8-23-2013

Conservation and Diversification of Appendage Identity Specification Mechanisms Along the Anteroposterior and Proximodistal Axes in Panarthropoda

Frank W. Smith III
University of Connecticut, frank.smith@uconn.edu

Conservation and Diversification of Appendage Identity Specification Mechanisms Along the Anteroposterior and Proximodistal Axes in Panarthropoda

Frank Wesley Smith III, PhD

University of Connecticut, 2013

A key characteristic of arthropods is their diverse serially homologous segmented appendages. This dissertation explores diversification of these appendages, and the developmental mechanisms producing them. In Chapter 1, the roles of genes that specify antennal identity in *Drosophila melanogaster* were investigated in the flour beetle *Tribolium castaneum*. Antenna-to-leg transformations occurred in response to RNA interference (RNAi) against *homothorax*, *extradenticle*, *spineless* and *Distal-less*. However, for *homothorax/extradenticle* RNAi, the extent of transformation along the proximodistal axis differed between embryogenesis and metamorphosis. This suggests that distinct mechanisms specify antennal identity during flour beetle embryogenesis and metamorphosis and leads to a model for the evolution of the *Drosophila* antennal identity mechanism. Homothorax/Extradenticle acquire many of their identity specification roles by acting as Hox cofactors. In chapter 2, the metamorphic roles of the *Hox* genes, *extradenticle*, and *homothorax* were compared in *T. castaneum*. *homothorax*/*extradenticle* RNAi and *Hox* RNAi produced similar body wall phenotypes but different appendage phenotypes. These results suggest that *Hox* genes require *extradenticle* and *homothorax* to specify sclerite identities in the thorax and abdomen during metamorphosis. On the other hand, the *Hox* genes act independently of *extradenticle* or *homothorax* to specify appendage identities along the body axis, while

extradenticle and *homothorax* do not require *Hox* genes to impart proximal identity to appendage podomeres.

Tardigrades are closely related to arthropods, but their ventral appendages retain the lobopodal leg-like morphology that is ancestral for arthropods. In Chapter 3, the body plan of the tardigrade *Hypsibius dujardini* was characterized using anti-β-tubulin immunostaining and phalloidin staining. These methods revealed differences in the nervous system and musculature that make each segment unique. These results raise the possibility that the arthropod/tardigrade ancestor already exhibited morphologically differentiated segments. In Chapter 4, the embryonic role of the gene *Distal-less* was investigated in *H. dujardini*. It is expressed in the pharyngeal stylets and across the entire proximodistal appendage axis. The uniform expression of *Distal-less* in developing appendages is consistent with the lesser degree of morphological regionalization exhibited in tardigrade appendages relative to arthropod appendages. The appendix provides an *in situ* hybridization protocol for *H. dujardini*.

Conservation and Diversification of Appendage Identity Specification Mechanisms Along the Anteroposterior and Proximodistal Axes in Panarthropoda

Frank Wesley Smith III

A.S., Community College of Rhode Island, 2004

B.S., University of Rhode Island, 2007

A Dissertation

Submitted in Partial Fulfillment of the

Requirements for the Degree of Doctor of Philosophy

at the

University of Connecticut

2013

APPROVAL PAGE

Doctor of Philosophy Dissertation

Conservation and Diversification of Appendage Identity Specification Mechanisms Along the Anteroposterior and Proximodistal Axes in Panarthropoda

Presented by

Frank Wesley Smith III, B.S.

Major Advisor_____
Elizabeth L. Jockusch

Associate Advisor_____
Steven Q. Irvine

Associate Advisor_____
Carl D. Schlichting

Associate Advisor_____
David L. Wagner

University of Connecticut
2013

Dedicated to my parents, Ann and Ken Hoover

Acknowledgments

Chapters 3 and 4 of this dissertation were supported by the following sources:

The Betty Decoursey Endowment and the James A. Slater Endowment Fund to the EEB Dept. and Connecticut State Museum of Natural History.

Sigma Xi Grants-in-Aid of Research Award

Society for the Study of Evolution (SSE) Rosemary Grant Graduate Research Award

EDEN Research Exchange Fund (NSF/EDEN grant IOS# 0955517)

I am deeply indebted to my advisor, Elizabeth L. Jockusch, for the wonderful opportunities and the invaluable advice she has provided for me during my journey through graduate school and growth as a scientist. Elizabeth was always happy to discuss my interests with me, and push me to take on challenges that I would have been reluctant to accept without her encouragement. Elizabeth taught me a wealth of knowledge about evolution and development and thanks to her, a window to an incredibly exciting world has been opened to me. She has revealed mysteries that I will spend the rest of my career working to solve. As a scientist, I cannot imagine a greater gift.

I would like to thank my other committee members for all that they have taught me. Carl Schlichting has been an incredible influence on the way I perceive organismal evolution. Dave Wagner has instilled in me an immense appreciation for the diversity of insects. Steve Irvine provided me with my first evo-devo research experience, which gave me the confidence to pursue a PhD. I want to thank all my committee for their excellent comments and advice concerning my dissertation. I owe them all for the excitement I feel about this tremendous accomplishment.

I would like to thank Dave Angelini for his excellence mentorship when I first started my PhD. He really got me excited about appendage development and evolution. I did not know that I would become an appendage biologist when I arrived at UCONN!

I would like to acknowledge Bob Goldstein for encouraging me to study tardigrades. Bob's encouragement extended all the way to hosting me in his lab during the summer of 2011. During my visit, I developed skills that were incredibly useful for my dissertation research. I cannot wait to join his lab for my postdoc. There is not another lab in the world that I would rather join!

I feel incredibly lucky for the opportunity to work along side so many great colleagues during my time in the Jockusch lab. I would like to thank my fellow graduate students in the Jockusch lab: Roberta Engel, Cera Fisher, Beth Timpe, and Tobias Landberg. They have provided me with incredible support. I would like to thank Iñigo Martinez-Solano, who was a postdoc in the Jockusch lab, for sharing his phylogenetic expertise with me and for being a great friend. Finally, I would like to thank all the undergraduates I have been lucky enough to mentor: Derek Cornetta, Matthew Gaudio, Daniel Madden, Devin O'Brien, and Chelsea Willet. It was incredibly exciting to watch them grow as scientists.

I would like to thank my professors in the EEB Department: Kurt Schwenk, Janine Caira, Charlie Henry, Chris Simon, Louise Lewis, Paul Lewis, and Andy Bush. The knowledge I accrued in their classes and seminars was critical for the development of my dissertation.

I would like to thank Marie Cantino, Bruce Goodwin, and Stephen Daniels of the University of Connecticut Electron Microscopy Laboratory. I would also like to thank Carol Norris of the University of Connecticut Confocal Microscopy Facility. Members of both

imaging facilities were kind enough to share their expertise, which enabled me to collect invaluable data for my dissertation research.

Special thanks to all of the graduate students in the EEB Department. It has been a treat!

I would like to thank my parents, Ann and Ken, my brother, Nick, sister in law Amy, and nieces, Halle and Hannah for their love and support.

Finally, I would like to thank Jackie Meier for her love and support for the last four years. I love you so much Jackie!! I hope you find some great artifacts!!

Table of Contents

Chapter 1.

Distinct mechanisms specify antennal identity during embryogenesis and metamorphosis of the flour beetle *Tribolium castaneum*

Introduction

While much of the incredible evolutionary success of the phylum Arthropoda can be attributed to the diversity of appendages characterizing this group, arthropods are descended from an ancestor that had morphologically homonymous appendages that functioned as legs (Prpic and Damen, 2008; Snodgrass, 1935). Fossil evidence suggests that the deuterocerebral appendage pair was the first to evolve distinct morphology (Boxshall, 2004; Legg et al., 2012), and that this morphology was antenniform (Yang et al., 2013). In extant arthropods, this appendage pair is represented by the chelicerae of Chelicerata, the first antennae of Crustacea, and the antennae of Myriapoda and Hexapoda (Fig. 1). Much effort has been given to elucidating the developmental mechanism that specifies antennal identity, because understanding this would lend insight into how morphologically diverse serial appendage homologs evolved in Arthropoda.

The first insights into antennal identity specification were gleaned through studies of four transcription factor mutants in *Drosophila melanogaster* that exhibit transformations of the antenna to leg. The TALE class homeobox transcription factor-coding genes *extradenticle* (*exd*) and *homothorax* (*hth*) are co-expressed throughout the antennal disc during the 1st and early 2nd instar (Emmons et al., 2007), and function as a heterodimer (Abu-Shaar and Mann, 1998; Abu-

Shaar et al., 1999; Kurant et al., 1998; Pai et al., 1998; Rieckhof, 1997). Hypomorphic or null mutants of either gene result in a transformation of the entire antenna to leg (Casares and Mann, 1998; Casares and Mann, 2001; Gonzales-Crespo and Morata, 1995; Rauskolb et al., 1995). *Distal-less* (*Dll*), which also codes for a homeobox transcription factor, is expressed in the developing distal antenna and hypomorphic alleles of this gene result in a transformation of the flagellum to leg (Dong et al., 2000; Sunkel and Whittle, 1987). Unlike the antenna of *hth* or *exd* mutants, the proximal antennal regions of *Dll* mutants are not affected. Lastly, like *Dll* mutations, hypomorphic and null mutations of the bHLH-PAS transcription factor-coding gene *spineless* (*ss*) also cause transformations of the flagellum to leg, but do not affect proximal regions (Struhl, 1982b; Duncan et al., 1998).

Studies of these *Drosophila* mutations laid the foundation for a model of antennal identity specification (Casares and Mann, 2001; Dong et al., 2000; Dong et al., 2001; Dong et al., 2002, Duncan et al., 1998). In the *Drosophila* model, *exd*/*hth* and *Dll* promote antennal identity by both activation and repression of downstream appendage patterning genes. In the antennal imaginal disc, *exd*/*hth* and *Dll* block leg disc expression patterns of the appendage patterning gene *dachshund* (*dac*) (Dong et al., 2001; Dong et al., 2002). Overexpressing *dac* in the antennal disc, which simulates leg expression, causes a transformation of the medial antenna to leg (Dong et al., 2001). Co-expression of *exd*/*hth* and *Dll* activates *ss* expression in the developing flagellum (Dong et al., 2002; Duncan et al., 1998). Therefore, mutations of *exd*, *hth*, or *Dll* cause transformations of the flagellum to leg because of reduced *ss* expression. *exd* and *hth* also specify identity of the proximal two antennal segments, the scape and pedicel, but this is not modulated through *ss*. Finally, *Hox* genes are not expressed in the antennal segment, but they are expressed in the imaginal discs of other ventral appendages, where they block antenna-

specific expression and functions of *hth*/*exd*, *Dll*, and *ss* (Casares and Mann, 1998; Duncan et al., 2010; Emmons et al., 2007; Struhl, 1982a). For example, unlike the extensive overlap in expression patterns of *hth*/*exd* and *Dll* in the antennal discs, there is little overlap in the expression domains of these genes in the leg discs (Abu-Shaar and Mann, 1998; Rauskolb, 2001).

The *Drosophila* model of antennal identity specification became the basis for models of the origin of the antenna (Casares and Mann, 2001; Duncan et al., 1998), even though the extent of conservation of this process across arthropods was unknown at the time. Sufficient data are now available to test the generality of two aspects of the *Drosophila* model. First, *Hox* genes are not expressed in the deuterocerebral segment (Hughes and Kaufman, 2002; Jager et al., 2006; Janssen and Damen, 2006; Manuel et al., 2006; Mittmann and Scholtz, 2003; Sharma et al., 2012b) and they block deuterocerebral segment identity in other body segments in all arthropod species investigated (Angelini et al., 2005; Brown et al., 2002; Hughes and Kaufman, 2000; Struhl, 1982a). Therefore, this aspect of appendage identity specification appears to be conserved. Second, extensive overlap of the expression domains of *exd*/*hth* and *Dll* in the deuterocerebral appendage is not conserved across arthropods. As in the *Drosophila* antennal disc, extensive overlap in the expression domains of these genes is found during embryogenesis in the chelicera of spiders (Abzhanov and Kaufman, 2000; Pechmann and Prpic, 2009; Prpic and Damen, 2004; Prpic et al., 2003), the harvestman *Phalangium opilio* (Sharma et al., 2012a), and the mite *Archegozetes longisetosus* (Barnett and Thomas, in press) and the antenna of the insects *Oncopeltus fasciatus* (Angelini and Kaufman, 2004) and *Tribolium castaneum* (Jockusch et al., 2004). On the other hand, there exist discrete expression domains of these genes during development of the antenna of the millipede *Glomeris marginata* (Prpic and Tautz, 2003) and the

orthopteran insects *Gryllus bimaculatus* (Mito et al., 2008; Ronco et al., 2008), *Acheta domesticus* (Abzanhov and Kaufmann, 2000) and *Schistocerca americana* (Jockusch et al., 2004). However, as in *Drosophila*, discrete expression domains of *exd*/*hth* and *Dll* exist in legs during embryogenesis of all arthropods investigated (Angelini and Kaufman, 2005; Barnett and Thomas, in press; Prpic and Damen, 2004; Sharma et al., 2012a). It has been proposed that the *Drosophila*-like expression patterns of *exd*/*hth*, *Dll*, and even *dac*, found in the deuterocerebral appendages of some insects and chelicerates reflect the independent evolution of highly derived appendage morphologies (Prpic and Damen, 2004; Prpic and Damen, 2008), often exhibiting reduction in both length and number of joints, rather than indicating conservation of an ancestral arthropod antennal identity specification mechanism.

Compared to expression data, a phylogenetically more limited sample of functional data for *exd, hth*, and *Dll* are available. Two cases match predictions based on the *Drosophila* model of antennal identity specification, supporting conservation. First, RNA interference (RNAi) against either *hth* or *exd* in the cricket *G. bimaculatus* results in transformation of the antenna to leg (Mito et al., 2008; Ronco et al., 2008). Second, *ss* is known to specify flagellum identity in *T. castaneum* during both embryogenesis and metamorphosis (Angelini et al., 2009; Shippy et al., 2009; Toegel et al., 2009). However, in beetles, the roles of *hth* and *Dll* in antennal identity specification are less clear (Angelini et al., 2009; Moczek and Rose, 2009; Suzuki et al., 2009), but it has been suggested that these genes lack antennal identity specification roles in *T. castaneum* (Angelini et al., 2009). Functional data for *exd* in beetles were previously unavailable.

One difficulty in comparing results of RNAi investigations in beetles to *Drosophila* mutant phenotypes stems from the highly derived mode of *Drosophila* development. It is

unclear how the ontogenetic sequence of *Drosophila* development relates to the ontogenetic sequence that gives rise to antennae in other insects, and direct comparisons between homologous developmental stages are required to determine the extent of conservation of the antennal identity specification mechanism. Here, we test the *Drosophila* model of antennal identity specification and models of arthropod appendage evolution using RNAi in *T. castaneum* and other flour beetles. In flour beetles, antennal identity is specified during embryogenesis, as in most arthropods, and again during metamorphosis. This similarity in development between *Tribolium* and other arthropods makes this group particularly informative. Studies of *T. castaneum* enable comparisons of beetle embryonic gene functions with the functions of orthologs in non-holometabolous arthropods; comparisons of both beetle embryonic and metamorphic functions with functions in *Drosophila* development; and comparisons between embryonic and metamorphic functions in *T. castaneum*. Based on these comparisons, we present an evolutionary model of stage-specific conservation of antennal identity specification mechanisms among insects.

Materials and methods

Beetle husbandry

In order to increase the phylogenetic breadth of this study, we have included RNAi data for *Tribolium confusum*, *T. brevicornis*, and *Latheticus oryzae*, along with the model short germ band insect *T. castaneum* (Fig. 1). These tenebrionid species are all stored product pests (Angelini and Jockusch, 2008). *T. castaneum* were obtained from Carolina Biological and all

other species were obtained from the USDA Stock Center (Manhattan, Kansas). These species exhibit a diversity of antennal morphologies (Sokoloff, 1972), within the conserved beetle pattern of a scape, pedicel, and 9-segmented flagellum. Beetles were reared in mason jars on a 9:1 mixture of organic whole-wheat pastry flour and nutritional yeast (Sokoloff ,1972). *T. brevicornis* were cultured at room temperature. The other species were cultured at 32°C. Roughly once a month, flour in the culture jars was replaced and excess beetles were sacrificed to prevent overcrowding.

Selection, molecular cloning, and sequencing of candidate genes

Genes were chosen for this investigation based on evidence that they play antennal specification roles in *D. melanogaster* (Table 1). Total RNA was collected using a PureLink RNA Mini Kit (Ambion). An oligo-dT primer and qScript Flex cDNA Synthesis Kit (Quanta Bioscience) were used to make cDNA. Genes were amplified from cDNA using regular or semi-degenerate primers designed from sequence data available for *T. castaneum* (Supplementary Table 1). PCR products were either cloned directly or purified using a Macherey-Nagel Nucleospin extract II kit and subsequently cloned into the pCR4-TOPO vector (Invitrogen). Clone inserts were amplified with vector primers and then sequenced on an Applied Biosystems 3130xl Genetic Analyzer using Big Dye v1.1. Sequences were blasted against *T. castaneum* nucleotide collection (nr/nt) to confirm identity. After confirmation of nucleotide sequence identity, amino acid sequences were predicted using the Translate DNA to Protein function in Mesquite (Maddison and Maddison, 2011).

RNA interference

Target gene fragments were amplified with PCR from clones using gene-specific primers designed with T7 RNA polymerase promoter sites added to the 5′ end (Supplementary Table 1). The resulting PCR product was used as a template for in vitro transcription using the MEGAscript T7 transcription kit (Ambion) following the procedure of Tomoyasu and Denell (2004). 20 µl reactions were incubated at 37° C for 16 hours. Double-stranded RNA (dsRNA) was purified by precipitation in ammonium acetate and ethanol and resuspended in nuclease-free water. Stocks of dsRNA were prepared at 0.01–1.00 µg/µl (Table 3, Table 4) in 1:20 McCormick green food coloring and 1:100 injection buffer (0.1 mM sodium phosphate, 5.0 mM KCl, 1:10 green food coloring).

We performed larval RNAi (Posnien et al., 2009; Tomoyasu and Denell, 2004) to investigate the antennal specification function of candidate genes during metamorphosis (Table 2). Injections of *GFP* dsRNA acted as a negative control. We injected late stage larvae, as suggested by Posnien et al. (2009), earlier than the prepupal stage that was injected in our previous investigation (Angelini et al., 2009). We have previously validated RNAi knockdown of *T. castaneum Dll*, *hth*, and *dac* with qRT-PCR (Angelini et al., 2012a). Because *hth* and *exd* are co-dependent for developmental function (Abu-Shaar and Mann, 1998; Kurant et al., 1998; Pai et al., 1998; Rieckhof, 1997), performing both *hth* and *exd* RNAi controls for off-target effects of these genes. For *dac* RNAi, we recovered a species-specific RNAi effect in *T. confusum* (Section 2.6), so we injected dsRNA for a non-overlapping *dac* fragment to control for off-target effects (Table 2). Larvae were anesthetized by placing them in a 33 mm petri dish on ice for ~5 minutes. Solutions of dsRNA were loaded into micropipets (VWR International 53432-783) that had been pulled on a Sutter Instrument Co. Model P-97 Flaming/Brown

micropipette puller. Larvae were then placed on a piece of double-sided tape on a microscope slide and injected with ~120 nl of dsRNA solution dorsally between the pro- and mesothoracic tergites under a Nikon SMZ645 dissecting scope using a microinjector. Injected larvae were then reared at 32° C in flour/yeast mix, and cultures were checked regularly for pupae. Pupae were removed and kept individually at 32° C. These pupae were monitored until eclosion or until they appeared dead, and were then prepared for scoring and imaging (Section 4.4).

To investigate the embryonic antennal specification function of candidate genes in *T. castaneum*, we injected female pupae or adults with dsRNA (Table 3), following closely the procedures described in Posnien et al. (2009). Pupae with darkly pigmented eyes were placed ventral side up on a piece of double-sided tape on a microscope slide and injected between the third and fourth sternites. Enough dsRNA solution was injected to straighten the normally curved abdomen. These females were then kept in standard flour/yeast mix at 32° C. After all surviving specimens had eclosed (~3–5 days post-injection), they were moved to organic white flour and males were added. Virgin female adults were anesthetized on ice following the procedure used for larvae, injected with dsRNA into the soft tissue of the dorsal abdomen, and then cultured in flour/yeast mix at 32° C. Enough dsRNA solution was injected to turn the abdomen green. Males were added 4 days after injection. For both pupal and adult injection experiments, after males were added, cultures were checked for embryos and larvae, weekly, for 1–4 weeks. Larvae were collected and prepared for scoring and imaging (see below), while embryos were maintained for four additional days, allowing sufficient time for the completion of embryogenesis. Any larvae or remaining embryos were then also prepared for scoring and imaging.

Specimen preparation and imaging

Adult RNAi specimens were prepared following the protocol of Van der Meer (1977). Briefly, specimens were soaked in 20% glycerol in acetic acid overnight at 50° C. Specimens were then rinsed with 20% glycerol in PB-tween (1X phosphate-buffered saline, 0.1% Tween20), while rocking gently for at least an hour. Specimens were stored in 80% glycerol in 1X PB-tween at 4° C.

Embryos and early instar larvae from maternal RNAi experiments were collected and washed in an embryo basket. Specimens were rinsed with distilled water briefly, and then washed with 50% bleach in distilled water for 2 minutes in order to remove the embryonic chorion (Jockusch et al., 2004). Next, specimens were washed twice briefly with distilled water and once with PB-tween. All embryos were immediately mounted on slides with 80% glycerol in 1X PB-tween. Larvae were mounted on slides or stored in 100% ethanol at 4° C.

For imaging, adult appendages were dissected off and mounted on slides in 80% glycerol in 1X PB-tween. Whole mount adults were washed three times in 100% ethanol over a 24-hour period to remove glycerol and then mounted on Styrofoam with double-sided tape. All light micrographs were taken with an Olympus digital camera. Light micrographs of whole mount adults were taken on a Nikon SMZ800 dissecting microscope. All other light micrographs were taken on a Zeiss Axioskop compound microscope. In some cases, images were taken in multiple focal planes and the Auto-Blend Layers command in Adobe Photoshop was used to maximize the focus of light micrographs of whole-mount adults and appendages. For Scanning Electron Microscopy (SEM), specimens were dehydrated with 3 washes of ethanol, followed by dehydration in hexamethyldisilazane, and then coated with gold-palladium. SEM images were taken on a Zeiss DSM982 Gemini field emission scanning electron microscope.

Results

Antennal morphology

There is disagreement in the literature on the podomere composition of the highly derived larval antennae of *T. castaneum* (Shippy et al., 2009; Sokoloff, 1972; Stanley 1965; Toegel et al., 2009). In the antenna during metamorphosis, *ss* only functions in the flagellum (Fig. 3A–C). Therefore we consider the antennal regions affected by *ss* RNAi during embryogenesis (Shippy et al., 2009; Toegel et al., 2009) to be homologous to the adult flagellum. In this interpretation, the larval antenna is composed of a proximal segment, homologous to the scape and/or the pedicel followed by a flagellum composed of two articles, and terminating in a seta (Fig. 2A). This pattern is conserved across flour beetles. The adult flagellum is annulated, consisting of nine articles (Fig. 1I–L). The adult flagellum is further regionalized into proximal funicle articles and somewhat larger distal club articles (Fig. 1I–L). Club articles are dorsoventrally flattened compared to more proximal antennal articles. Basiconic sensilla are associated with the apical margin of club articles and absent from funicle articles (Fig. 6A–C). At the adult stage, variation in antennal regionalization patterns exists among flour beetle species. The flagellum of *L. oryzae*, *T. confusum*, and *T. brevicornis* has five club segments, while *T. castaneum* exhibits a derived flagellar morphology with a three-segmented club (Sokoloff, 1972) (Fig. 1I–L). Across species, variation is also apparent in bristle and basiconic sensillum number and distribution, and how distinctly abrupt the club articles appear (Sokoloff, 1972). There are also differences in the shape of flagellar articles between species. For example, the first flagellar article of both *T. brevicornis* and *T. confusum* has a noticeable basal constriction (Fig. 1F, H). This feature is absent from both *T. castaneum* and *L. oryzae* (Fig. 1E, G).

Molecular analysis

In most cases, orthologs of *hth*, *exd*, *Dll*, and, *dac* were cloned from all species. As expected, given the close relationship among the flour beetles of this study, nucleotide (nt) and predicted amino acid (aa) sequences were highly conserved (Table 1). Identities ranged from 85%–96% (nt) and 98%–100% (aa) for *T. confusum*; 81%–91% (nt) and 98%–100% (aa) for *T. brevicornis*; and 80%–93% (nt) and 98%–99% (aa) for *L. oryzae*. We failed to clone an *hth* orthologue from *T. brevicornis* or a *Dll* orthologue from *L. oryzae*. In these cases, double-stranded RNA (dsRNA) produced from *T. castaneum* clones was used to investigate *hth* function in *T. brevicornis* and *Dll* function in *L. oryzae*. This approach yielded highly penetrant phenotypes (Table 2) that matched results from *T. castaneum* and other flour beetle species (Section 2.4, 2.5).

For the gene *dac*, we found variation among species in the nucleotide and predicted amino acid sequence lengths. This variation was 3′ from sequence coding for the highly conserved bilaterian Ski-Sno domain. Both *T. confusum* Dac[a] and *L. oryzae* Dac lack two serine residues at the N-terminus of the amino acid sequence relative to other flour beetles (Supplementary Fig. 1A). Synthesized dsRNAs spanned this region for all species. *Tribolium brevicornis* Dac included an 11 amino acid residue domain that was absent from other flour beetles (Supplementary Fig. 1B). Synthesized *dac* dsRNAs for *T. castaneum*, *T. confusum*, and *L. oryzae* spanned this region; the dsRNA sequence for *T. brevicornis* did not. We also sequenced a new *T. castaneum dac* clone that shared 99% nt identity (537/538) with the clone used in our previous studies (Angelini et al., 2009, 2012a, 2012b; Aspiras et al., 2011). The predicted amino acid sequence for the new clone was missing the two serine residues, like *L. oryzae* Dac, and included the 11 amino acid residue domain, as in *T. brevicornis* Dac

(Supplementary Fig. 2). These results are consistent with the existence of alternatively spliced *dac* transcripts in flour beetles, which explains some of the *dac* sequence length differences among these species.

In the C-terminus of our sequences, the predicted *T. brevicornis* Dac sequence was missing a 31 amino acid residue domain present in other flour beetles. This domain exists in the lightning bug *Photuris* sp. (Supplementary Fig. 1C), demonstrating that it is not a synapomorphy of the *T. castaneum* + *T. confusum* + *L. oryzae* clade. Either lack of this sequence is a genomic synapomorphy of the *T. brevicornis* lineage, or this result stems from alternative splicing of the *T. brevicornis dac* transcript.

Embryonic RNAi phenotypes

spineless RNAi has been shown to cause transformations of the flagellum to leg during embryogenesis in *T. castaneum* (Shippy et al., 2009; Toegel et al., 2009). We performed maternal RNAi in order to determine if *hth*/*exd* and *Dll* also play roles in embryonic antennal identity specification in *T. castaneum* (Table 3). At 1 μg/μl dsRNA, pupal-stage maternal *Dll* RNAi resulted in extreme truncations of all appendages except the mandible (Fig. 2E), including the complete deletion of the antennal flagellum, consistent with the phenotype of *T. castaneum Dll* mutants (Beermann et al., 2001). In order to attenuate the RNAi effect of *Dll* to prevent complete deletion of the flagellum, we tried 0.1 μg/μl and 0.01 μg/μl dsRNA concentrations. At these concentrations, specimens developed to the larval stage and had normal appendages. Therefore, although *Dll* specifies distal appendages in *T. castaneum*, as in other arthropods, we were unable to determine whether a role exists for *Dll* in embryonic antennal identity specification.

For pupal-stage maternal *exd* RNAi, at 1 μg/μl dsRNA, all eggs lacked a visible germ-band, while at 0.1 μg/μl and 0.01 μg/μl *exd* dsRNA, specimens developed into normal larvae (Table 3). At 1 μg/μl dsRNA, pupal-stage maternal *hth* RNAi resulted in the death of 16/17 injected pupae (Table 3). The surviving female produced 27 offspring. Twenty-five of these embryos developed into normal larvae. One embryo exhibited a very reduced head and was missing all head appendages, but eyes were present (Fig. 2C). The legs of this specimen also appeared normal. At 0.1 μg/μl and 0.01 μg/μl *hth* dsRNA, specimens developed into normal larvae.

Because of the high mortality associated with pupal-stage maternal *hth* RNAi, we injected virgin adult females with 1 μg/μl *hth* dsRNA (Table 3). In parallel, we injected adult females with either *Dll* or *exd* dsRNA to test if embryonic RNAi phenotypes were consistent between pupal and adult female injections for dsRNA targeting these genes. Embryos produced by adults injected with *Dll* dsRNA exhibited the same phenotypes as embryos produced by pupae injected with *Dll* dsRNA. No embryos were produced from adult females injected with *exd* dsRNA. Adult females injected with *hth* dsRNA produced embryos with very reduced heads with identifiable eyes. Similar head reductions were reported for *hth* RNAi in the cricket *G. bimaculatus* (Ronco et al., 2008) and the milkweed bug *O. fasciatus* (Angelini et al., 2004). Most *T. castaneum hth* RNAi specimens had three pairs of legs with the full complement of podomeres, although two specimens had only two pairs of legs and lacked all head appendages. Embryos with three pairs of legs were missing all (12/17 embryos) or some (5/17 embryos) head appendages. In most cases, it was difficult to identify the segmental affiliation or morphological identity of head appendages when they were present. A single *hth* RNAi specimen had an appendage pair anterior and dorsal to the eye (Fig. 2D). Based on the location of these

appendages, we interpret these as antennae. However, these appendages lacked antennal setae and the shape of the podomeres was not consistent with antennal identity, suggesting a partial homeotic transformation. When appendages were present on body segments between the eyes and the legs (5/17 embryos), they lacked endites associated with the labium and maxillae, and were composed of multiple podomeres, unlike the mandible (Fig. 2D). These appendages were also directed posteriorly, which is similar to the legs, but atypical for the prognathous mouthparts of *T. castaneum*, suggesting a partial homeotic transformation of a gnathal appendage pair towards leg identity.

Adult Dll *and* ss *RNAi phenotypes*

As previously reported (Angelini et al., 2009; Shippy et al., 2009; Toegel et al., 2009), *T. castaneum ss* larval RNAi led to transformations of the adult flagellum toward leg identity, but did not affect the morphology of the scape or pedicel (Fig. 3A–C). The most severely affected specimens showed the presence of both a claw and a tibial spur (Fig. 3C), resembling *T. castaneum ss* mutants (Shippy et al., 2009). In all appendages, *Dll* RNAi resulted in reduction of growth and loss of normal segmentation patterns. In the leg, the tarsus was almost completely deleted and there was no evidence of a claw (Fig. 3D–F, lower panels). Antennal morphology was so disrupted that in most cases it was difficult to assign an identity to antennal elements (Figure 3D–F, upper panels). In addition, we also recovered clear antenna to leg transformations (Fig. 3F), evidenced by a tarsal claw on the distal antenna (Table 2). We only found claws on both antennae in 1/5 specimens exhibiting homeotic transformation. *Dll* RNAi also caused severely truncated and malformed appendages in the other species (Fig. 3G–I), but no clear homeosis. Antenna to leg transformations were probably recovered at such a low frequency with

Dll RNAi because *Dll* RNAi normally causes deletions of tarsal claws and other leg components that are useful for determining leg identity. This likely explains why antennal transformations were not found in our earlier study (Angelini et al., 2009).

Adult exd *and* hth *RNAi phenotypes*

As expected, given the co-dependence of Hth and Exd for nuclear localization, *exd* and *hth* RNAi resulted in largely overlapping phenotypes for all species in this study. RNAi resulted in a range of phenotypic severity, resembling a hypomorphic series. In the antenna flagellum, *hth* and *exd* RNAi in *T. castaneum* caused fusions between proximal articles in severely affected specimens (Fig. 4D, F, G), while complete joints formed between all flagellar articles in less severely affected individuals (Fig. 4B, C, E). In severely affected specimens, the scape and pedicel were altered in size and shape, suggesting homeotic transformations to femur and tibia, respectively (Fig. 4D, G). This transformation included the following changes: denser leg-like bristle patterns on the scape and pedicel; the scape became much larger with flatter lateral surfaces, like the femur; the articulation between the scape and pedicel resembled the hinge joint characteristic of the femur tibia-joint; and finally, the pedicel became elongate and tapered proximally, like the tibia (compare Fig. 1A, D). Even in more mildly affected specimens, the scape and pedicel were larger and more elongate than in the *GFP* RNAi control specimens and showed a greater bristle density, suggesting a transformation toward leg identity (Fig 4B, C, E, F). The identity of the flagellum was not affected with either *exd* or *hth* larval RNAi.

Similar results were found for both *exd* and *hth* RNAi for the other species of this study, and suggest a role for these genes in specifying scape and pedicel. In all cases, distal elements of the flagellum were the least sensitive to RNAi, while proximal articles were often fused. In *T.*

confusum (Fig. 4H, I) and *L. oryzae* (Fig. 4J, K), the most severe transformations were of similar magnitude between *hth* and *exd* RNAi. However, in *T. brevicornis*, *exd* RNAi lead to more severe transformations than *hth* RNAi, including an almost complete transformation of the scape to femur identity (Fig. 4L, M).

Both *exd* and *hth* RNAi resulted in additional anterior head phenotypes. The gena and clypeus, anterior head sclerites, were deleted in the most severely affected specimens of all species. For *exd* and *hth* RNAi treatments, all species also showed marked reductions in the number of ommatidia in the eyes, consistent with the role of *hth* in promoting cell proliferation in the *Drosophila* antennal-eye disc (Bessa et al., 2002; Lopes and Casares, 2010). However, in severely affected *Tribolium* specimens, the ventral eye lobe was transformed into a dorsoventrally flattened cuticular outgrowth, which tapered distally (Fig. 5D–I). The wrinkled appearance of these structures closely resembled the appearance of elytra of recently molted adults. We used Scanning electron microscopy (SEM) to more closely examine the microstructure of *T. confusum hth* RNAi specimens. Regular hexagonally-shaped cuticle cells were present on both the elytron of a *GFP* RNAi specimen and the transformed eyes of an *hth* RNAi specimen (Fig. 5K, L), while cuticle cells of the head capsule of a *GFP* RNAi specimen were hexagonal, but stretched laterally (Fig. 5J). The pits of sensory bristles on the elytron of the *GFP* RNAi specimen and the pits on the cuticular outgrowths resulting from *hth* RNAi were both shallow with circular, flat bases (Fig. 5K, L). In contrast, sensory pits on the head capsule of the *GFP* RNAi specimen were deeper and did not have flat circular bases (Fig. 5J). These results are all consistent with the transformation of the ventral eye towards an elytron-like identity in *hth* larval RNAi.

Adult dac *RNAi phenotypes*

The transcription factor coding gene *dac* is expressed in intermediate appendage domains across arthropods (Angelini and Kaufman, 2005; Sharma et al., 2012; Barnett and Thomas, 2013). In *Drosophila*, *dac* null mutations dramatically reduce the intermediate leg region, but cause only subtle effects on antennal morphology (Mardon et al., 1994; Dong et al., 2002). In flour beetle species, larval *dac* RNAi resulted in fusions, deletions, and other patterning disruptions of the first seven flagellar elements (Fig. 6E–G, I), and also resulted in dramatic reduction of the intermediate leg domain (Angelini et al. 2012b). However, we found differences among species in the role *dac* plays in specifying the proximodistal flagellar identity of articles. As reported by Angelini et al. (2009), in *T. castaneum dac* RNAi caused transformations of the distal two funicle segments to club identity (Fig. 6F). This was evidenced by an increase in the number of bristles and the presence of an apical row of bristles on these articles.

Surprisingly, *dac* RNAi in *T. castaneum* did not effect the development of basiconic sensilla associated with the club. Scanning EM inspection of a severely disrupted *T. castaneum dac* RNAi specimen confirmed ectopic apical bristle rows, but no ectopic basiconic sensilla were found on transformed funicle segments. Because *dac* RNAi also disrupts normal segmentation in the antenna, and basiconic sensilla are normally found at the boundaries between club segments (Fig. 6A), we reasoned that *dac* RNAi might be causing the loss of a molecular boundary that is required for basiconic sensilla specification. *Notch* pathway genes are responsible for specifying joints between appendage articles in *T. castaneum* (Angelini et al., 2009, 2012a, 2012b), as in other arthropods (Prpic and Damen, 2009). *dachshund* regulates Notch pathway genes in *Drosophila* (Rauskolb, 2001), which explains disruptions of normal

segmentation associated with *dac* RNAi. However, while RNAi in *T. castaneum* against the Notch ligand *Serrate* (*Ser*) caused a loss of normal segmentation in the flagellum, it did not affect the development of basiconic sensilla in the club (Fig. 6H). This suggests that in *T. castaneum* these sensilla are specified by a mechanism that functions independently of the joint formation pathway and of *dac*-mediated regional identity.

In *T. confusum*, *dac* RNAi caused a transformation of the proximal most funicle article, as evidenced by loss of the basal constriction and the presence of ectopic basiconic sensilla (Fig. 6E). This transformation occurred even in moderately affected specimens, where all flagellum articles were present. In terms of shape, bristle pattern, and presence of basiconic sensilla, this article adopted the morphology of a more distal flagellar article. While RNAi in *L. oryzae* and *T. brevicornis* produced defects in antenna growth and segmentation (Fig. 6G, I), there was no evidence of proximodistal transformation of flagellar articles in these species.

Discussion

Flour beetles are an exceptional system for investigations into the evolution of developmental processes. The four species used in this study are amenable to RNAi and easily reared in the lab. Here we also demonstrate the feasibility of heterospecific knockdown in gene function using dsRNA based on *T. castaneum* sequences. For example, we recovered deletions of distal appendages with *T. castaneum Dll* dsRNA in *L. oryzae*, as well as transformations of the proximal antennae with *T. castaneum hth* dsRNA in *T. brevicornis*. Beetles also develop appendages during both embryogenesis and metamorphosis, enabling comparisons between

appendage patterning processes during these two stages. The utility of these methods and the diversity of antenna, eye and other morphologies in these beetles, makes the group an attractive system for investigating the developmental underpinnings of morphological diversity and its evolution.

Below, we present a model of the evolution of embryonic and metamorphic antennal identity specification in insects, and test the predictions of several hypotheses for the evolution of arthropod appendages. We also present a model of flour beetle eye identity specification.

The evolution of antennal specification mechanisms in insects

Our results suggest that similar but distinct mechanisms specify antennal identity during *T. castaneum* embryogenesis and metamorphosis. We have injected *exd* and *ss* dsRNA at early larval instars, but this does not affect either antennal morphology or identity at later instars (data not shown). This suggests that the identity of the larval antenna is fixed during embryogenesis, and that metamorphic antennal identity specification is not an extension of a mechanism active during the larval period. Below we compare our data to those from other insects and present a model of the evolution of insect antennal identity specification.

During *T. castaneum* embryogenesis, both *hth* (Fig. 2D) and *ss* RNAi (Shippy et al., 2009; Toegel et al., 2009) cause transformations of the flagellum, consistent with Hth activating *ss* in the flagellum of this species. Activation of *ss* may be non-autonomous in *T. castaneum*, given that *hth* expression has not been observed in the flagellum (Toegel et al., 2009). During embryogenesis, *Dll* is expressed throughout the flagellum (Beermann et al., 2001), and *Dll* RNAi causes the complete deletion of this structure (Fig. 2E). This makes it difficult to determine the role of *Dll* in embryonic antennal identity specification. However, because the expression and

functional domains of *Dll* completely overlap those of *ss*, it seems likely that, like *hth*, *Dll* activates *ss* in the flagellum. During embryogenesis of the cricket *G. bimaculatus*, RNAi against either *hth* or *exd* causes a transformation of the flagellum to leg during embryogenesis (Mito et al., 2008; Ronco et al., 2008). Co-expression of *exd* and *hth* has only been observed in the proximal antennal domain (Ronco et al., 2008), as in *T. castaneum*, so they must be modulating flagellar identity through non-autonomous activation of a distal factor, such as *ss*. The function of *G. bimaculatus Dll* has yet to be determined, but it is expressed across the flagellum during embryogenesis (Ronco et al., 2008), consistent with a conserved function in specifying the flagellum. Embryonic *Dll* expression in the flagellum, antennal transformations associated with maternal *hth* RNAi in both *T. castaneum* and *G. bimaculatus*, and embryonic *ss* expression and function are all consistent with predictions of the *Drosophila* model of antenna specification. This conservation suggests the model represents an ancestral embryonic mechanism for Neoptera, a lineage that includes 98% of insects (Grimaldi and Engel, 2005) (Fig. 7A, C).

Holometabola, which include both flour beetles and *Drosophila*, accounts for 83% of insect diversity (Grimaldi and Engel, 2005). In most holometabolous insect orders, larval antennae and other ventral appendages develop during embryogenesis, and are later remodeled during metamorphosis to produce adult appendage morphologies that differ from larval morphologies. This ontogeny is ancestral for Holometabola and is retained in flour beetles, but not in *Drosophila*. *Drosophila* do not produce antennae or other ventral appendages during embryogenesis; imaginal discs are set aside during embryogenesis, and it is cells of the discs, rather than larval appendages, that give rise to adult appendages and other structures. During *T. castaneum* metamorphosis, *hth* and *exd* modulate scape and pedicel identity (Fig. 4), but are not required for *ss* function or flagellum identity. These results are inconsistent with the *Drosophila*

model for antenna specification, which are based on a mechanism active in the *Drosophila* eye-antennal disc up to late 2nd larval instar (Emmons et al., 2007). However, during the third (final) larval instar in *Drosophila*, *hth* is no longer required for *ss* expression, and inducing *hth* mutations at this stage causes transformations of the proximal antenna to leg but does not affect flagellum identity (Emmons et al., 2007). During this period, *Dll* is still required for *ss* expression. The antennal identity specification roles of *ss*, *Dll*, and *hth*/*exd* during the *Drosophila* 3rd instar resemble the roles of these genes during the last larval instar of *T. castaneum* (Fig. 3, Fig. 4).

Based on the comparisons of antennal identity specification mechanisms presented here, we propose that the early period of *Drosophila* antennal development is derived from the embryonic antennal identity specification mechanism in other insects and that the mechanism active during the *Drosophila* third instar represents metamorphic antennal identity specification in other holometabolous insects, like *T. castaneum* (Fig. 7A–C). Although these mechanisms independently specify larval and adult antennal identity in *T. castaneum* and presumably other holometabolous insects, in *Drosophila* they are apparently concatenated into a single process that specifies adult antennal identity.

Models for the evolution of serially homologous appendage types

Two developmental models for the evolution of arthropod appendage types have previously been presented. In the first model, new appendage identities and morphologies appear by the evolution of novel selector gene expression in a subset of appendages (Casares and Mann, 1998; Duncan et al., 1998; Joulia et al., 2006). In *Drosophila hth* mutants, the antenna is transformed to a leg with a single proximal podomere and a distal tarsus, and Casares and Mann

(2001) have suggested that this phenotype represents both the developmental and evolutionary ground state of the arthropod appendage. In other words, modifications of this appendage morphology are or have been accomplished in development and evolution by the addition of selector genes to developmental pathways. Under this model, ancestral appendage morphologies can be produced in extant insects by interfering with the activity of selector genes.

The second model accounts for the fact that selector genes, like *hth* and *exd*, also play generic appendage patterning roles, such as regulating appendage growth and joint formation (Herke et al., 2005; Prpic and Damen, 2008). In this model, the generic patterning roles of these genes predate their selector function, and generic patterning and selector functions evolve independently. Under this model, loss of selector gene activity would not result in the production of ancestral insect or arthropod morphologies, because the generic ancestral patterning roles of these genes would also be compromised. This view suggests that, even if the two-segment morphology of *Drosophila hth* antenna represents a developmental ground state, it is unlikely to represent an ancestral appendage morphology.

Our results support the second model for the evolution of distinct appendage morphologies. In *Drosophila hth* mutants, appendages are reduced because the proximal podomeres are fused into a single proximal article (Casares and Mann, 2001). Similar fusion and reduction of appendages were reported for *hth* and *exd* RNAi in *Gryllus* (Mito et al., 2008; Ronco et al., 2008) and for *hth* RNAi in *Oncopeltus* (Angelini and Kaufman, 2004), suggesting that *hth*/*exd* played a role in promoting growth and joint formation ancestrally in insect appendages. However, in flour beetles, maternal *hth* RNAi did not result in the loss of distinct leg podomeres during embryogenesis. Moreover, during metamorphosis, proximal antennal and leg podomeres actually become enlarged with *hth*/*exd* RNAi (Fig. 4; Angelini et al., 2012a,

2012b), as a consequence of their transformation toward a more distal appendage identity. These results suggest that generic appendage patterning functions of these genes can evolve unique properties in different lineages.

Generic appendage patterning functions continue to evolve in insects, even in cases where the identity of appendages and their morphology appear conserved. For example, the developmental "ground state" morphology of flour beetles has clearly diverged from that of other insects. Furthermore, some appendage patterning mechanisms predate the origin of the arthropods. For example, *hth*/*exd*, *dac*, and *Dll* show "leg gap" like expression patterns in the appendages of Onychophora (Janssen et al., 2010; Panganiban et al., 1997), which diverged from the arthropods before the evolution of jointed appendages and the heteronymous appendage condition of arthropods (Campbell et al., 2011; Legg et al., 2012). For these reasons, a genetic loss-of-function phenotype in any insect is unlikely to reproduce the morphology of an arthropod ancestor.

The role of dac *in deuterocerebral appendage specification is evolutionarily labile*

The transcription factor coding gene *dac* is expressed in legs across Arthropoda (Angelini and Kaufman, 2005; Sewell et al., 2008; Sharma et al., 2012a; Barnett and Thomas, in press), but its expression and function in the deuterocerebral appendage of arthropods is highly variable. In *Drosophila*, leg patterning functions and expression levels of *dac* are repressed by *hth*/*exd* and *Dll* in the antenna and inducing leg-like expression of *dac* in the antenna results in a transformation of the intermediate antennal domain into leg (Dong et al., 2001). However the only function of *dac* in the *Drosophila* antenna is to specify the joint between the fifth antennal segment and the arista (Dong et al., 2002), while in the leg it is required for development of a

large intermediate domain (Mardon et al., 1994). Many other examples exist of a reduced role of *dac* in development of the deuterocerebral appendage, relative to legs, in arthropods. In the milkweed bug *O. fasciatus*, there is reduced expression of *dac* in the antennae compared to legs and *dac* RNAi shortens the legs but has no effect on antennal morphology (Angelini and Kaufman, 2004). There is also reduced expression of *dac* in the antennae relative to legs in the cricket *G. bimaculatus* (Inoue et al., 2002, 2004). In the crustacean *Porcellio scaber*, *dac* is expressed in legs but not antennae (Abzhanov and Kaufman, 2000). Finally, *dac* is downregulated in the chelicera of spiders and mites compared to legs (Abzhanov and Kaufman, 2000; Prpic et al., 2003; Prpic and Damen, 2004; Pechmann and Prpic, 2009; Barnett and Thomas, in press). These examples suggest that distinct deuterocerebral appendage identity in arthropods may have partly evolved through downregulation of *dac* by *hth*/*exd* and *Dll* in the appendage primordia of the deuterocerebral segment.

However, there are also examples where expression patterns and functions of *dac* do not differ greatly between antennae and legs. For example, in the millipede *Glomeris marginata*, expression of *dac* in the antennae is very similar to expression in the legs (Prpic and Tautz, 2003). In the harvestman *O. opilio*, the cheliceral *dac* expression domain is similar in size to the leg domain (Sharma et al., 2012a) and RNAi against *dac* results in deletion of the proximal cheliceral podomere (Sharma et al., 2013). This podomere is plesiomorphic for Chelicerata, but has been lost in spiders. Sharma et al. (2013) reasoned that the lack of a distinct *dac* expression domain in the spider chelicera reflects the loss of a proximal cheliceral podomere in the spider lineage, and that in the chelicerate ancestor, *dac* did have a distinct expression domain in the chelicera, specifying this podomere. Finally, during *T. castaneum* metamorphosis, *dac* is expressed in a large intermediate domain in both the antennae and legs (Suzuki et al., 2009) and

dac RNAi results in drastic reduction of the intermediate domain in both appendage types (Angelini et al., 2009; Angelini et al., 2012b; Suzuki et al., 2009; Yang et al., 2009).

More functional and expression data for *dac* are required from unexplored insect and arthropod lineages before phylogenetic reconstructions of the ancestral roles of *dac* in deuterocerebral appendage patterning and identity specification can be determined with confidence. However available studies highlight the evolutionary lability of *dac*'s role in these processes. Here we have reported differences in the role of *dac* in antennal patterning even between closely related species of beetles. In *T. confusum*, *dac* RNAi causes a transformation of the proximal funicle article towards a more distal identity, while in *T. castaneum dac* RNAi results in transformations of distal funicle segments toward club identity. These data suggest that *dac* has evolved novel roles in specifying the identity of flagellar articles in the *T. castaneum* and *T. confusum* lineages. The role of *dac* in the *T. castaneum* antenna may underlie the evolution of the three-segmented club in this species.

hth *and* exd *repress elytron identity in the eye primordia of* Tribolium

The eyes of flour beetles were reduced in size in response to either *exd* or *hth* RNAi. Interference with *hth* function causes reduced eyes in both *Drosophila* (Bessa et al., 2002; Lopes and Casares, 2010) and the horned beetle *Onthophagus taurus* (Moczek and Rose, 2009), suggesting that promoting proliferation of primordial eye cells during metamorphosis is an ancestral function of *hth*/*exd*. RNA interference in *Tribolium* also resulted in transformations of the eye (Fig. 5), which were not found for experiments in other species. Based on the winglet-like shape of the transformed eyes, the shape of the cells comprising these structures, and the morphology of bristle bases, we interpret this as a homeotic transformation of eye to elytron.

In *Drosophila*, *hth* expression is down-regulated in wing discs relative to the body wall, and ectopic expression of *hth* in the wing disc results in reduction of the wing blade (Azpiazu and Morata, 2000**;** Casares and Mann, 2000), suggesting that *hth* represses wing development. *homothorax* expression in *T. castaneum* is also down-regulated in both mesothoracic (elytra) and metathoracic (membranous) wing primordia relative to the body wall (Tomoyasu et al., 2009), consistent with an ancestral role for *hth* in blocking wing development in Holometabola. In all holometabolous insects, including flour beetles, the development of the compound eyes and wings is suppressed during embryogenesis and commences during metamorphosis. Therefore, it is plausible that there are similarities between the regulatory states of the primordia producing these structures.

Here we present a model in which compound eye identity is determined in part by *hth* and *exd*. In arthropods, including *T. castaneum*, *Hox* genes are not expressed in the protocerebral segment where eyes develop (Hughes and Kaufman, 2002). Therefore, Hox genes do not specify eye identity. In *T. castaneum* wing primordia, elytron identity is the default state, and emerges without input from *Hox* genes, while membranous wing identity requires expression of the Hox gene *Ultrabithorax* (*Ubx*; Tomoyasu et al., 2005). Our model posits that *hth* and *exd* block elytron identity in the eye primordium of *Tribolium* beetles, promoting differentiation of the eyes. Therefore, with RNAi targeting *hth* or *exd*, the eye primordium acquires a "*Hox*-less*"* regulatory state similar to the T2 elytron primordium, and elytron development is activated. Future studies in *T. castaneum* could test whether ectopic expression of *hth*/*exd* in the elytron primordium is sufficient to transform the elytron into eyes. In hemimetabolous insects the development of compound eyes and wings is temporally decoupled, and this is the ancestral state for winged insects. Therefore, *hth*/*exd* may not have blocked wing identity during eye

development ancestrally in insects. The antiquity of the mechanism we present here remains to be determined.

Conclusions

We present an evolutionary model for antennal identity specification that includes distinct embryonic and metamorphic antennal identity specification mechanisms (Fig. 7). In light of this study, the model of antennal identity specification that was first established from work in *Drosophila* (Casares and Mann, 2001; Dong et al., 2000; Dong et al., 2001; Dong et al., 2002; Duncan et al., 1998) describes a mechanism active during embryogenesis in *T. castaneum* and other insects, while the processes active during metamorphosis in *T. castaneum* (and other holometabolous insects with juvenile antennae) corresponds to a mechanism active in the third instar antennal imaginal disc of *Drosophila*. It is possible that metamorphic antennal identity specification across Holometabola is derived from a late embryonic- or nymphal-stage mechanism present in hemimetabolous insects. Despite the derived form of *Drosophila* antennal development, the original mechanism proposed for *Drosophila* antennal identity specification is likely the ancestral mechanism for insect embryogenesis, and perhaps for all arthropods. Future studies will allow testing these possibilities. However, since RNAi against *exd*/*hth* and *Dll* causes reduction of the head (Fig. 2C, D) (Angelini and Kaufman, 2004; Mito et al., 2008; Ronco et al., 2008) and distal appendages (Fig. 3D–I) (Angelini and Kaufman, 2004; Angelini et al., 2009, 2012a, 2012b; Kato et al., 2011; Khila and Grbic, 2007; Moczek and Rose, 2009; Niimi et al., 2005; Ohde et al., 2009; Pechmann et al., 2011; Shoppmeier and Damen, 2001; Sharma et al., 2013; Suzuki et al., 2009; Yoshiyama et al., 2013), respectively, these genes may be poor targets for comparative studies. We propose focusing on the expression pattern,

function, and *cis*-regulatory elements of *ss* in order to determine the degree of conservation of deuterocerebral appendage identity specification mechanisms in arthropods.

References

Abu-Shaar, M., Mann, R.S., 1998. Generation of multiple antagonistic domains along the proximodistal axis during *Drosophila* leg development. *Development* 125, 3821–3830.

Abu-Shaar, M., Ryoo, H.D., Mann, R.S., 1999. Control of the nuclear localization of Extradenticle by competing nuclear import and export signals. *Genes Dev.* 13, 935–945.

Abzhanov, A., Kaufman, T.C., 2000. Homologs of *Drosophila* appendage genes in the patterning of arthropod limbs. *Dev. Biol.* 227, 673–689.

Angelini, D.R., Jockusch, E.L., 2008. Relationships among pest flour beetles of the genus *Tribolium* (Tenebrionidae) inferred from multiple molecular markers. *Mol. Phylogenet. Evol.* 46, 127–141.

Angelini, D.R., Kaufman, T.C., 2005. Insect appendages and comparative ontogenetics. *Dev. Biol.* 286, 57–77.

Angelini, D.R., Kaufman, T.C., 2004. Functional analyses in the hemipteran *Oncopeltus fasciatus* reveal conserved and derived aspects of appendage patterning in insects. *Dev. Biol.* 271, 306–321.

Angelini, D.R., Kikuchi, M., Jockusch, E.L., 2009. Genetic patterning in the adult capitate antenna of the beetle *Tribolium castaneum. Dev. Biol.* 327, 240–251.

Angelini, D.R., Liu, P.Z., Hughes, C.L., Kaufman, T.C., 2005. Hox gene function and interaction in the milkweed bug *Oncopeltus fasciatus* (Hemiptera). *Dev. Biol.* 287, 440–455.

Angelini, D.R., Smith, F.W., Aspiras, A.C., Kikuchi, M., Jockusch, E.L., 2012a. Patterning of the adult mandibulate mouthparts in the red flour beetle, *Tribolium castaneum. Genetics* 190, 639–654.

Angelini, D.R., Smith, F.W., Jockusch, E.L., 2012b. Extent with modification: Leg patterning in the beetle *Tribolium castaneum* and the evolution of serial homologs. *G3 (Bethesda)* 2, 235–248.

Aspiras, A.C., Smith, F.W., Angelini, D.R., 2011. Sex-specific gene interactions in the patterning of insect genitalia. *Dev. Biol.* 360, 369–380.

Azpiazu, N. and Morata, G., 2000. Function and regulation of homothorax in the wing imaginal disc of *Drosophila*. *Development.* 127, 2685–2693.

Barnett, A.A., Thomas, R.H., 2013. The expression of limb gap genes in the mite *Archegozetes longisetosus* reveals differential patterning mechanisms in chelicerates. *Evol. Dev.* 15, 280–292.

Beermann, A., Jay, D.G., Beeman, R.W., Hulskamp, M., Tautz, D., Jurgens, G., 2001. The *Short antennae* gene of *Tribolium* is required for limb development and encodes the orthologue of the *Drosophila* Distal-less protein. *Development* 128, 287–297.

Bessa, J., Gebelein, B., Pichaud, F., Casares, F., Mann, R.S., 2002. Combinatorial control of *Drosophila* eye development by Eyeless, Homothorax, and Teashirt. *Genes Dev.* 16, 2415–2427.

Boxshall, G.A., 2004. The evolution of arthropod limbs. *Biol. Rev. Camb. Philos. Soc.* 79, 253–300.

Brown, S.J., Shippy, T.D., Beeman, R.W., Denell, R.E., 2002. *Tribolium Hox* genes repress antennal development in the gnathos and trunk. *Mol. Phylogenet. Evol.* 24, 384–387.

Campbell, L.I., Rota-Stabelli, O., Edgecombe, G.D., Marchioro, T., Longhorn, S.J., Telford, M. J., Philippe, H., Rebecchi, L., Peterson, K.J., Pisani, D., 2011. MicroRNAs and phylogenomics resolve the relationships of Tardigrada and suggest that velvet worms are the sister group of Arthropoda. *Proc. Natl. Acad. Sci. U. S. A.* 108, 15920–15924.

Casares, F., Mann, R.S., 2001. The ground state of the ventral appendage in *Drosophila. Science* 293, 1477–1480.

Casares, F. and Mann, R.S., 2000. A dual role for homothorax in inhibiting wing blade development and specifying proximal wing identities in *Drosophila*. *Development.* 127, 1499-1508.

Casares, F., Mann, R.S., 1998. Control of antennal versus leg development in *Drosophila. Nature* 392, 723–726.

Dong, P.D., Chu, J., Panganiban, G., 2001. Proximodistal domain specification and interactions in developing *Drosophila* appendages. *Development* 128, 2365–2372.

Dong, P.D., Chu, J., Panganiban, G., 2000. Coexpression of the homeobox genes *Distal-less* and *homothorax* determines *Drosophila* antennal identity. *Development* 127, 209–216.

Dong, P. D., Dicks, J. S., Panganiban, G., 2002. *Distal-less* and *homothorax* regulate multiple targets to pattern the *Drosophila* antenna. *Development* 129, 1967–1974.

Duncan, D.M., Burgess, E.A., Duncan, I., 1998. Control of distal antennal identity and tarsal development in *Drosophila* by *spineless-aristapedia*, a homolog of the mammalian dioxin receptor. *Genes Dev.* 12, 1290–1303.

Duncan, D.M., Kiefel, P., Duncan, I., 2010. Control of the *spineless* antennal enhancer: Direct repression of antennal target genes by Antennapedia. *Dev. Biol.* 347, 82–91.

Emmons, R.B., Duncan, D., Duncan, I., 2007. Regulation of the *Drosophila* distal antennal determinant *spineless*. *Dev. Biol.* 302, 412–426.

Gonzalez-Crespo, S., Morata, G., 1995. Control of *Drosophila* adult pattern by *extradenticle. Development* 121, 2117–2125.

Grimaldi, D., Engel, M.S., 2005. Evolution of the Insects. Cambridge University Press, Cambridge.

Herke, S.W., Serio, N.V., Rogers, B.T., 2005. Functional analyses of *tiptop* and *Antennapedia* in the embryonic development of *Oncopeltus fasciatus* suggests an evolutionary pathway from ground state to insect legs. *Development* 132, 27–34.

Hughes, C.L., Kaufman, T.C., 2002. Hox genes and the evolution of the arthropod body plan. *Evol. Dev.* 4, 459–499.

Hughes, C.L., Kaufman, T.C., 2000. RNAi analysis of *Deformed*, *proboscipedia* and *sex combs reduced* in the milkweed bug *Oncopeltus fasciatus*: Novel roles for Hox genes in the Hemipteran head. *Development* 127, 3683–3694.

Inoue, Y., Mito, T., Miyawaki, K., Matsushima, K., Shinmyo, Y., Heanue, T.A., Mardon, G., Ohuchi, H., Noji, S., 2002. Correlation of expression patterns of *homothorax*, *dachshund*, and *Distal-less* with the proximodistal segmentation of the cricket leg bud. *Mech. Dev.* 113, 141-148.

Inoue, Y., Miyawaki, K., Terasawa, T., Matsushima, K., Shinmyo, Y., Niwa, N., Mito, T., Ohuchi, H., Noji, S., 2004. Expression patterns of *dachshund* during head development of *Gryllus bimaculatus* (cricket). *Gene Expression Patterns.* 4, 725-731.

Jager, M., Murienne, J., Clabaut, C., Deutsch, J., Le Guyader, H., Manuel, M., 2006. Homology of arthropod anterior appendages revealed by Hox gene expression in a sea spider. *Nature* 441, 506–508.

Janssen, R., Damen, W.G., 2006. The ten *Hox* genes of the millipede *Glomeris marginata. Dev. Genes Evol.* 216, 451–465.

Janssen, R., Eriksson, B.J., Budd, G.E., Akam, M., Prpic, N.M., 2010. Gene expression patterns in an onychophoran reveal that regionalization predates limb segmentation in pan-arthropods. *Evol. Dev.* 12, 363–372.

Jockusch, E.L., Williams, T.A., Nagy, L.M., 2004. The evolution of patterning of serially homologous appendages in insects. *Dev. Genes Evol.* 214, 324–338.

Joulia, L., Deutsch, J., Bourbon, H.M., Cribbs, D.L., 2006. The specification of a highly derived arthropod appendage, the *Drosophila* labial palps, requires the joint action of selectors and signaling pathways. *Dev. Genes Evol.* 216, 431–442.

Kato, Y., Shiga, Y., Kobayashi, K., Tokishita, S., Yamagata, H., Iguchi, T., Watanabe, H., 2011. Development of an RNA interference method in the cladoceran crustacean *Daphnia magna*. *Dev. Genes Evol.* 220, 337–345.

Khila, A., Grbic, M., 2007. Gene silencing in the spider mite *Tetranychus urticae*: dsRNA and siRNA parental silencing of the *Distal-less* gene. *Dev. Genes Evol.* 217, 241–251.

Kobayashi, M., Fujioka, M., Tolkunova, E.N., Deka, D., Abu-Shaar, M., Mann, R.S., Jaynes, J.B., 2003. Engrailed cooperates with *extradenticle* and *homothorax* to repress target genes in *Drosophila*. *Development* 130, 741–751.

Kurant, E., Pai, C.Y., Sharf, R., Halachmi, N., Sun, Y.H., Salzberg, A., 1998. *dorsotonals/homothorax*, the *Drosophila* homologue of *meis1*, interacts with *extradenticle* in patterning of the embryonic PNS. *Development* 125, 1037–1048.

Legg, D.A., Sutton, M.D., Edgecombe, G.D., Caron, J.B., 2012. Cambrian bivalved arthropod reveals origin of arthrodization. *Proc. Biol. Sci.* 279, 4699–4704.

Lopes, C.S., Casares, F., 2010. *hth* maintains the pool of eye progenitors and its downregulation by Dpp and Hh couples retinal fate acquisition with cell cycle exit. *Dev. Biol.* 339, 78–88.

Maddison, W.P., Maddison, D.R., 2011. Mesquite: a modular system for evolutionary analysis. Version 2.75 http://mesquiteproject.org

Manuel, M., Jager, M., Murienne, J., Clabaut, C., Le Guyader, H., 2006. Hox genes in sea spiders (pycnogonida) and the homology of arthropod head segments. *Dev. Genes Evol.* 216, 481–491.

Mardon, G., Solomon, N.M., Rubin, G.M., 1994. *dachshund* encodes a nuclear protein required for normal eye and leg development in *Drosophila. Development* 120, 3473–3486.

Mito, T., Ronco, M., Uda, T., Nakamura, T., Ohuchi, H., Noji, S., 2008. Divergent and conserved roles of extradenticle in body segmentation and appendage formation, respectively, in the cricket *Gryllus bimaculatus. Dev. Biol*. 313, 67–79.

Mittmann, B., Scholtz, G., 2003. Development of the nervous system in the "head" of *Limulus polyphemus* (Chelicerata: Xiphosura): morphological evidence for a correspondence between the segments of the chelicerae and of the (first) antennae of Mandibulata. *Dev. Genes Evol.* 213, 9–17.

Moczek, A.P., Rose, D.J., 2009. Differential recruitment of limb patterning genes during development and diversification of beetle horns. *Proc. Natl. Acad. Sci. U. S. A.* 106, 8992–8997.

Niimi, T., Kuwayama, H., Yaginuma, T., 2005. Larval RNAi applied to the analysis of postembryonic development in the ladybird beetle, *Harmonia axyridis. J. Insect Biotechnol. Sericology* 74, 95–102.

Ohde, T., Masumoto, M., Yaginuma, T., Niimi, T., 2009. Embryonic RNAi analysis in the firebrat, *Thermobia domestica* [Zygentoma: Lepismatidae]: *Distal-less* is required to form caudal filament. *J. Insect Biotechnol. Sericology* 78, 99–105.

Pai, C.Y., Kuo, T.S., Jaw, T.J., Kurant, E., Chen, C.T., Bessarab, D.A., Salzberg, A., Sun, Y.H., 1998. The Homothorax homeoprotein activates the nuclear localization of another homeoprotein, Extradenticle, and suppresses eye development in *Drosophila. Genes Dev*. 12, 435–446.

Panganiban, G., Irvine, S.M., Lowe, C., Roehl, H., Corley, L.S., Sherbon, B., Grenier, J.K., Fallon, J.F., Kimble, J., Walker, M., Wray, G.A., Swalla, B.J., Martindale, M.Q., Carroll, S.B., 1997. The origin and evolution of animal appendages. *Proc. Natl. Acad. Sci. U.S.A.* 94, 5162–5166.

Pechmann, M., Khadjeh, S., Turetzek, N., McGregor, A.P., Damen, W.G., Prpic, N.M., 2011. Novel function of *Distal-less* as a gap gene during spider segmentation. *PLoS Genet.* 7: e1002342.

Pechmann, M., Prpic, N.M., 2009. Appendage patterning in the south american bird spider *Acanthoscurria geniculata* (Araneae: Mygalomorphae). *Dev. Genes Evol.* 219, 189–198.

Peifer, M., Wieschaus, E., 1990. Mutations in the *Drosophila* gene *extradenticle* affect the way specific homeo domain proteins regulate segmental identity. *Genes Dev.* 4, 1209–1223.

Posnien, N., Schinko, J., Grossmann, D., Shippy, T.D., Konopova, B., Bucher, G., 2009. RNAi in the red flour beetle (*Tribolium*). *Cold Spring Harb. Protoc.* 2009, pdb.prot5256.

Prpic, N.M., Damen, W.G.M., 2009. *Notch*-mediated segmentation of the appendages is a molecular phylotypic trait of the arthropods. *Dev. Biol.* 326, 262–271.

Prpic, M., Damen, W.G.M., 2008. Arthropod appendages: a prime example for the evolution of morphological diversity and innovation, in: Fusco, G., Minelli, A. (Eds.), Evolving Pathways: Key Themes in Evolutionary Developmental Biology. Cambridge University Press, Cambridge, pp. 381–398.

Prpic, N.M., Damen, W.G.M., 2004. Expression patterns of leg genes in the mouthparts of the spider *Cupiennius salei* (Chelicerata: Arachnida). *Dev. Genes Evol.* 214, 296–302.

Prpic, N.M., Janssen, R., Wigand, B., Klingler, M., Damen, W.G., 2003. Gene expression in spider appendages reveals reversal of *exd*/*hth* spatial specificity, altered leg gap gene dynamics, and suggests divergent distal morphogen signaling. *Dev. Biol.* 264, 119–140.

Prpic, N.M., Tautz, D., 2003. The expression of the proximodistal axis patterning genes *Distal-less* and *dachshund* in the appendages of *Glomeris marginata* (Myriapoda: Diplopoda)

suggests a special role of these genes in patterning the head appendages. *Dev. Biol.* 260, 97–112.

Rauskolb, C., 2001. The establishment of segmentation in the *Drosophila* leg. *Development* 128, 4511–4521.

Rauskolb, C., Smith, K.M., Peifer, M., Wieschaus, E., 1995. *extradenticle* determines segmental identities throughout *Drosophila* development. *Development* 121, 3663–3673.

Rieckhof, G.E., Casares, F., Ryoo, H.D., Abu-Shaar, M., Mann, R.S., 1997. Nuclear translocation of Extradenticle requires *homothorax*, which encodes an Extradenticle-related homeodomain protein. *Cell* 91, 171–183.

Ronco, M., Uda, T., Mito, T., Minelli, A., Noji, S., Klingler, M., 2008. Antenna and all gnathal appendages are similarly transformed by *homothorax* knock-down in the cricket *Gryllus bimaculatus. Dev. Biol.* 313, 80–92.

Schoppmeier, M., Damen, W.G., 2001. Double-stranded RNA interference in the spider *Cupiennius salei*: the role of *Distal-less* is evolutionarily conserved in arthropod appendage formation. *Dev. Genes Evol.* 211, 76–82.

Sewell, W., Williams, T., Cooley, J., Terry, M., Ho, R., Nagy, L., 2008. Evidence for a novel role for dachshund in patterning the proximal arthropod leg. *Dev. Genes Evol.* 218, 293-305.

Sharma, P.P., Schwager, E.E., Giribet, G., Jockusch, E.L., Extavour, C.G., 2013. *Distal-less* and *Dachshund* pattern both plesiomorphic and apomorphic structures in chelicerates: RNA interference in the harvestman *Phalangium opilio* (opiliones). *Evol. Dev.* 15, 228–242.

Sharma, P.P., Schwager, E.E., Extavour, C.G., Giribet, G., 2012a. Evolution of the chelicera: a *dachshund* domain is retained in the deutocerebral appendage of Opiliones (Arthropoda, Chelicerata). *Evol. Dev.* 14, 522–533.

Sharma, P.P., Schwager, E.E., Extavour, C.G., Giribet, G., 2012b. Hox gene expression in the harvestman *Phalangium opilio* reveals divergent patterning of the chelicerate opisthosoma. *Evol. Dev.* 14, 450–463.

Shippy, T.D., Yeager, S.J., Denell, R.E., 2009. The *Tribolium spineless* ortholog specifies both larval and adult antennal identity. *Dev. Genes Evol.* 219, 45–51.

Snodgrass, R.E., 1935. Principles of Insect Morphology. Cornell University Press, Ithaca.

Sokoloff, A., 1972. The Biology of Tribolium, Volume 1. Clarendon Press, Oxford.

Stanley, M.S.M., 1965. Teratology in *Tribolium confusum*. *Tribolium Inf. Bull.* 8, 158-159.

Struhl, G., 1982a. Genes controlling segmental specification in the *Drosophila* thorax. *Proc. Natl. Acad. Sci. U. S. A.* 79, 7380–7384.

Struhl, G., 1982b. *spineless-aristapedia*: a homeotic gene that does not control the development of specific compartments in *Drosophila. Genetics* 102, 737–749.

Sunkel, C.E, Whittle, J.R.S., 1987. *Brista:* a gene involved in the specification and differentiation of distal cephalic and thoracic structures in *Drosophila melanogaster. Dev. Genes Evol.* 196, 124–132.

Suzuki, Y., Squires, D.C., Riddiford, L.M., 2009. Larval leg integrity is maintained by *Distal-less* and is required for proper timing of metamorphosis in the flour beetle, *Tribolium castaneum. Dev. Biol.* 326, 60–67.

Toegel, J.P., Wimmer, E.A., Prpic, N.M., 2009. Loss of *spineless* function transforms the *Tribolium* antenna into a thoracic leg with pretarsal, tibiotarsal, and femoral identity. *Dev. Genes Evol.* 219, 53–58.

Tomoyasu, Y., Arakane, Y., Kramer, K.J., Denell, R.E., 2009. Repeated co-options of exoskeleton formation during wing-to-elytron evolution in beetles. *Curr. Biol.* 19, 2057–2065.

Tomoyasu, Y., Denell, R.E., 2004. Larval RNAi in *Tribolium* (Coleoptera) for analyzing adult development. *Dev. Genes Evol.* 214, 575–578.

Tomoyasu, Y., Wheeler, S.R., Denell, R.E., 2005. *Ultrabithorax* is required for membranous wing identity in the beetle *Tribolium castaneum*. *Nature.* 433, 643–647.

Van der Meer, J., 1977. Optical clean and permanent whole mount preparation for phase-contrast microscopy of cuticular structures of insect larvae. *Dros. Inf. Serv.* 52, 160.

Yang, J., Ortega-Hernandez, J., Butterfield, N.J., Zhang, X.G., 2013. Specialized appendages in fuxianhuiids and the head organization of early euarthropods. *Nature* 494, 468–471.

Yang, X., ZarinKamar, N., Bao, R., Friedrich, M., 2009. Probing the *Drosophila* retinal determination gene network in *Tribolium* (I): The early retinal genes *dachshund*, *eyes absent* and *sine oculis*. *Dev. Biol.* 333, 202–214.

Yoshiyama, N., Tojo, K., Hatakeyama, M., 2013. A survey of the effectiveness of non-cell autonomous RNAi throughout development in the sawfly, *Athalia rosae* (Hymenoptera). *J. Insect Physiol.* 59, 400–407.

Tables

Table 1. Candidate genes investigated in this study. Identities of genes cloned for this study were determined by aligning coding sequences of the cloned candidate genes against *T. castaneum* sequences (*homothorax*, NM_001039400; *extradenticle*, NM_001039412; *Distal-less*, NM_001039439; *dachshund*, XM_964678), using the bl2seq algorithm at NCBI. Gaps and insertions were not considered when determining amino acid identity. Abbreviations: aa, amino acid; bp, base pairs; lg, linkage group; nt, nucleotide.

Species	Gene name	Symbol	Protein class	LG	GenBank	Clone source	Sequence length (bp)	Identity	
								nt	aa
T. castaneum	*homothorax*	*hth*	homeobox TXF	7	NM_001039400	this study	663	99%	98%
	extradenticle	*exd*	homeobox TXF	10	NM_001039412	this study	545	99%	99%
	Distal-less	*Dll*	homeobox TXF	7	NM_001039439	Jockusch et al. 2004	-	-	-
	spineless	*ss*	bHLH/PAS TXF	10	XM_962783	Angelini et al. 2009	-	-	-
	dachshund	*dac*	Ski/Sno-related TXF	4	XM_964678	Prpic et al. 2001	-	-	-
T. confusum	*homothorax*	-	-	-		this study	663	96%	100%
	extradenticle	-	-	-		this study	308	82%	98%
	Distal-less	-	-	-		this study	476	92%	98%
	dachshund[1]	-	-	-		this study	411	90%	98%
	dachshund[2]	-	-	-		this study	374	85%	98%
T. brevicornis	*extradenticle*	-	-	-		this study	475	81%	100%
	Distal-less	-	-	-		this study	345	91%	96%
	dachshund	-	-	-		this study	358	91%	98%
L. oryzae	*homothorax*	-	-	-		this study	310	93%	99%
	extradenticle	-	-	-		this study	475	75%	99%
	dachshund	-	-	-		this study	597	80%	98%

Table 2. Results of larval RNAi experiments. Phenotypic penetrance was calculated by dividing the number of adult beetles showing abnormal phenotypes for an RNAi treatment by the number scored for that treatment. In cases where the sample size is different than the number scored, we provide the sample size in parentheses. The other appendages scored are the maxillae, labium, and legs. Antennal homeosis shows the frequency of transformations of the antenna to leg. Eye homeosis shows the frequency of transformations of the eye. We recovered

appendages with minor fusions with *GFP* RNAi controls at very low frequency. Phenotypic abnormalities of this degree are distinct from RNAi phenotypes and are found at low frequencies in unmanipulated beetle cultures. Abbreviations: aa, amino acid; nt, nucleotide.

					Phenotypic penetrance			
Species	dsRNA sequence	dsRNA size (bp)	Concentration (μg/μl)	Number scored	Antennae	Antennal homeosis	Other appendages	Eye homeosis
T. castaneum	*GFP*	600	1.00	65	3%	0%	8%	0%
	hth	174	1.00	177	97%	28% (173)	94%	6% (174)
	exd	236	1.00	53	94% (50)	57% (37)	92%	5% (37)
	Dll	462	1.00	91	99%	4%	99%	0%
	"	"	0.10	12	100%	0%	100%	0%
	"	"	0.01	18	100%	6%	100%	0%
	ss	335	1.00	97	90%	77%	45%	0%
	dac	359	1.00	52	71%	0%	60%	0%
T. confusum	*GFP*	600	1.00	26	0%	0%	4%	0%
	hth	174	1.00	116	79%	63% (108)	87% (114)	32% (113)
	exd	249	0.75	29	90%	83%	93%	17%
	Dll	132	0.10	24	100%	0%	100%	0%
	dac1	394	1.00	186	94%	0%	96%	0%
	dac2	374	0.60	26	92%	0%	92%	0%
T. brevicornis	*GFP*	600	1.00	41	2%	0%	2%	0%
	hth	174	1.00	18	86%	50%	81% (16)	19% (16)
	"	"	0.10	17	83%	6%	59%	7% (14)
	exd	204	0.10	12	67%	67%	75%	58%
	Dll	132	1.00	26	100%	4%	96%	0%
	dac	180	1.00	20	95%	0%	95%	0%
	"	"	0.10	10	100%	0%	100%	0%
L. oryzae	*GFP*	600	1.00	34	0%	0%	6%	0%
	hth	145	1.00	14	71%	29%	50%	0%
	"	"	0.10	96	84%	25%	74%	0%
	exd	204	0.10	11	75%	80% (10)	73%	0% (10)
	Dll	132	1.00	29	100%	0%	100%	0%
	dac	520	1.00	48	98%	0%	98%	0%

Table 3. Results of *T. castaneum* maternal RNAi. Penetrance was calculated as in Table 2. Hyphens represent instances where all specimens developed to the larval stage, so no embryos were scored, or only embryos were scored because no specimens made it to the larval stage.

dsRNA	Concentration	Stage	Number	Number	Number Scored		Penetrance	
sequence	(µg/µl)	injected	injected	survived	eggs	larvae	eggs	larvae
GFP	1.00	pupa	20	18	0	258	-	0%
hth	1.00	adult	5	4	16	0	100%	-
	1.00	pupa	17	1	2	25	100%	0%
	0.10	pupa	10	10	0	205	-	0.49%
	0.01	pupa	27	21	0	116	-	0%
exd	1.00	adult	5	2	0	0	-	-
	1.00	pupa	37	13	13	94	100%	0%
	0.10	pupa	10	9	0	130	-	0.77%
	0.01	pupa	25	16	7	140	100%	0%
Dll	1.00	adult	5	2	10	0	100%	-
	1.00	pupa	19	19	34	0	100%	-
	0.1	pupa	25	15	0	86	-	1.16%
	0.01	pupa	25	12	0	208	-	0%

Supplementary Table 1. Primers used to clone genes and to produce dsRNA. Abbreviations: *brv*, *T. brevicornis*; *cnf*, *T. confusum*; *cst*, *T. castaneum*; *ory*; *L. oryzae*. Primer sequences used to produce dsRNA also include a 5' T7 recognition site (TAATACGACTCACTATAGGG).

sequence	gene	species	purpose
			cloning
	dachshund		
ATHCARCCVGGNGTNAACAGATGCAA GGCATNCCYTGRTTYTTDATNACNCT		*cnf* (A)	
CCGATCACAGTCCCGTGCTNAA CCTTTCTCGTAGTTGATCTGNCGYT		*cnf* (B)	
ATHCARCCVGGNGTNAACAGATGCAA TGTTTRCADATRTCTTCRTANGCNGC		*brv*	
GGNCARAAGGTNGCCGCNTTYATHAT TGTTTRCADATRTCTTCRTANGCNGC		*ory*	
	Distal-less		
CGTATTATCGCGGTAATTGTGC CAGGTGTCCCATTATTGTTATTGC		*cst*	
GGCAAGAAGATGAGGAAACCGAGR GTACCACGAGTATTGTGGGAGGTNG		*cnf*, *brv*	
	extradenticle		
GTTCTCCGTGCTGTGCGAAATCAA ATCCCGCATTTCCTAGCCAACTCT		*cst*	
CAAATCCGCCAAATCTACCAYCARG CCCGCATTTCCTAGCNARYTCYTC		*cnf*	
AGATCCTCCAGCAGATCATGAACATH AGTCGACTGTTTCAGCTGCATCTG		*brv*, *ory*	
	homothorax		
CAGTGTACACGACAGTGCAGT TCAGACAACTGATATACCGATG		*cst*, *cnf*, *ory*	
	spineless		
AGCCTGAAGCCAACGCCCAAAGA CCCACATACTCCCGCTCCTCCATT		*cst*	
			dsRNA
	dachshund		
ATGCAAAGACTTCGATACAC CTTGTGAGATTGTGGGGCAT		*cst*	
AACAGATGCAAACTACTCTC CTATGGCTTCCATCGTAGGC		*cnf* (A)	
CCGATCACAGTCCCGTGCTAAA CCTTTCTCGTAGTTGATCTGGCGCT		*cnf* (B)	
CCAGGAGTCAACAGATGCAA ATCACCGTTGTCGAGGCGCT		*brv*	
ACATCTCGTAGGCGGTTAGC CGCTATGGCCTCCATCGT		*ory*	
	Distal-less		
ACGGGATACCATTTAGGATC GAGTGCTGCATGTACCCTGT		*cst*	
CTGGGTTTGCGTTAAACC ATGAGGAAACCGAGG		*cnf*, *brv*	
	extradenticle		
ATCGAGCGGATGGTGCAAGTCATA ATCCCGCATTTCCTAGCCAACTCT		*cst*	
TGCTGAGAGAACAGTCACGGACT CTTCCTCACTGGGGTAGGGGTT		*cnf*	
CTCCAGCAGATCATGAACAT MGCWATCAACATGTTATCCA		*brv*, *ory*	
	homothorax		
TATGACGACGGCATCCACC CATGACGTGGTTGGCGGTTG		*cst*, *cnf*	
CCAAACAGATCCGACAAGAA ATACCGATGGCAGAAATTAT		*ory*	
	spineless		
ACAAAGACAGTTAATGTGGA CGATAACATTTTTCCTCTCT		*cst*	

Figure 1. Wild-type morphologies of adult flour beetles. Species are identified at the top of the figure. (A–D) Ventral views of whole mount specimens of the flour beetle species studied. Scale bars equal 500 μm. (E–H) SEMs of wild-type adult antennae. Scale bars equal 100 μm. Arrowheads show basal constriction of first flagellum article of *T. confusum* and *T. castaneum*. (I–L) *GFP* RNAi specimens illustrate wild-type antennal morphology. The adult antenna consists of a scape, pedicel, and flagellum. Flagellum articles are numbered. Purple and orange lines denote funicle and club articles, respectively. (M–P) *GFP* RNAi specimens illustrate wild-type leg morphology. Black arrows point to the unique hinge joint between the femur and the tibia. Proximal is to the left in all appendage panels. (Q) A phylogenetic tree showing hypothesized relationships among flour beetles studied (based on Angelini and Jockusch 2008). The red hash mark denotes the branch where the tripartite club of *T. castaneum* evolved. Abbreviations: ant, antenna; c, coxa; fe, femur; fl, flagellum; k, knob; p, pedicel; scape, s; T, thoracic segment; ta, tarsus; tc, tarsal claw; ti, tibia; tr, trochanter; sp, tibial spur.

Figure 1.

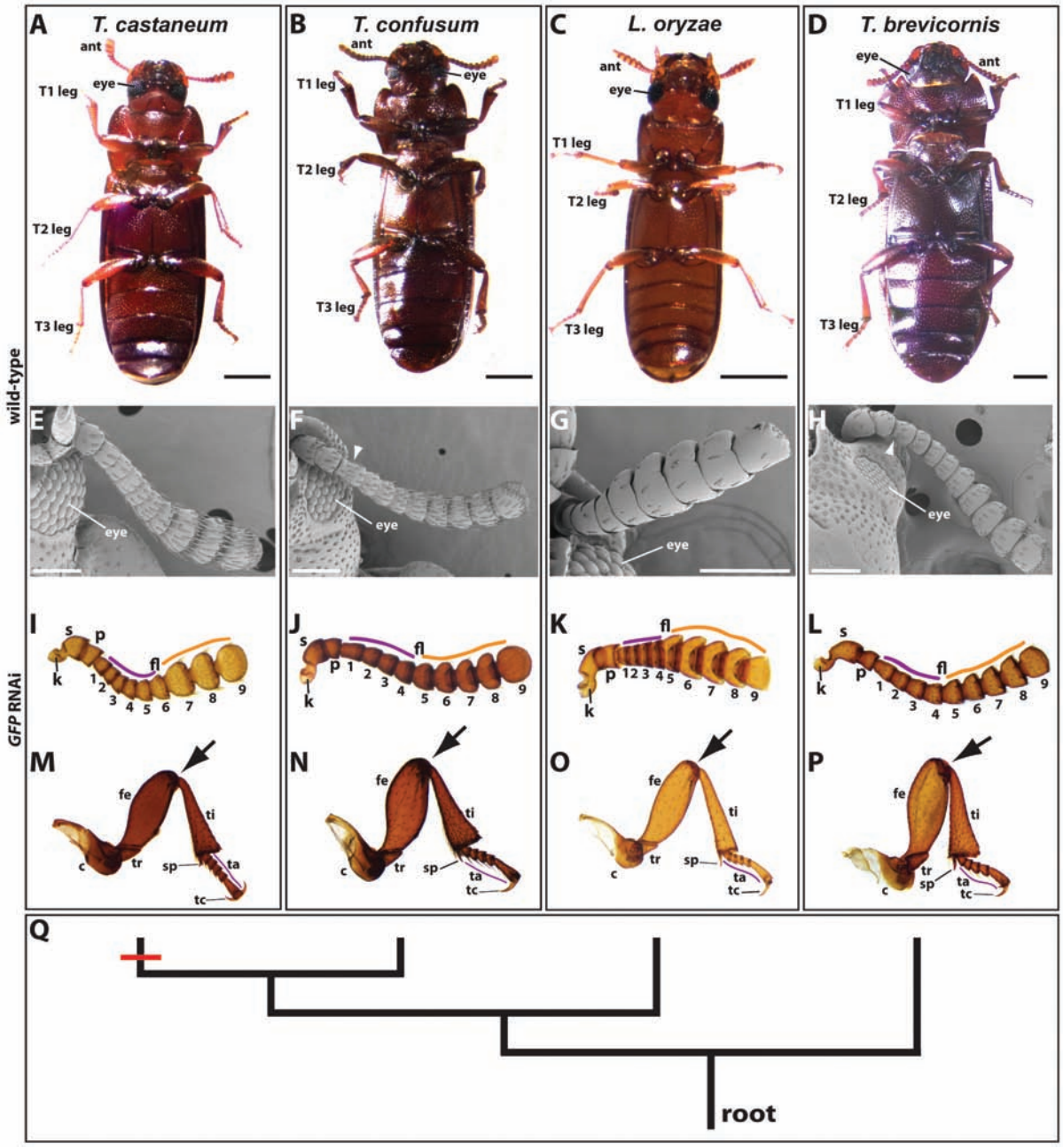
A T. castaneum
B T. confusum
C L. oryzae
D T. brevicornis
ant
eye
T1 leg
T2 leg
T3 leg
wild-type
GFP RNAi
E
F
G
H
I
J
K
L
M
N
O
P
Q
root
s
p
fl
k
fe
ti
c
tr
sp
ta
tc

Figure 2. Embryonic phenotypes resulting from *T. castaneum* maternal RNAi experiments. Appendages affected by RNAi are labeled red. Scale bars equal 100 μm. (A) Scanning electron micrograph of a wild-type larval antenna. (B) Wild-type embryo resulting from *GFP* RNAi. (*B*) A DIC micrograph magnification of the area within the black box in panel A. Flagellum articles are numbered in A and B. (C) Severely affected *hth* RNAi embryo. The head is greatly reduced and lacks appendages. (D) Moderately affected *hth* RNAi embryos exhibited three pairs of legs, antennae, and a pair of gnathal appendages (app2) with unknown morphological and segmental identity. The red arrowhead points to the distal end of the left antennae. (E) Light micrograph of a *Dll* RNAi embryo. All appendages except the mandible are truncated. The antenna lacks a flagellum and seta. The legs appear truncated. Small nodules are found distally (*), which may be remnants of distal leg tissue. (*E*) Same specimen as panel E, but at a deeper focal plane. The mandible appears normal, while the maxillae and labium lack palpi. Abbreviations: app, appendage pair; lab, labium; man, mandible; max, maxilla; ps, proximal antennal segment; set, seta; tt, tibiotarsus. All other abbreviations are as in Figure 1.

Figure 2.

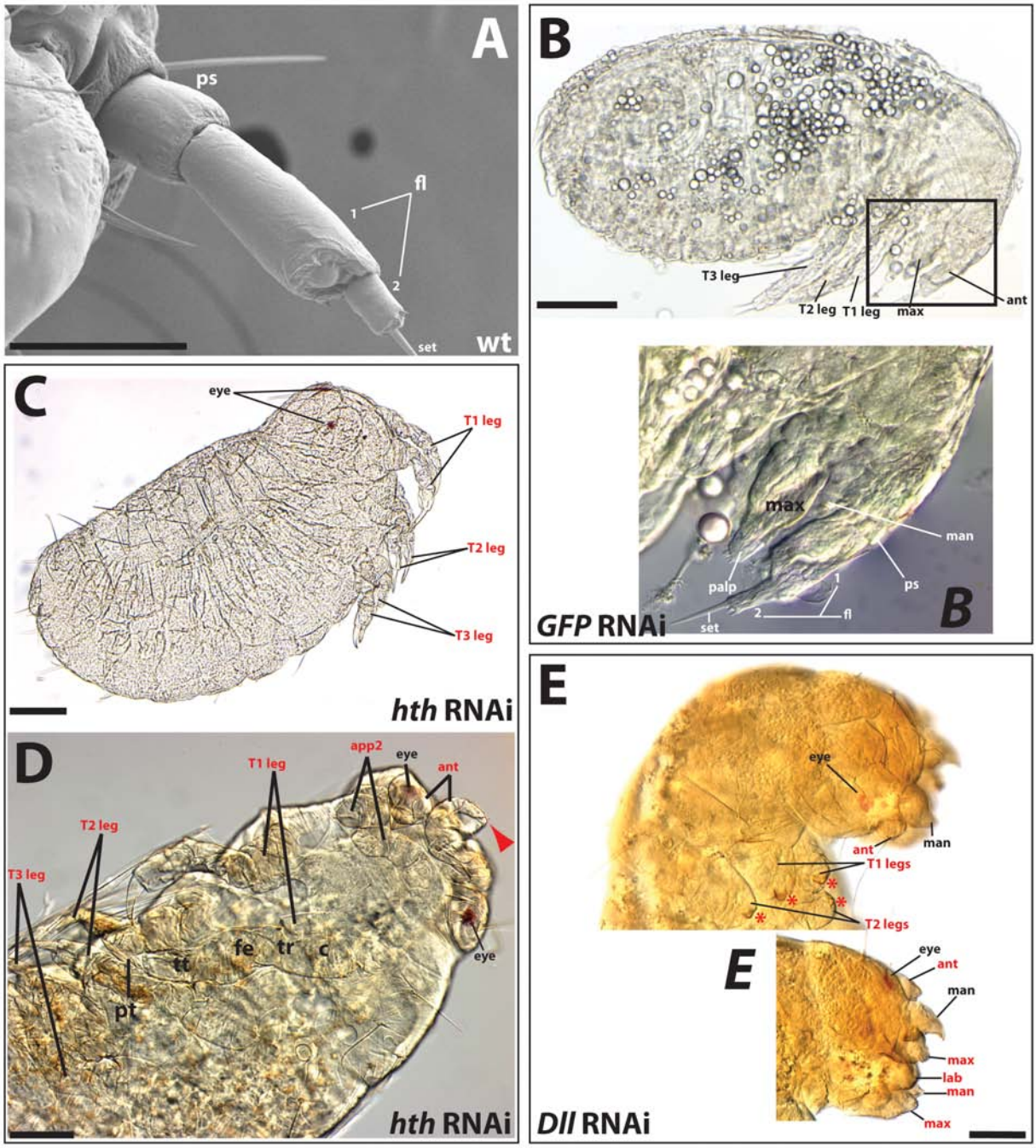
A
ps
fl
1
2
set
wt
B
T3 leg
T2 leg
T1 leg
max
ant
max
man
palp
ps
1
2
fl
set
B
GFP RNAi
C
eye
T1 leg
T2 leg
T3 leg
hth RNAi
D
app2
eye
ant
T1 leg
T2 leg
T3 leg
fe
tr
c
tt
pt
eye
hth RNAi
E
eye
man
ant
T1 legs
T2 legs
E
eye
ant
man
max
lab
man
max
Dll RNAi

Figure 3. Larval *ss* and *Dll* RNAi both result in homeotic transformations of the antenna toward leg. Appendage components affected by RNAi are labeled in red. Red arrows point to homeotically transformed structures. (A–C) Three examples of *T. castaneum ss* RNAi, with the most severely affected antenna to the right. Only the flagellum is transformed toward leg. The identity and morphology of the scape and pedicel are unaffected. (D–F) Examples of antennae and prothoracic legs from three *T. castaneum Dll* RNAi specimens. *Dll* RNAi antennae and legs of the other species (G–I). Antennae are at 2X the magnification of the legs. *Dll* RNAi results in loss of segmentation and truncation of both the antennae and legs. The antennae are so severely affected that in many cases flagellar structures are unidentifiable (red arrow heads). Some *T. castaneum* specimens show claws on the antennae, suggesting a role for *Dll* in antennal identity specification. In all species, *Dll* RNAi results in misshapen leg segments, including shortening of the femur and tibia, and truncation of the tarsus. Abbreviations: *brv*, *T. brevicornis*; *cnf*, *T. confusum*; *cst*, *T. castaneum*; *ory*, *L. oryzae.* Other abbreviations are as in Figure 1.

Figure 3.

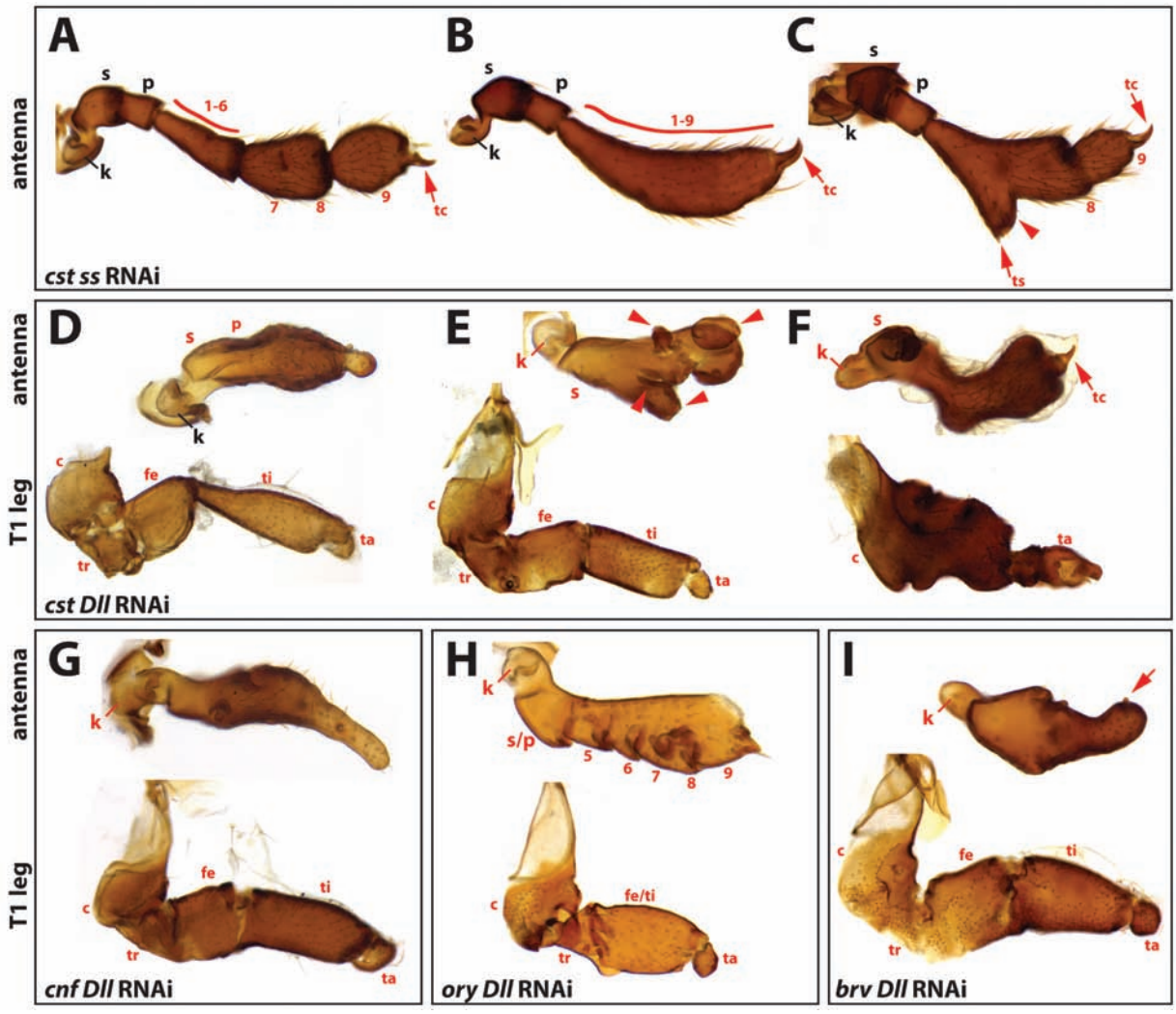
A
B
C
antenna
s
p
k
1-6
7
8
9
tc
1-9
ts
cst ss RNAi
D
E
F
T1 leg
c
fe
ti
ta
tr
cst Dll RNAi
G
H
I
s/p
5
6
fe/ti
cnf Dll RNAi
ory Dll RNAi
brv Dll RNAi

Figure 4. Larval *hth* and *exd* RNAi result in homeotic transformations of the antennal scape and pedicel toward leg identity. Appendage components affected by RNAi are labeled red. Red arrows denote homeotic transformation of antennal segments toward leg segment identity. (A) Wild-type T2 leg. The black arrowhead denotes the femur-tibia joint. (B–D) *T. castaneum exd* RNAi causes transformation of the scape and pedicel to femur and tibia, respectively, and fusions between flagellum articles. (*D*) Magnification of boxed region in D. Red arrowhead denotes a homeotic transformation of the scape-pedicel joint to a femur-tibia joint. (E–G) *T. castaneum hth* RNAi resembles *exd* RNAi. Phenotypic severity of RNAi increases from left to right in B–D and E–G. (H–M) Phenotypes of *exd* and *hth* RNAi recovered for the other species of this study are consistent with RNAi results from *T. castaneum.* Abbreviations are as in Figures 1 and 3.

Figure 4.

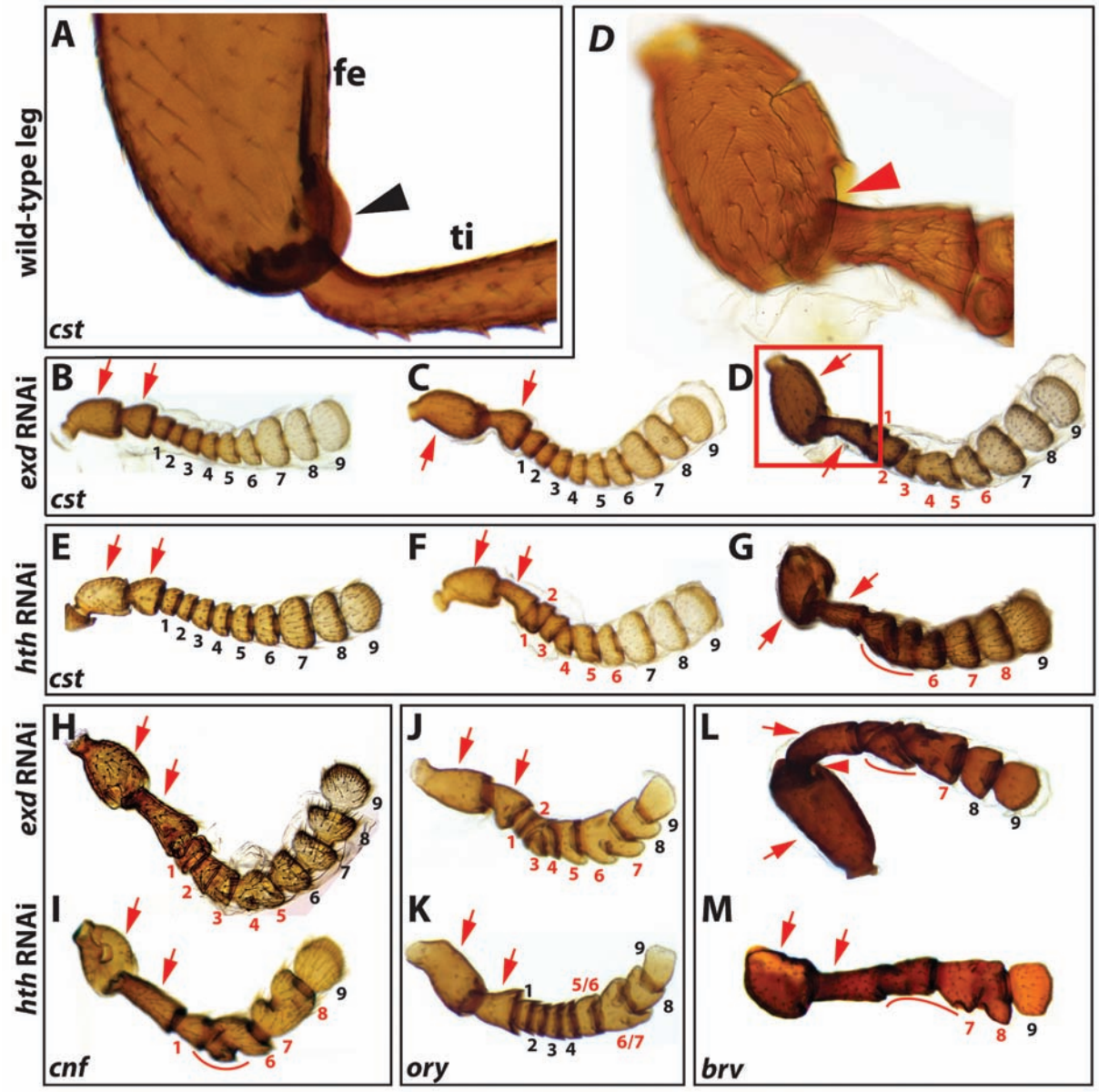
wild-type leg
A
fe
ti
cst
D
exd RNAi
B
C
D
cst
hth RNAi
E
F
G
cst
exd RNAi
H
J
L
hth RNAi
I
K
M
cnf
ory
brv

Figure 5. Larval *hth* and *exd* RNAi result in homeotic transformations of the eye, and deletions of the gena and clypeus. (A–C) Ventral head of *GFP* RNAi specimens. (D–F) Ventral head of *exd* RNAi specimens. (G–I) Ventral head of *hth* RNAi specimens. Red arrows point to ectopic structures replacing the eye. (J–L) SEM images of *T. confusum* support elytra identity of ectopic structures. (J) Ventral head of *GFP* RNAi specimen. Note the irregular shape of the cells surround the sensory bristle, which lacks a flat circular base. (*J*) Magnification of boxed region in J. (K) Elytron of *GFP* RNAi specimen. Note the regular hexagonal shape of the cells and flat circular base surrounding the sensory bristle. (*K*) Magnification of boxed region in K. (L) Ventral head of *hth* RNAi specimen. Note the elytron cell-like shape of the cells and flat circular base surrounding the sensory bristle. (*L*) Magnification of boxed region in L. Abbreviations: cl, clypeus; *cnf*, *T. confusum*; gn, gena.

Figure 5.

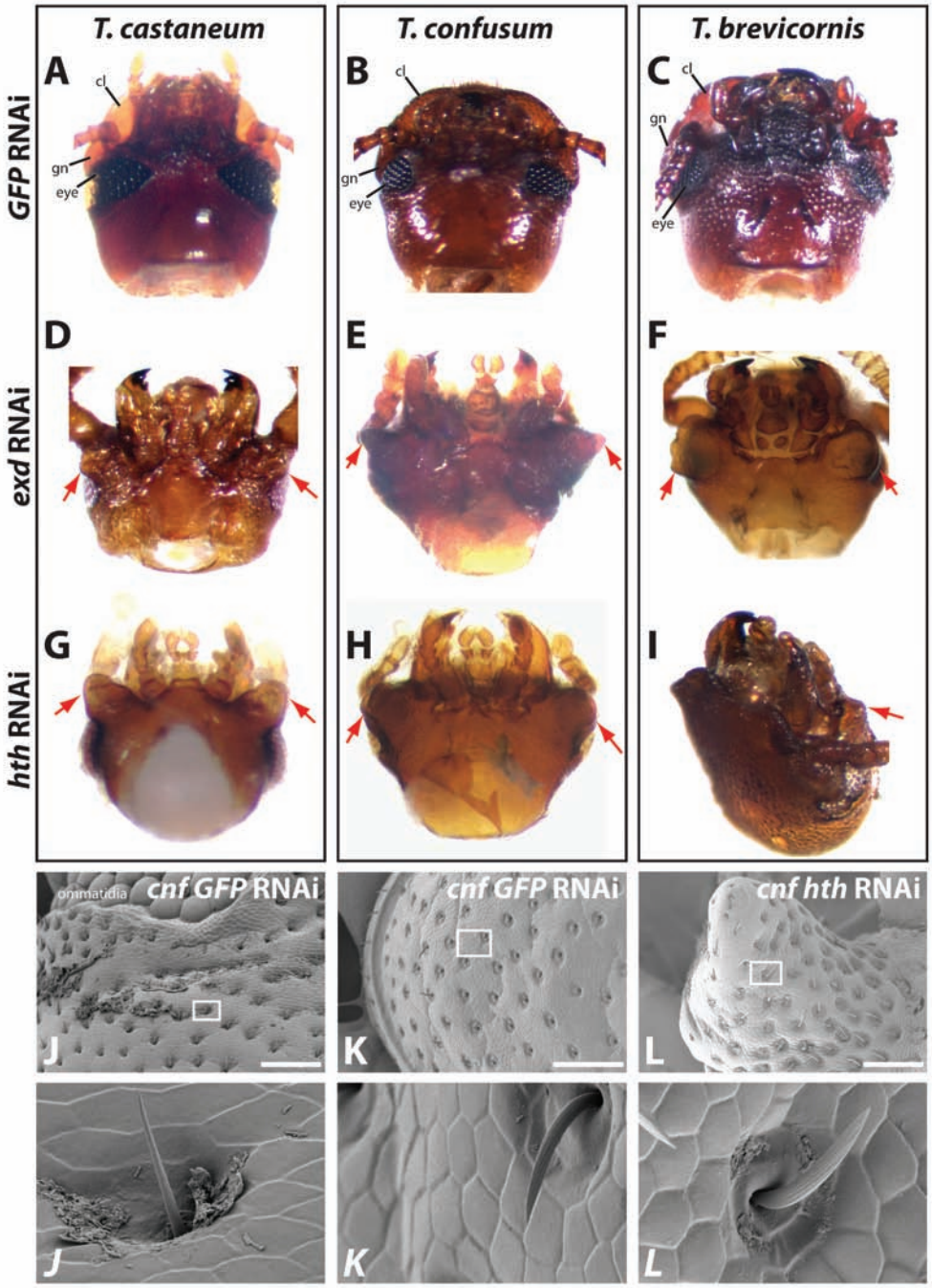
T. castaneum
T. confusum
T. brevicornis
GFP RNAi
exd RNAi
hth RNAi
A
B
C
D
E
F
G
H
I
cl
gn
eye
cnf GFP RNAi
cnf hth RNAi
J
K
L

Figure 6. Larval *dac* RNAi causes fusion and deletions of intermediately located antennal articles. (A) Like all club segments of flour beetles, the wild-type apical margin of *T. castaneum* flagellar article 7 houses basiconic sensilla (white arrows). Basiconic sensilla range from simple to 7-pronged varieties (Sokoloff, 1972). (B) A wild-type tri-pronged basiconic sensillum of *T. confusum*. (C) Distal two funicle segments (5, 6) of *T. castaneum* wild-type antenna. Note the absence of basiconic sensilla. (D) Wild-type proximal antenna of *T. confusum*. The white arrowhead denotes the basal constriction associated with the first flagellar article. (E) *T. confusum dac* RNAi specimen. Note the loss of the basal constriction of the first flagellum article and the presence of ectopic single-pronged basiconic sensilla (inset). (F) *T. castaneum dac* RNAi specimen. Normal apically located rows of bristles on club articles 7 and 8 are denoted with white arrowheads. Red arrowheads denote ectopic club-like apical rows of bristles on funicle articles. No ectopic basiconic sensilla were detected in the funicle. (*F*) Magnification of specimen in F. (G) *L. oryzae dac* RNAi specimen. (H) Results of *T. castaneum Ser* RNAi. Joint formation is disrupted, but basiconic sensilla are still found at the juncture of club articles. (I) *T. brevicornis dac* RNAi specimen. Note the presence of the normal basal constriction on the first flagellar article (white arrowhead). Structures labeled with red denote elements affected by *dac* RNAi. Scale bars equal 25 μm in all panels except B, where it is equal to 5 μm. Abbreviation: wt, wild-type. Other abbreviations are as in Figures 1 and 3.

Figure 6.

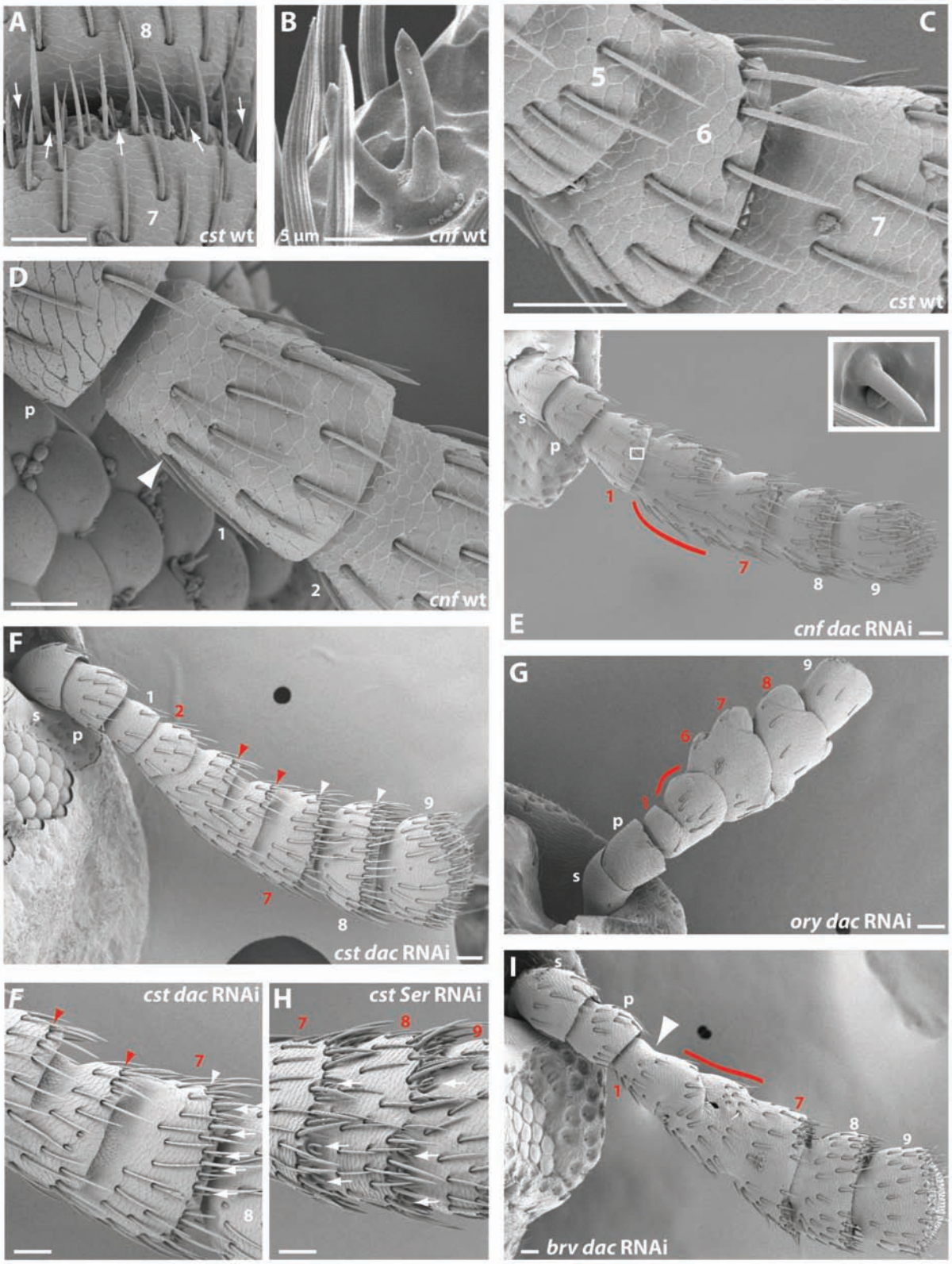
A
8
7
cst wt
B
5 µm
cnf wt
C
5
6
7
cst wt
D
p
1
2
cnf wt
s
p
1
7
8
9
E
cnf dac RNAi
F
1
2
s
p
9
7
8
cst dac RNAi
G
9
8
7
6
1
p
s
ory dac RNAi
F
cst dac RNAi
7
8
H
cst Ser RNAi
7
8
9
I
s
p
1
7
8
9
brv dac RNAi

Figure 7. Developmental and evolutionary models of antennal identity specification. Gene regulatory interactions are inferred based on data from *Drosophila* studies. (A) Embryonic insect and early *Drosophila* instar antennal identity specification. Scape and pedicel identity require *hth* and *exd*. The flagellum is specified by *ss*, which requires *hth*/*exd* and *Dll* for activation. (B) Metamorphic insect and late *Drosophila* instar antennal identity specification. *ss* does not require *hth*/*exd* for activation. (C) Model of evolution of antennal specification mechanisms in insects. The red dashed line traces the embryonic mechanism in insects, and the blue dashed traces the metamorphic mechanism. In this view, the imaginal specification mechanism of *Drosophila* includes components of both the ancestral embryonic and metamorphic antennal identity specification mechanisms (purple dashed line).

Figure 7.

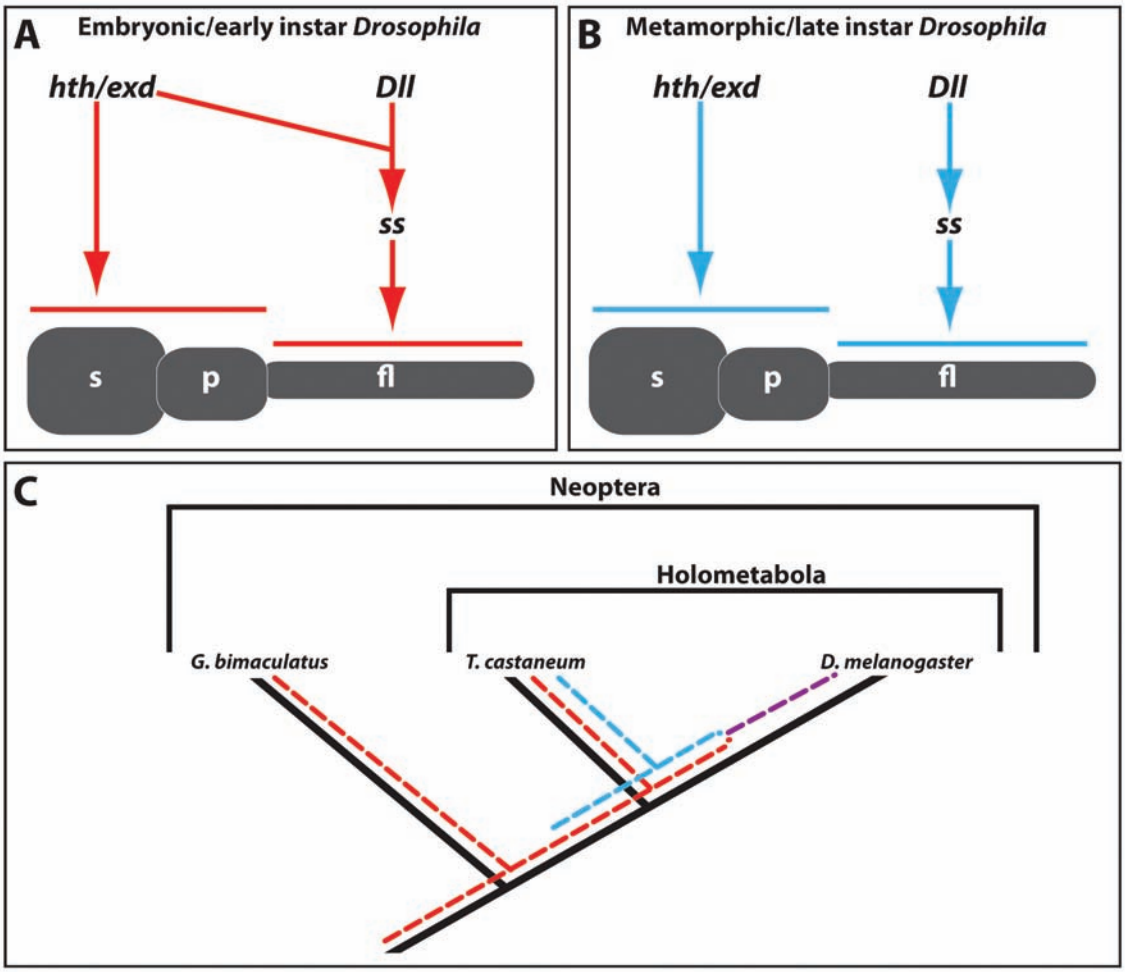
A
Embryonic/early instar Drosophila
hth/exd
Dll
ss
s
p
fl
B
Metamorphic/late instar Drosophila
hth/exd
Dll
ss
s
p
fl
C
Neoptera
Holometabola
G. bimaculatus
T. castaneum
D. melanogaster

Supplementary Figure 1. Alignment of predicted Dac sequences from flour beetles and a lightning bug (*Photuris sp.*, Lampyridae). Boxed regions are discussed in text. Sequence designations: XM_964678, *T. castaneum* Dac; cnf_Dac, *T. confusum* Dac; ory_Dac, *L. oryzae* Dac; brv_Dac, *T. brevicornis* Dac; AGG09248, *Photuris sp.* Dac.

Supplementary Figure 1.

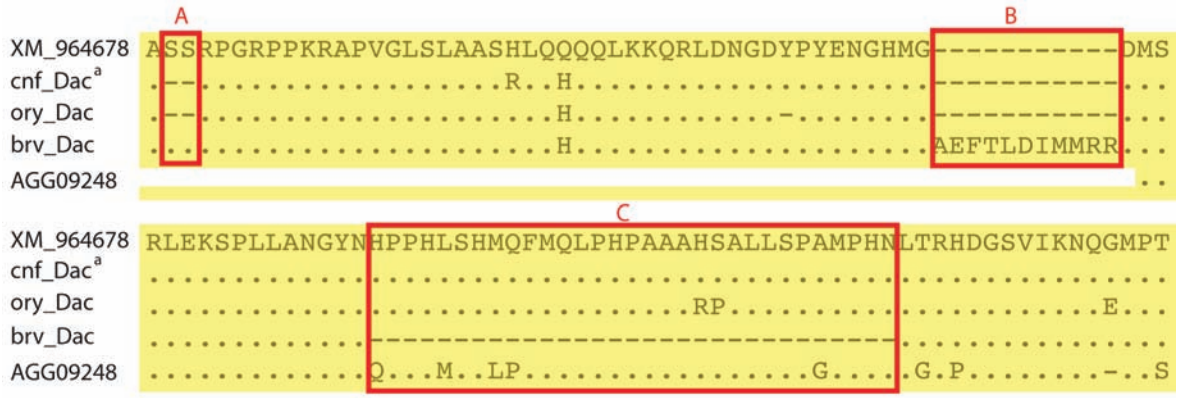

Supplementary Figure 2. Alignment of *T. castaneum dac* sequences of region showing amino acid sequence length variation in flour beetles. Predicted amino acid sequence is provided above the nucleotide alignment. Boxed regions correspond to boxed regions A and B in Supplemental Information Figure S1. Sequence designations: XM_964678, *T. castaneum dac*; new cst_dac, new *T. castaneum dac* sequence.

Supplementary Figure 2.

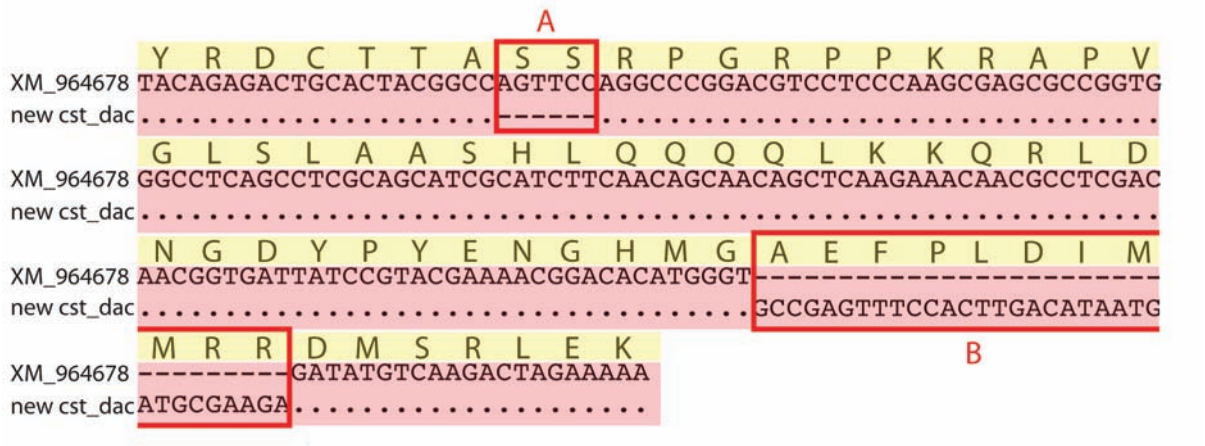

Chapter 2.

Hox genes require *homothorax* and *extradenticle* for sternite and tergite identity specification but not for appendage identity specification during metamorphosis of *Tribolium castaneum*

Introduction

In terms of species number, Arthropoda is by far the most successful animal phylum (Grimaldi and Engel, 2005). This success can partly be attributed to the evolution of their characteristic modular metameric body plans (Carroll, 2001). Metameres are grouped into morphologically distinct tagmata, which house a diversity of serially homologous ventral appendages. How these modular body plans evolved from an ancestor that lacked tagmosis (Manton et al., 1977; Snodgrass, 1935) is a salient issue in evolutionary developmental biology (Eriksson et al., 2010). In insects, the metameres are grouped into head, thoracic and abdominal tagmata. The head segments include ventral appendages that serve sensory (antennae) and food processing (mandibles, maxillae, labium) functions. The thorax includes three pairs of legs that ancestrally all served locomotory functions, while in extant lineages, the prothoracic leg is sometimes modified for prey capture. Two pairs of wings are also found on the thorax of most insects. For the most part, the abdomen lacks appendages, although developmental genetic data support the hypothesis that the genitalia of the terminal segments are derived from ventral appendages (Aspiras et al., 2011).

The earliest insight into the development of the modular insect body plan emerged from investigations of *Drosophila* mutants. Of significant interest were mutants for the TALE-class homeodomain transcription factor genes *homothorax* (*hth*) and *extradenticle* (*exd*). Mutations of these genes cause fusions among proximal segments in the antenna and leg (Casares and Mann, 2001), cause homeotic transformations of the antenna to leg (Casares and Mann, 1998; Casares and Mann, 2001; González-Crespo and Morata, 1995; Rauskolb et al., 1995), and cause other homeoses along the anteroposterior body axis during both embryogenesis and metamorphosis (González-Crespo and Morata, 1995; Jürgens et al., 1984; Peifer and Wieschaus, 1990; Rauskolb et al., 1993; Rauskolb et al., 1995; Rieckhof et al., 1997). Exd is nuclearly localized only when bound to Hth (Abu-Shaar et al., 1999; Pai et al. 1998; Rieckhof et al. 1997) and Hth is stabilized only in this dimer complex (Abu-Shaar and Mann, 1998; Kurant et al., 1998), explaining why mutants of these genes exhibit largely overlapping phenotypes in *Drosophila* (Casares and Mann, 1998).

hth/*exd* determine segmental identity through interactions with the *Hox* genes (Chan et al. 1994), which also code for homeodomain transcription factors (McGinnis et al., 1984, Scott and Weiner, 1984). During arthropod development, the particular identity of a segment, including its appendages, is determined by the complement of *Hox* genes expressed in the segment, and the boundaries between tagmata correspond to expression boundaries of particular *Hox* genes (Hughes and Kaufman, 2002). *Hox* genes select for specific appendage identities, in part, by modulating the activity of *exd* and *hth* (Abzhanov et al. 2001; Casares and Mann, 1998; Yao et al., 1999), which are co-expressed in the proximal domain of all ventral appendages. In some contexts Exd/Hth are cofactors of Hox proteins and increase their DNA binding specificity (Chan et al., 1994; Chan and Mann, 1996; Mann and Chan, 1996; Ryoo and Mann, 1999; Ryoo

et al., 1999; Slattery et al., 20011b; van Dijk and Murre, 1994). In most cases, this complex is formed between a conserved YPWM domain N-terminal to the Hox homeodomain (Chang et al., 1995; Chan et al., 1996; Johnson et al., 1995) and the homeodomain and C-terminal region of Exd (Chang et al., 1995). However, only a single Exd interaction residue of the ancestral YPWM domain is conserved in the Hox protein Abdominal-B (Abd-B) (LaRonde-LeBlanc and Wolberger, 2003), and it is unclear whether Exd and Abd-B interact in *Drosophila* (Sambrani et al., 2013). The interaction between Exd and Hox proteins explains why *Drosophila hth* and *exd* mutants phenocopy many *Hox* homeotic mutations (González-Crespo and Morata, 1995; Peifer and Wieschaus, 1990); phenocopies result from Hox proteins losing their affinity for specific enhancers when not complexed with Exd and Hth, which leads to the loss of segment specific regulatory states. This interaction between Exd and Hox proteins is at least as ancient as Bilateria (Chang et al., 1995; van Dijk et al., 1995; Lu et al., 1995; Neuteboom, et al., 1995; Phenlen, et al. 1995), suggesting that the evolution of this interaction predates the evolution of tagmosis in arthropods and other animal lineages, such as the vertebrates and annelids.

Unlike most other insects and non-insect arthropods, *Drosophila* do not produce ventral appendages during embryogenesis. Instead, imaginal discs are set aside during embryogenesis and patterned during the larval period, a period, in *Drosophila*, where the characteristic insect tagmosis pattern is hardly detectable. The adult appendages and many other components of the adult body plan emerge from the imaginal discs during metamorphosis, and the characteristic head, thorax, and abdomen tagmata become evident in the adult. Given the highly derived mode of *Drosophila* development, investigations of insect species that retain ancestral modes of development must be investigated in order to determine the ancestral roles of *hth*/*exd* and the *Hox* genes in producing heteronomous metamerism and tagmosis patterns in insects.

The red flour beetle *Tribolium castaneum* is a suitable system to further explore evolution and development of modular insect body plans for several reasons. First, in *T. castaneum* ventral appendages are patterned both during embryogenesis, as in most other insects, and again during metamorphosis, as in most other holometabolous insects. Second, *T. castaneum* retain ancestral mandibulate mouthpart anatomies, unlike *Drosophila*. These two features suggest that conclusions based on *T. castaneum* embryogenesis may be broadly applicable to other insects, while conclusion based on metamorphosis may be broadly applicable to other holometabolous insects. Third, gene function can be studied during both embryogenesis and metamorphosis in *T. castaneum* utilizing RNA interference (RNAi) (Posnien et al., 2009).

We have previously investigated the metamorphic role of *hth* in ventral appendage patterning in *T. castaneum* (Angelini et al., 2009; Angelini et al., 2012a; Angelini et al., 2012b) and have investigated the roles of both *hth* and *exd* in embryonic and metamorphic antennal identity specification (see Chapter 1). We found that *hth* and *exd* play a generic role in all ventral appendages in specifying proximal appendage identity during metamorphosis. Our results also suggest that distinct identity specification mechanisms are active in the antenna *anlagen* during embryogenesis and metamorphosis, providing developmental insight into the evolution of holometaboly. In order to aid in interpretation of our *T. castaneum exd* and *hth* RNAi specimens, we have investigated the metamorphic functions of the *Hox* genes (Table 1). Although *T. castaneum Hox* mutants are available (Beeman et al., 1989; Beeman et al., 1993), functional data are lacking for some genes; in some cases it is unclear whether mutant phenotypes are the result of loss or gain of function (Tomoyasu et al., 2005); and metamorphic investigations of double or triple *Hox* mutants have not been reported. Here, we supplement existing functional data for *T. castaneum Hox* genes with metamorphic RNAi to identify

developmental roles of *hth*/*exd* that require and do not require *Hox* function, and vice versa. These data show: a) that segmental identity specification of dorsal tergites and ventral sternites requires *exd*/*hth* and *Hox* function during metamorphosis; b) the role of *hth*/*exd* in specifying proximodistal podomere identity does not require *Hox* function; and c) the *Hox* genes do not require *hth*/*exd* to specify ventral appendage identities. Additionally, like antennal identity, distinct mechanisms specify the identities of other ventral appendages during embryogenesis and metamorphosis, lending further insight into the evolution of holometaboly.

Materials and methods

Beetle husbandry

T. castaneum were purchased from Carolina Biological. Beetles were cultured at 32° C on a diet of equal parts wheat and white flour at a ratio of 1 part nutritional yeast to 19 parts flour (Sokoloff, 1972). Beetles were culled regularly in order to regulate population size.

Molecular cloning and sequencing of candidate genes

Total pupal RNA was extracted with Trizol Reagent (Invitrogen). cDNA was synthesized with a qScript Flex cDNA Synthesis Kit (Quanta Bioscience), selecting for poly(A)+ transcripts with an oligo-dT primer. Gene fragments were cloned into the pCR4-TOPO vector (Invitrogen) (see Supplementary Table 1 for primer sequences). We cloned fragments of each *Hox* gene, *hth*, and *exd* (Table 1). Plasmid Mini preps were prepared using a NucleoSpin Plasmid Quick Pure Kit (Machery-Nagel). Clones were sequenced with vector primers using

Big Dye v1.1 on an ABI 3130*xl* Genetic Analyzer. Sequence identity was determined using blastn at the NCBI website.

RNA interference

Gene fragments were amplified from minipreps using gene specific primers with T7 reverse transcriptase promoter sites added to the 5' end (see Supplementary Table 1 for primer sequences). Double-stranded RNA (dsRNA) was synthesized with a MEGAscript T7 kit (Ambion) (Table 2). To control for off-target effects of *Hox* RNAi, we synthesized and tested two non-overlapping dsRNA constructs for each *Hox* gene. *exd* and *hth* have overlapping functions, so investigating functions of both genes controls for off-target RNAi affects. *GFP* dsRNA acted as a negative control. Double-stranded RNA (dsRNA) solution was prepared in 1:20 McCormick green food coloring and 1:100 injection buffer (0.1 mM sodium phosphate, 5.0 mM KCl, 1:10 green food coloring). To investigate metamorphic gene functions, approximately 120 nl of 0.1–3.1 ng/µl dsRNA was injected into ultimate instar larvae prior to the wandering stage (Table 2). Larvae were anesthetized in a petri dish on ice for ~5 minutes. Anesthetized larvae were injected dorsally between the prothoracic and mesothoracic tergites with pulled 50 µl calibrated pipets (VWR International) (Posnien et al., 2009; Tomoyasu and Denell, 2004). Injected larvae were cultured in flour mix at 32° C until pupation. After pupation, specimens were stored individually at 32° C until they reached the adult stage.

Specimen preparation and imaging

Adults, including pharate specimens, were cleared for scoring and imaging following the procedure of Van der Meer (1977). Briefly, they were heated at 50° C overnight in 20% glycerol

in glacial acetic acid with 0.1% Tween20. Specimens were then washed in 20% glycerol with 0.1% Tween20. Finally, they were stored at 4° C in 80% glycerol wit 0.1% Tween20 for later scoring and imaging. Heads, thoraces, and abdomens were placed in wells of a 9 well dish filled with H_2O and imaged under a Nikon SMZ800 dissecting microscope. Ventral appendages were mounted in 80% glycerol in PB-tween (1X phosphate-buffered saline, 0.1% Tween20) on slides and imaged on a Ziess Axioskop2. All light micrographs were taken with an Olympus camera and Magnafire Digital Microimaging software. In some cases, multiple focal planes of a specimen were imaged and stitched together with the Auto-Blend Layers command in Adobe Photoshop CS4 to maximize focus. For Scanning electron microscopy (SEM), specimens stored in glycerol were rinsed several times quickly with 100% ethanol, followed by an overnight wash. Specimens were then dehydrated in hexamethyldisilazane, sputter coated with Gold-palladium and imaged on a Zeiss DSM982 Gemini field emission SEM.

Scoring RNAi phenotypes

RNAi phenotypes of whole mount adult specimens were scored using a dissecting microscope. Ventral appendages were scored on either a compound microscope or SEM. All ventral appendages were scored for losses and fusions of articles and proximodistal and anteroposterior homeosis. We also scored body wall defects and homeotic transformations of sternites, tergites and wings.

Results

Although the *Hox* gene *labial* is known to function during *T. castaneum* embryogenesis (Posnien and Bucher, 2010), we did not recover specific adult phenotypes with larval *labial* RNAi, and do not discuss this gene further in this report. For other *Hox* genes, we recovered matching adult phenotypes with larval RNAi treatments using non-overlapping dsRNA fragments, suggesting these phenotypes are not the result of off-target effects. We also recovered matching adult phenotypes from larval *exd* and *hth* RNAi treatments, suggesting specificity of these RNAi treatments. Adult RNAi specimens could be ranked in terms of phenotypic severity (Table 2), with mildly affected specimens showing minor patterning defects, including fusions between or losses of appendage articles, but lacking evidence of homeosis. Moderately affected specimens exhibited minor patterning defects, along with homeotic transformations, including segmental identity transformations of ventral appendages, wings, and/or sclerites. Severely affected specimens included phenotypes of moderately affected specimens, but also included the development of ectopic appendages in body regions that normally lack appendages. Below, we describe phenotypes recorded in roughly anterior posterior order.

Mandibles

exd RNAi did not affect mandible identity or morphology. This result is consistent with our previous report of *hth* RNAi in *T. castaneum* (Angelini et al., 2012a). Of the *Hox* genes, only *Dfd* RNAi treatments in *T. castaneum* affected mandible morphology (Fig. 1C). *Dfd* RNAi caused reduced scleritozation of the mandible, accompanied by reduction in pigmentation of the

molar. The posterior edge of the mandible normally curves gently from the base of the condyle to the point of the distal tooth. In *Dfd* RNAi specimens, this edge hardly curved until just below the incisor lobe, and then curved sharply forming a shoulder. The teeth and condyles appeared normal. On this basis, we conclude that mandible identity was not affected by depletion of *Dfd.*

Maxillae

The adult maxilla of flour beetles is composed of the proximal-most cardo; the stipes, which includes a basal sclerite and palpifer; two medial endites, the proximal lacinia and the distal galea; and finally the distal palp, which is composed of four palpomeres (Fig. 1A). Maxillary phenotypes resulting for larval *exd* RNAi were consistent with our previous report for larval *hth* RNAi (Angelini et al., 2012a). However, the phenotypic series of *T. castaneum exd* RNAi specimens included more severely affected specimens than the phenotypic series of *hth* RNAi. For both genes, the moderately affected specimens exhibited proximal defects (Fig. 1M, O); the region of effect expanded distally in more severely affected specimens (Fig. 1N, P). In moderately affected specimens for RNAi against either gene, the proximal palpomere became greatly enlarged, consistent with a transformation toward a more distal palpomere identity. The cardo and basal sclerite of the stipes became misshapen, often accompanied by fusions between these elements and a reduction in the size of the cardo. The palpifer adopted a rod-like shape, possibly representing a transformation to maxillary palp identity. In more severely affected individuals, the proximal palpomere was completely deleted. Both the galea and lacinia were severely reduced, but the identity of these structures was not affected. We found no evidence of homeotic transformations of the most distal two palpomeres. We also did not see evidence of transformation of the maxilla to a different appendage identity.

Deformed (*Dfd*) RNAi affected maxilla morphology, but not identity (Fig. 1D). It resulted in overall reduction of the cardo, similar to results of *exd* and *hth* RNAi. The basal sclerite of the stipes was also reduced, and the palpifer became wider distally. The joint between the first two maxillary palpomeres became more exposed in response to *Dfd* RNAi. *proboscipedia* (*pb*) RNAi resulted in transformation of the maxillary palp to leg identity (Fig. 1E) consistent with *pb* mutations affecting *T. castaneum* metamorphosis (Beeman et al, 1989). This appendage included a proximal palpomere, followed by a femur and short tibia connected by a characteristic hinge joint; a tarsus with variable number of jointed and fused tarsomeres; and a misshapen pretarsus with a single pronged claw. Neither the cardo nor the stipes and associated endites were affected by *pb* RNAi. *Sex combs reduced* (*Scr*) larval RNAi did not affect adult maxillae morphology (Fig. 1F). Maxillary morphology of specimens that were co-injected with *Dfd* and *Scr* dsRNA did not differ from *Dfd* RNAi specimens (Fig. 1G). Maxillary phenotypes resulting from co-injection of *pb* and *Scr* did not differ from phenotypes resulting from *pb* RNAi (Fig. 1H). However, co-injection of *Dfd* and *pb* dsRNA resulted in the transformation of the palpifer and palp to an antenna (Fig. 1IJ). Maxillary phenotypes resulting from co-injection of *Dfd*, *pb*, and *Scr* dsRNA resembled phenotypes resulting from co-injection of *Dfd* and *pb* dsRNA (Fig. 1K-L). Unlike the maxillary phenotypes recovered with *hth* and *exd* RNAi, maxillary phenotypes recovered with *Hox* RNAi did not include proximodistal transformations.

Labium

The adult labium of flour beetles is intercalated between the paired maxillae. This appendage is composed of a proximal-most mentum, followed by the prementum with an

associated distal ligula, and a palp with three palpomeres, which articulates with a palpiger on either side of the base of the prementum (Fig. 1A). As in all insects, the unpaired labium is formed by a fusion of the ventral appendages of the labial segment. Results of larval *exd* RNAi were consistent with our previous report of *hth* function in the labium (Angelini et al., 2012a). Similar to the maxillary palps of *exd* and *hth* RNAi specimens, the labial palps of these specimens exhibited transformations of the proximal-most palpomere toward distal identity in moderately affected specimens (Fig. 1M, O), while the proximal two palpomeres were completely deleted in more severely affected individuals (Fig. 1N, P). Both the mentum and prementum became narrower, while the base of the prementum became elongate relative to the wild-type condition. The part of the prementum normally found between the two palps was severely reduced. As in the maxillae, larval *exd* RNAi phenotypes were more severe than larval *hth* RNAi in the labium (Fig. 1N, P). In the most severely affected *exd* RNAi specimens, the mentum was transformed to two rounded sclerites; the base of the prementum became markedly thinner and elongate; the ligula and large sclerite of the prementum normally found between the labial palps were completely deleted; and the labial palps were reduced and fused medially (Fig. 1P). We recovered phenotypes of this degree of severity with both *hth* and *exd* RNAi in *Tribolium brevicornis* (Supplementary Fig. 1B–C), a closely related beetle species (Angelini and Jockusch, 2008), meeting our expectation of completely overlapping functions of *exd* and *hth*. Labial identity was retained in the labium of *T. castaneum* and *T. brevicornis exd* and *hth* RNAi specimens.

Dfd RNAi did not affect labium identity by itself or in combinations with RNAi against *pb* and/or *Scr* (Fig. 1G, J–K). In these RNAi combinations, the maxilla adopted identities and morphologies consistent with those produced with RNAi against *pb* and/or *Scr*. Larval RNAi

against *pb* resulted in a transformation of the labial palps to leg identity (Fig. 1E), as do mutations of this gene that affect metamorphosis (Beeman et al., 1989). The distal palp was transformed to leg identity, exhibiting a pretarsus and a variable number of complete and fused tarsomeres. The proximal most element of the transformed palp most resembled a tibia. The ligula was deleted and the prementum was markedly reduced. *Scr* RNAi caused a slight reduction in size of the mentum, a dramatic decrease in the size of the prementum, and the palpiger became rounded at the edges (Fig. 1F). Most notably, the distal labial palpomere acquired the size and shape of the wild-type distal maxillary palpomere and the ligula acquired galea morphology, supporting a homeotic transformation of the labium toward maxillary identity.

Specimens co-injected with *pb* and *Scr* dsRNA produced both phenotypes similar to those resulting from *pb* RNAi and *Scr* RNAi alone as well as novel phenotypes (Fig. 1H). The prementum was greatly reduced, as with *Scr* RNAi. The ligula was reduced and the palps articulated with the prementum in these specimens, as they did with *pb* RNAi specimens. The proximal two palp segments adopted morphologies like those of *pb* RNAi specimens, suggesting a transformation to leg identity like that found with *pb* RNAi. However, the palps lacked both the distal sensory region normally found on palps and claws normally found on legs, suggesting a transformation to an identity other than those adopted with *pb* or *Scr* RNAi alone. The shape of the distal palp segments was very similar to the shape of distal maxillary palp segments in combination *Dfd* and *pb* RNAi specimens, which exhibited a clear transformation toward antennal identity. In sum, RNAi combinations targeting *pb* and *Scr* caused the labial palps to adopt a mixed identity, possibly leg proximally and antenna distally, but did not result in

transformations of proximal maxillary elements to more distal identity, unlike both *hth* and *exd* RNAi.

Legs

Leg segmentation patterns are highly conserved across insects and flour beetles exhibit the generalized pattern. Briefly, there is a proximal coxa, followed by the trochanter, femur, tibia, tarsus and pretarsus (Fig. 2A). Leg podomeres are distinguishable by shape, joint structure, bristle and setae patterns, and cuticular sculpting patterns (Fig 3A–D). Although pro- meso- and metathoracic legs are very similar in morphology, they can be distinguished based on podomere morphology and the distribution of setae. The body of the coxa of the prothoracic leg is globose in shape with a large laterally directed lobe; the coxa of the mesothoracic leg is globose in shape, but larger than the body of the prothoracic leg, and has a much smaller laterally facing lobe; the coxa of the metathoracic leg is much larger than that of either the prothoracic or mesothoracic legs and lacks a lateral lobe. The dorsal edge of the prothoracic femur slopes concavely to where it meets the trochanter, while the dorsal edge of the femur slopes convexly to meet the trochanter in meso- and metathoracic legs (Fig. 2A). The prothoracic leg exhibits tibial teeth along the ventral edge of the tibia and a medial tibial spur that is markedly more robust than the lateral spur (Fig. 3B), while the meso- and metathoracic legs lack tibial teeth on the ventral edge of the tibia and the medial and lateral tibial spurs are very similar in size and shape (Fig. 3C–D). Unlike the pro- and mesothoracic legs, the metathoracic legs lack tibial teeth along the dorsal edge of the tibia (3B–D). Finally, the pro- and mesothoracic tarsi are divided into five tarsomeres, while the metathoracic tarsus is divided into only four tarsomeres (Fig. 2A).

In *T. castaneum*, leg phenotypes recovered in *exd* RNAi specimens were consistent with *hth* RNAi phenotypes we previously reported (Angelini et al. 2012b). As with other appendages, leg phenotypes resulting from *exd* RNAi were more severe than those resulting from *hth* RNAi. RNAi targeting either of these genes resulted in transformations of the coxa and trochanter toward more distal podomere identity (Fig. 2F–G). In line with this interpretation, the coxa and trochanter became more elongate, and a flexible joint resembling the normal joint between the femur and tibia developed between these two podomeres. We also recovered *exd* RNAi specimens that had tibial spurs at the apex of the elongate 2nd leg segment. We examined the mesothoracic leg of an *hth* RNAi specimen with SEM. The femur of this specimen showed a clear tibial cuticular sculpting pattern and exhibited distal tibial teeth (Fig. 3E), suggesting that the femur was transformed toward tibia. These results suggest that *exd* and *hth* specify the proximodistal identity of the coxa, trochanter, and femur of the leg by repressing identities distal to these elements. In general, more distal articles were less affected, and the tarsus and pretarsus appeared wild-type in morphology in these treatments. Neither treatment affected the segmental identity of the legs.

Larval *Scr* RNAi caused the prothoracic coxa to adopt a rectangular shape (Fig. 2B). The medial tibial spur lost its normally robust morphology and the ventral edge of the tibia lacked the tibial teeth that normally characterize the prothoracic leg (Fig. 3F). These phenotypes are consistent with a homeotic transformation of the prothoracic leg to mesothoracic leg. *Antennapedia* (*Antp*) RNAi did not affect leg morphology or identity (Fig. 2C). *Ubx* (*Ultrabithorax*) RNAi affected both the meso- and metathoracic legs. The coxa of both appendages adopted a rectangular shape not observed in any wild-type leg, but similar to the prothoracic coxae of *Scr* RNAi specimens (Fig. 2B–D). The femurs of both the meso- and

metathoracic legs of *Ubx* RNAi specimens slope concavely like those of normal prothoracic legs. The tibia of the metathoracic leg exhibited tibial teeth along the dorsal edge, but lacked tibial teeth along the ventral edge (Fig. 3G), and the tarsus was divided into five tarsomeres (Fig. 2D). Results of *Ubx* RNAi are consistent with a transformation of the tibia and tarsus of the metathoracic leg to mesothoracic leg identity. Neither RNAi targeting individual thoracic *Hox* genes, nor RNAi targeting pairs or all three of these genes caused transformations of legs toward antennal identity.

Based on what is known about leg identity specification during *T. castaneum* embryogenesis (Brown et al., 2002) and *Drosophila* metamorphosis (Struhl, 1981, 1982) (see discussion), we were surprised that *Ubx* was playing a role in providing identity to both the meso- and metathoracic legs during metamorphosis, while *Antp* was playing no detectable identity specification role. In order to gain further insight into these results, we also investigated leg expression profiles of the thoracic *Hox* genes using RT-PCR. As expected, we detected expression of all thoracic *Hox* genes from cDNA produced from whole pupae (Fig. 3H). Interestingly, our *Scr* primers amplified two fragments, a 422 base pair *Scr* fragment and a larger fragment of unknown identity, possibly representing an alternatively spliced *Scr* transcript. Consistent with our RNAi results, we detected *Scr* expression at high levels in the prothoracic leg, compared to our reference gene *rsp18*, and at low levels in the meso- and metathoracic legs (Fig. 3I). Not surprisingly, given our RNAi results, we only detected faint expression of *Antp* in the meso and metathoracic legs (Fig. 3J). Surprisingly, given the identity determining roles we detected with *Ubx* RNAi, we did not detect expression of *Ubx* in any legs. This suggests that *Ubx* can perform its leg morphogenesis functions at very low expression levels, or that it is only highly expressed in a small subset of leg cells.

Membranous wings and elytra

Beetle forewings have evolved into elytra, hard cuticular structures that cover the membranous hind wings and are not used in flight (Fig. 4A). In *T.* castaneum, *hth* RNAi resulted in the development of ectopic elytra tissue on the prothorax (Fig. 4E), rather than complete elytra, suggesting only a partial transformation of the T1 segment to T2 identity. We did not recover ectopic elytra tissue on the prothoraces of *exd* RNAi specimens of *T. castaneum* specimens (Fig. 4F), but did recover this transformation in both *T. brevicornis hth* and *exd* RNAi specimens (Supplementary Fig. 1E–F), consistent with completely overlapping regulatory functions of *exd* and *hth*. These specimens resembled moderately affected *Scr* RNAi specimens in their degree of transformation (see below). RNAi against these genes also caused a loss of both the medial and scutoscutellar ridges of the mesonotum (Fig. 4E–F) and disrupted metascutum morphology.

Scr RNAi resulted in the development of ectopic elytra on the prothorax (Fig. 4B, Tomoyasu et al. 2005), consistent with a *Scr* mutation affecting metamorphosis (Beeman et al., 1989). *Antp* RNAi did not affect wing identity, but did cause loss of the scutoscutellar ridge of the mesonotum (Fig. 4C, Tomoyasu et al., 2005), like *hth* and *exd* RNAi. Finally, *Ubx* RNAi resulted in the transformation of the membranous hind wing to elytra (Fig. 4D; Tomoyasu et al., 2005).

Thoracic tergites and sternites

hth and *exd* RNAi resulted in reduction and patterning disruption of all thoracic sternites (Fig. 4E–F), causing the coxae to become completely exposed. This was especially true of the metasternite, which became closer in size to the more anterior thoracic sternites. In general, the

sternites of the three thoracic segments appeared more similar to each other in *hth* and *exd* RNAi specimens than wild-type specimens. However, they did not resemble any wild-type sternite, suggesting that convergent morphologies could be due to reduction of all sternites, rather than homeotic transformation in response to *hth* or *exd* RNAi.

Scr RNAi resulted in shortened and bent epimera (Fig. 4B). However, these specimens were often bent forward at the pro-mesothoracic boundary during pupation, which could have physically disrupted growth of this structure, leaving open the possibility that *Scr* may not function directly in epimeron patterning. *Antp* RNAi resulted in transformation of the mesosternellum to a structure resembling the wild-type prosternellum of the prothorax, and the development of bilaterally paired pits on the posterior metasternite (Fig. 4C). Finally, *Ubx* RNAi caused a transformation of the metasternite to mesosternite, evidenced by the much smaller size of this sclerite compared to the mesosternite of wild-type specimens and the presence of a mesosternellum (Fig. 4D).

Abdominal segments

The abdomen of adult *T. castaneum* is composed of ten segments. The anterior two abdominal segments (A1, A2) are internalized, and sit under the metathoracic coxae. The anterior most visible abdominal segment is A3 (Fig. 5A). A3 has a very distinctly curved anterior margin that abuts the posterior edge of the metathoracic coxae, and has a pointed intercoxal process that sits between the coxae, while the sternites of A4–A7 have straight anterior margins. The posterior margins of A3–A6 are straight while the posterior margin of A7 is rounded. The posterior-lateral margins of sternites A5–A7 are heavily schlerotized and extend from the body, increasing in size and conspicuousness from anterior to posterior. A8–A10 are

membranous and normally pulled within the abdomen, but are telescoped out during mating (Sokoloff, 1972). The male aedeagus articulates with A8, and the female ovipositor is composed of parts of A8–A10 (Aspiras et al., 2011).

In severely affected *hth* or *exd* RNAi specimens, at the pupal molt, the abdomen remained trapped in the larval cuticle, and at the adult molt, the abdomen remained trapped in both the larval and pupal molt and did not fully sclerotize. In less severely affected specimens, larval *hth* or *exd* RNAi resulted in exposure of the anterior two sternites (Fig. 5G, I) [as with *Ubx* RNAi (see below)], but they did not develop legs, nota, or elytra. Sternite 3 lost the intercoxal process and sternite 7 was not rounded along the posterior margin. In general, all abdominal sternites adopted morphology most similar to wild-type sternites 4–6. Abdominal sternite 8 became sclerotized in response to *hth* or *exd* RNAi (Fig. 5H, J). We did not find evidence of homeotic transformations of the dorsal abdomen or genitalia in response to either *exd* or *hth* RNAi treatments.

As with *hth* and *exd* RNAi, *Ubx* larval RNAi resulted in abdominal sternites 1 and 2 becoming exposed (Fig. 5F). In severely affected specimens, A1 was transformed to mesothoracic identity, complete with legs and elytra (Fig. 4D). A2 became sclerotized, suggesting this segment was being transformed to either a thoracic segment or a more posterior abdomen segment. Moderately affected *abd-A* RNAi specimens exhibited transformations of abdominal sternites 4–7 to sternite 3 identity, complete with intercoxal processes (Fig. 5B). The abdomens of severely affected specimens remained trapped in the pupal cuticles. The abdomens of these specimens became smaller and never fully sclerotized, as was previously reported for a *T. castaneum abdominal-A* (*abd-A*) mutation that affects metamorphosis (Beeman et al., 1989). No intercoxal process could be identified in these specimens. Similar to *hth* and *exd* RNAi

results, *Abd-B* RNAi resulted in transformations of abdominal sternites 7–9 toward more anterior identity, evidenced by a straight sternite 7 posterior margin and sclerotization of sternites 8–10 (Fig. 5C, E). The genitalia also became heavily sclerotized, while in males the aedeagus was transformed distally into a two-pronged structure (Fig. 5D–E).

Discussion

The discovery of the *Hox* cofactor roles of *exd* and *hth* provided insight into how *Hox* genes differentially regulate expression of downstream factors even though they all share a highly conserved DNA binding homeodomain, with similar in vitro DNA binding specificity (Chan et al., 1994; Chan and Mann, 1996; Mann and Chan, 1996; Ryoo and Mann, 1999; Ryoo et al., 1999; van Dijk and Murre, 1994). Much effort has been given to distinguishing the developmental roles that *Hox* genes play that require *exd* and *hth* function from those that do not require Exd and Hth as cofactors, and elucidating how *Hox* genes differentially regulate expression of downstream factors in contexts that do not require Exd/Hth cofactors. For example, Slatterly et al. (2011) recently reported a genome-wide analysis of Hth and Ubx DNA motif occupancy during development of the *Drosophila* metathoracic leg and haltere discs. They found several examples in both tissues of motifs that bound both Hth and Ubx, suggesting these factors are acting in concert in some contexts to regulate target gene expression, presumably in a complex including Exd. They also discovered motifs that bound either Hth or Ubx, but not both, which presumably reflects contexts where Ubx does not form a complex with Hth or Exd (and vice versa) when regulating target gene expression. Galant et al. (2002) found that Ubx did not

require Exd or Hth to repress expression of the wing gene *spalt* in the *Drosophila* haltere. In this case, they found that multiple Ubx monomer binding sites were found upstream of *spalt*, and that these multiple sites enabled Ubx to additively block *spalt* expression without Exd or Hth; whereas, reducing the number of binding sites resulted in an incomplete suppression of *spalt* expression. In another example, both Abd-A and Ubx require Hth and Exd as cofactors to block *Distal-less* expression in the legless *Drosophila* abdomen (Gebelein et al., 2002). On the other hand, Abd-B represses *hth* and *exd* expression in the abdominal segments 8 and 9, and blocks *Dll* expression in these segments through interactions with other cofactors (Sambrani et al., 2013). In order to determine shared and independent roles of *T. castaneum hth*/*exd* and *Hox* genes in *T. castaneum* metamorphosis, we compared phenotypes resulting from RNAi targeting these genes. We reasoned that in developmental contexts where a *Hox* gene requires Hth/Exd for normal function, RNAi targeting either that *Hox* gene or *hth*/*exd* would produce similar knockdown phenotypes. On the other hand, in developmental contexts where a *Hox* gene is performing developmental functions that do not require Hth/Exd, RNAi targeting that *Hox* gene or *hth*/*exd* would not produce similar knockdown phenotypes.

Hox *genes require* hth *and* exd *to specify segmental identity in the thorax and abdomen*

We found several cases of specification processes that required both *Hox* genes and *hth*/*exd*. We found that both *Scr* RNAi and *hth* RNAi result in the development of ectopic elytra on the prothorax. The transformation of the prothorax in response to *hth* RNAi (Fig. 4E) was much less severe than that produced by *Scr* RNAi (Fig. 4B). Although the development of ectopic wing tissue on the prothorax of *Drosophila* in response to loss of function of *hth* or *exd* has not been reported, RNAi targeting either *hth* or *Scr* causes the development of ectopic elytra

on the prothorax of horned beetles in the genus *Onthophaus* (Moczek and Rose, 2009; Walik et al., 2010). This suggests the existence of evolutionary ancient interactions between these genes in repressing elytra development within Coleoptera, and possibly other insect lineages. Also in the thorax, *Antp* (Fig. 4C) requires *hth*/*exd* (Fig. 4E–F) for development of mesonotal ridges. It is also possible that *Hox* genes require *hth*/*exd* to specify thoracic sternite identity, but the sternites were so reduced with either *hth* or *exd* RNAi that we could not determine if segmental identity transformations were occurring.

In the abdomen, we found that *Ubx* (Fig. 4D, 5F) required *hth*/*exd* (Fig. 5G, I) to repress thoracic identity in the first two abdominal segments. Transformations resulting from *Ubx* RNAi were much more severe than transformations resulting from *hth* or *exd* RNAi, and included the development of ectopic elytra (forewings) and legs on abdominal segments (Fig. 4D). Tomoyasu et al. (2005) previously reported the development of ectopic wing discs in the first abdominal segment of *T. castaneum* larvae in response to *Ubx* RNAi, and ectopic wing discs in abdominal segments 1–8 in response to simultaneous RNAi against *Ubx* and *abd-A*, suggesting both genes play roles in blocking wing development in the abdomen. Supporting this conclusion, RNAi targeting *Ubx* and *abd-A* in the beetle *Tenebrio molitor* resulted in six pairs of ectopic wings in the pupal abdomen (Ohde et al., 2013).

In severely affected *hth*, *exd*, and *abd-A* RNAi specimens, we found that the adult abdomen remained encased in the pupal cuticle, and the abdomens never fully sclerotized. Beeman et al. (1989) interpreted this lack of sclerotization in adult *T. castaneum abd-A* mutants as a transformation of posterior abdominal segments to anterior abdominal segment identity, either abdominal segment 1 or 2. The reduced size of the abdomen in specimens of *abd-A* RNAi treatments, and the fact that in moderately affected specimens abdominal segment 4 develops a

intercoxal process characteristic of abdominal segment 3 support the conclusion that *abd-A* blocks anterior abdominal segment identities during metamorphosis. The fact that the abdomen often remains stuck in the pupal molt in response to *hth*, *exd*, or *abd-A* RNAi might reflect shared metamorphic functions among these genes. However, we did not find reductions in the size of the abdomen in specimens of *hth* or *exd* RNAi treatments, as we would expect if these genes were required by *abd-A* to specify abdominal segment identity.

Interestingly, we found that *hth* and *exd* are required for abdominal segment 3 identity, evidenced by the loss of the intercoxal process and similarity of segment 3 to wild-type segment 4 in response to either RNAi targeting *hth* or *exd*. This segment, although transformed, remained fully sclerotized. This phenotype was not recovered in any *Hox* RNAi treatment. A similar phenotype was reported in response to *tiptop*/*teashirt* RNAi in *T. castaneum* (Shippy et al., 2008), suggesting that *hth* and *exd* may be determining the identity of this segment though interactions with this gene. This is not surprising, given the number of developmental roles shared between *hth*/*exd* and the *tiptop*/*teashirt* orthologues in *Drosophila* (Azpiazu and Morata, 2000; Azpiazu and Morata, 2002; Bessa et al., 2002; Casares and Mann, 2000; Wu and Cohen, 2000).

Finally, we found that *Abd-B* requires *hth* and *exd* for identity specification of abdominal segments 7 and 8. RNAi targeting any of these genes caused abdominal segment to develop a straight rather than rounded posterior margin (Fig. 5F–J), and abdominal segment 8 became sclerotized. This was surprising, given that *Abd-B* does not require *hth*/*exd* to impart segmental identity to the posterior abdominal segments in *Drosophila* (Sambrani et al., 2013). In contrast to the requirement of *hth*/*exd* in posterior abdominal sternite metamorphosis, *Abd-B* did not require *hth*/*exd* to specify genitalia. Transformations of abdominal sternite to tergite identity

have been reported for *Drosophila exd* null abdominal clones (González-Crespo and Morata, 1995). However, we did not recover transformations of abdominal sternites to tergites with either *hth* or *exd* RNAi.

hth/exd and Hox *genes specify identities along different axes during* Tribolium *metamorphosis*

RNAi targeting either *hth* or *exd* resulted in patterning defects of the labium, maxillae and legs, which included homeotic transformations of proximal elements to more distal identity (Angelini et al., 2012a, b; Fig. 1–3). We did not find evidence of segmental transformations of appendages in response to *hth* or *exd* RNAi. However, we did recover multiple transformations of appendage identity in response to RNAi targeting *Hox* genes, as expected given results of depletion of *Hox* function in *T. castaneum* embryogenesis (Brown et al, 2002) and embryogenesis (Chesboro et al., 2009; Hrycaj et al., 2010; Hughes and Kaufman, 2000) and metamorphosis of other species (Kaufman, 1978; Pattatucci et al., 1991; Percival-Smith et al., 1997; Pultz et al., 1988; Struhl 1981, 1982). *pb* RNAi resulted in transformation of the maxillary palps to legs (Fig. 2E) and double knockdowns of *pb* and *Dfd* resulted in transformations of these appendages to antennae (Fig. I–J). *pb* RNAi resulted in transformation of the labial palps to legs (Fig. 2E), *Scr* RNAi resulted in transformation of these appendages to maxillary palp identity (Fig. 2F), and double knockdowns of these genes resulted in these appendages adopting a mixed identity (Fig. 2H), possibly including leg identity proximally and antennal identity distally. In the legs, we found that *Scr* RNAi resulted in transformations of the prothoracic tibia to mesothoracic tibia identity (Fig. 3F), and the coxa adopted a rectangular shape, but the identity of the femur was not affected. *Ubx* RNAi caused the transformation of the metathoracic tarsus and tibia to mesothoracic identity (Fig. 2D; Fig. 3G), the proximal femur of both the

mesothoracic and metathoracic femurs to adopt a shape characteristic of the prothoracic femur (Fig. 2D), and the metathoracic and mesothoracic coxa to adopt a rectangular shape similar to that seen in the prothoracic leg with *Scr* RNAi.

Investigations of the roles of the *Hox* genes in leg identity specification in *Drosophila* predict that mesothoracic leg identity is the default identity that legs adopt in the absence of *Hox* activity (García-Bellido, 1977; Struhl, 1982). Our results suggest that in *T. castaneum*, in the default state, distal elements adopt mesothoracic identity, but the proximal femur adopts prothoracic femur morphology, while the coxa adopts a novel morphology, possibly representing an unspecified state. Although *Hox* RNAi resulted in homeotic transformations of appendages, the proximodistal podomere order in homeotically transformed appendages reflected the wild-type condition of the transformed appendage identity. This is in contrast with results of *hth*/*exd* RNAi, which included proximodistal transformations of podomere identity. Thus our results suggest that *hth*/*exd* and *Hox* genes independently specify different aspects of identity in the ventral appendages during metamorphosis.

It is clear that Hth/Exd are not cofactors of Hox factors in specifying appendage identities in distal appendage domains, because Hth and Exd are not nuclearly localized in distal appendage domains and thus play no role in gene regulation in these regions (Galant et al., 2002). Our data suggest that *Hox* genes do not require *hth*/*exd* as cofactors in specifying appendage identities in proximal appendage domains during metamorphosis either. This raises the question as to how *Hox* genes are modulating *hth* and *exd* activity so that correct appendage identities are produced in the proximal appendage domain of the gnathal appendages and legs. In *Drosophila* leg imaginal discs, Antp represses antennal identity by blocking Distal-less from binding to a *spineless* regulatory element that Distal-less activates in the antennal imaginal disc

(Duncan et al., 2010). We predict that regions of the genome bound by Hth/Exd in the proximal appendage domain of ventral appendages are also in part determined by regions of the genome bound by Hox factors, with appendage specific suites of Hox genes blocking specific suites of regulatory elements. This leads to appendage specific genomic Hth/Exd binding profiles, which results in appendage specific regulatory states. These appendage specific regulatory states ultimately cause the production of appendage specific proximal appendage morphologies.

Distinct mechanisms specify appendage identities during embryogenesis and metamorphosis

We have found that distinct mechanisms specify antennal identity in *T. castaneum* embryogenesis and metamorphosis (see Chapter 1). *Hox* genes are not expressed in the antennal segment during arthropod development (Hughes and Kaufman, 2002; Jager et al., 2006; Janssen and Damen, 2006; Manuel et al., 2006; Mittmann and Scholtz, 2003; Sharma et al., 2012). In order to test whether distinct mechanisms specify other appendage identities during embryogenesis and metamorphosis, here we compare the function of *Hox* genes between these two ontogenetic stages, and highlight apparent differences.

We have found evidence of differential embryonic and metamorphic regulation of the *Hox* gene *pb*. *pb* specifies maxillary identity during both *T. castaneum* embryogenesis (Beeman et al., 1993) and during metamorphosis (Fig. 1E). During embryogenesis, *pb* activity in the maxilla requires either Dfd or Scr, presumably because either of these factors are sufficient to activate embryonic *pb* expression in the maxilla (Brown et al., 2002). Therefore, loss of either Dfd or Scr independently has no effect on maxilla identity (Beeman et al., 1993; Brown et al., 1999; Curtis et al., 2001), but loss of Scr and Dfd concurrently results in a transformation of the maxilla to antennal identity because this leads to loss of *pb* expression (Brown et al., 2002). In

contrast, concurrently targeting *Dfd* and *Scr* with RNAi during *T. castaneum* metamorphosis does result in homeotic transformations of the maxillae (Fig. 1G). Scr also activates expression of *pb* in the labium (DeCamillis et al., 2001) during embryogenesis, and *Scr* loss of function causes a transformation of the larval labial palps to antennae (Beeman et al., 1993). In contrast, targeting *Scr* with RNAi during metamorphosis causes the labial palps to adopt maxillary palp identity rather than antennal identity (Fig. 1F). Results of our RNAi investigations suggest that *pb* expression is not regulated by other *Hox* genes in the maxillary and labial segments during metamorphosis. This explains why the maxilla retains its identity in response to concurrent *Dfd* and *Scr* RNAi; *pb* is still expressed during maxilla metamorphosis in specimens of this RNAi treatment. Likewise, *pb* remains expressed in the labium in specimens of *Scr* RNAi treatments, resulting in the labium adopting maxilla identity.

Our results also suggest interesting differences in the potential for homeotic transformation between embryogenesis and metamorphosis of the mandibles and legs. During *T. castaneum* embryogenesis, loss of *Dfd* function results in transformation of the mandibles to antennae (Brown et al., 1999; Brown et al., 2000; Coulcher and Telford, 2012). On the other hand, we did not recover homeotic transformations of the mandible with RNAi targeting *Dfd* during metamorphosis (Fig. 1C). However, concurrently targeting *Dfd* and *pb* with RNAi during metamorphosis resulted in transformations of the maxilla to antenna, unlike results of RNAi targeting either of these genes individually. Because there is no reason to expect *Dfd* RNAi to be more penetrant in the maxillae compared to the mandibles, we conclude that the lack of mandible transformations accompanying *Dfd* RNAi represents a true difference between embryonic and metamorphic mandible specification, rather than representing an incomplete knockdown of *Dfd* during mandible metamorphosis. Regarding legs, loss of function of *Antp* during *T. castaneum*

embryogenesis results in transformation of all legs to antennae (Beeman et al., 1993), but we did not recover homeotic transformations of legs in response to larval *Antp* RNAi. Our results suggest that mandible and leg identity are fixed during embryogenesis in *T. castaneum*, unlike antenna, maxilla, or labium identity.

Phylogenetic comparison of gnathal appendage identity specification in insects

Given the highly derived developmental mode of *Drosophila*, we expected to discover differences between the mechanisms producing differential segment morphologies between *Drosophila* and *T. castaneum*. Here we discuss one such example, identity specification of gnathal appendages, for which there is enough data from other insect species to make phylogenetic inferences. *Hox* genes specify gnathal appendage identities during both embryogenesis (Beeman et al., 1993; Brown et al., 1999; Brown et al., 2000; Brown et al., 2002; Coulcher and Telford, 2012; Curtis et al., 2001; DeCamillis et al., 2001) and metamorphosis in *T. castaneum* (Fig. 1). We recovered transformations of gnathal appendages toward leg identity in *T. castaneum* embryos in response to maternal *hth* RNAi (see Chapter 1), suggesting that the *Hox* genes require *hth* and *exd* to impart gnathal appendage identities during embryogenesis in this species. However, our data suggest that the *Hox* genes do not require *hth*/*exd* to specify adult gnathal appendage identities during metamorphosis (Fig. 1). In contrast, *exd* null clones produce leg bristles in the *Drosophila* proboscis (Rauskolb et al., 1995), suggesting that the *Hox* genes do require *hth*/*exd* to specify adult gnathal identities in this species.

Relevant data exists from two hemimetabolous insect species. In the milkweed bug *Oncopeltus fasciatus*, both embryonic *hth* RNAi (Angelini and Kaufman, 2004) and *pb* RNAi (Hughes and Kaufman, 2000) result in transformations of the labium to leg. RNAi targeting

either embryonic *hth* (Ronco et al., 2008) or *exd* (Mito et al., 2008) also results in transformation of gnathal appendages to legs in the cricket *Gryllus bimaculatus*. Based on data from *T. castaneum*, *O. fasciatus*, and *G. bimaculatus*, we infer the requirement of *hth*/*exd* for the *Hox* genes to specify gnathal appendage identity during embryogenesis as ancestral for insects, an embryonic plesiomorphy retained in holometabolous insects that produce appendages during this period.

In *Drosophila*, imaginal discs are produced during embryogenesis, but patterning and specification of ventral appendage identity takes place in ventral appendage discs throughout the larval period. This contrast with most other holometabolous insects, where ventral appendage identity is determined during embryogenesis, fixed throughout the larval period, and specified again during metamorphosis. Previously, based on a detailed comparison among insect species, we suggested that the antennal identity specification process in *Drosophila* is a concatenation of ancestral embryonic and metamorphic processes (see Chapter 1). This could also be true of the proboscis in this species, explaining the differences apparent in adult mouthpart identity specification between this species and *T. castaneum*. In this view, transformation of the adult *Drosophila* proboscis toward leg identity with loss of *exd* function reflects the activity of ancestral insect embryonic specification mechanisms during the earliest stages of identity specification of the adult *Drosophila* proboscis. Therefore, the lack of a requirement of *hth*/*exd* for *Hox* genes to specify gnathal identities during metamorphosis could be the ancestral state for holometabolous insects. This could be tested by investigating the metamorphic functions of *exd* and *hth* in mouthpart identity specification in species of Hymenoptera, the earliest diverging holometabolous insect class (Trautwein et al., 2012), that retain larval and adult ventral appendages.

Conclusion

The *Hox* genes require *exd* and *hth* for specifying sclerite identity in the thorax and abdomen during *T. castaneum* metamorphosis. However, *hth* and *exd* specify proximodistal podomere identities and the *Hox* genes specify appendage identities independently during metamorphosis. On the other hand, *Hox* genes do appear to require *hth* and *exd* to specify gnathal appendage identities during insect embryogenesis. *hth* and *exd* also play distinct embryonic and metamorphic roles in specifying antennal identity (see Chapter 1) as do the *Hox* genes in specifying the identities of more posterior appendages. *T. castaneum* present a practical system for investigating differences between embryogenesis and metamorphosis, because like most insects, this species produces appendages during both ontogenetic stages. Future studies could elucidate the genomic motifs that bind Hth/Exd, those that bind Hox proteins, and those that bind both Hth/Exd and Hox proteins, and differences in motif binding profiles between embryogenesis and metamorphosis. This would provide further insight into the production of unique morphologies during embryogenesis and metamorphosis in holometabolous insect.

References

Abu-Shaar, M., Ryoo, H.D., Mann, R.S., 1999. Control of the nuclear localization of Extradenticle by competing nuclear import and export signals. *Genes Dev.* 13, 935–945.

Abu-Shaar, M., Mann, R.S., 1998. Generation of multiple antagonistic domains along the proximodistal axis during *Drosophila* leg development. *Development* 125, 3821–3830.

Abzhanov, A., Holtzman, S., Kaufman, T.C., 2001. The *Drosophila* proboscis is specified by two *Hox* genes, *proboscipedia* and *Sex combs reduced*, via repression of leg and antennal appendage genes. *Development* 128, 2803–2814.

Angelini, D.R., Smith, F.W., Aspiras, A.C., Kikuchi, M., Jockusch, E.L., 2012. Patterning of the adult mandibulate mouthparts in the red flour beetle, *Tribolium castaneum*. *Genetics* 190, 639–654.

Angelini, D.R., Smith, F.W., Jockusch, E.L., 2012. Extent with modification: Leg patterning in the beetle *Tribolium castaneum* and the evolution of serial homologs. *G3 (Bethesda)* 2, 235–248.

Angelini, D.R., Jockusch, E.L., 2008. Relationships among pest flour beetles of the genus *Tribolium* (Tenebrionidae) inferred from multiple molecular markers. *Mol. Phylogenet. Evol.* 46, 127–141.

Angelini, D.R., Kikuchi, M., Jockusch, E.L., 2009. Genetic patterning in the adult capitate antenna of the beetle *Tribolium castaneum*. *Dev. Biol.* 327, 240–251.

Angelini, D.R., Kaufman, T.C., 2004. Functional analyses in the hemipteran *Oncopeltus fasciatus* reveal conserved and derived aspects of appendage patterning in insects. *Dev. Biol.* 271, 306–321.

Aspiras, A.C., Smith, F.W., Angelini, D.R., 2011. Sex-specific gene interactions in the patterning of insect genitalia. *Dev. Biol.* 360, 369–380.

Azpiazu, N., Morata, G., 2002. Distinct functions of *homothorax* in leg development in *Drosophila*. *Mech. Dev.* 119, 55–67.

Azpiazu, N., Morata, G., 2000. Function and regulation of *homothorax* in the wing imaginal disc of *Drosophila*. *Development* 127, 2685–2693.

Beeman, R.W., Stuart, J.J., Haas, M.S., Denell, R.E., 1989. Genetic analysis of the homeotic gene complex (HOM-C) in the beetle *Tribolium castaneum*. *Dev. Biol.* 133, 196–209.

Beeman, R.W., Stuart, J.J., Brown, S.J., Denell, R.E., 1993. Structure and function of the homeotic gene complex (HOM-C) in the beetle, *Tribolium castaneum*. *Bioessays* 15, 439–444.

Bessa, J., Gebelein, B., Pichaud, F., Casares, F., Mann, R.S., 2002. Combinatorial control of *Drosophila* eye development by *eyeless*, *homothorax*, and *teashirt*. *Genes Dev*. 16, 2415–2427.

Brown, S., DeCamillis, M., Gonzalez-Charneco, K., Denell, M., Beeman, R., Nie, W., Denell, R., 2000. Implications of the *Tribolium Deformed* mutant phenotype for the evolution of *Hox* gene function. *Proc. Natl. Acad. Sci. U. S. A.* 97, 4510–4514.

Brown, S.J., Shippy, T.D., Beeman, R.W., Denell, R.E., 2002. *Tribolium Hox* genes repress antennal development in the gnathos and trunk. *Mol. Phylogenet. Evol.* 24, 384–387.

Brown, S.J., Mahaffey, J.P., Lorenzen, M.D., Denell, R.E., Mahaffey, J.W., 1999. Using RNAi to investigate orthologous homeotic gene function during development of distantly related insects. *Evol. Dev.* 1, 11–15.

Carroll, S.B., 2001. Chance and necessity: The evolution of morphological complexity and diversity. *Nature* 409, 1102–1109.

Casares, F., Mann, R.S., 2001. The ground state of the ventral appendage in *Drosophila*. *Science* 293, 1477–1480.

Casares, F., Mann, R.S., 2000. A dual role for homothorax in inhibiting wing blade development and specifying proximal wing identities in *Drosophila*. *Development* 127, 1499–1508.

Casares, F., Mann, R.S., 1998. Control of antennal versus leg development in *Drosophila*. *Nature* 392, 723–726.

Chan, S.K., Popperl, H., Krumlauf, R., Mann, R.S., 1996. An extradenticle-induced conformational change in a HOX protein overcomes an inhibitory function of the conserved hexapeptide motif. *EMBO J.* 15, 2476–2487.

Chan, S.K., Jaffe, L., Capovilla, M., Botas, J., Mann, R.S., 1994. The DNA binding specificity of Ultrabithorax is modulated by cooperative interactions with Extradenticle, another homeoprotein. *Cell* 78, 603–615.

Chang, C.P., Shen, W.F., Rozenfeld, S., Lawrence, H.J., Largman, C., Cleary, M.L., 1995. Pbx proteins display hexapeptide-dependent cooperative DNA binding with a subset of hox proteins. *Genes Dev*. 9, 663–674.

Chesebro, J., Hrycaj, S., Mahfooz, N., Popadić, A., 2009. Diverging functions of Scr between embryonic and post-embryonic development in a hemimetabolous insect, *Oncopeltus fasciatus*. *Dev. Biol.* 329, 142–151.

Coulcher, J.F., Telford, M.J., 2012. *Cap'n'collar* differentiates the mandible from the maxilla in the beetle *Tribolium castaneum*. *Evodevo* 3, 25–9139–3–25.

Curtis, C.D., Brisson, J.A., DeCamillis, M.A., Shippy, T.D., Brown, S.J., Denell, R.E., 2001. Molecular characterization of *Cephalothorax*, the *Tribolium* ortholog of *Sex combs reduced*. *Genesis* 30, 12–20.

DeCamillis, M.A., Lewis, D.L., Brown, S.J., Beeman, R.W., Denell, R.E., 2001. Interactions of the *Tribolium Sex combs reduced* and *proboscipedia* orthologs in embryonic labial development. *Genetics* 159, 1643–1648.

Duncan, D., Kiefel, P., Duncan, I., 2010. Control of the *spineless* antennal enhancer: Direct repression of antennal target genes by Antennapedia. *Dev. Biol.* 347, 82–91.

Eriksson, B.J., Tait, N.N., Budd, G.E., Janssen, R., Akam, M., 2010. Head patterning and *Hox* gene expression in an onychophoran and its implications for the arthropod head problem. *Dev. Genes Evol.* 220, 117–122.

Galant, R., Walsh, C.M., Carroll, S.B., 2002. Hox repression of a target gene: extradenticle-independent, additive action through multiple monomer binding sites. *Development* 129, 3115–3126.

García-Bellido, A., 1977. Homoeotic and atavic mutations in insects. *Am. Zool.* 17, 613–629.

Gebelein, B., Culi, J., Ryoo, H.D., Zhang, W., Mann, R.S., 2002. Specificity of *Distalless* repression and limb primordia development by abdominal Hox proteins. *Dev. Cell.* 3, 487–498.

Gonzalez-Crespo, S., Morata, G., 1995. Control of *Drosophila* adult pattern by *extradenticle*. *Development* 121, 2117–2125.

Hrycaj, S., Chesebro, J., Popadić, A., 2010. Functional analysis of *Scr* during embryonic and post-embryonic development in the cockroach, *Periplaneta americana*. *Dev. Biol.* 341, 324–334.

Hughes, C.L., Kaufman, T.C., 2002. Hox genes and the evolution of the arthropod body plan. *Evol. Dev.* 4, 459–499.

Hughes, C.L., Kaufman, T.C., 2000. RNAi analysis of *Deformed*, *proboscipedia* and *Sex combs reduced* in the milkweed bug *Oncopeltus fasciatus*: novel roles for Hox genes in the hemipteran head. *Development* 127, 3683–3694.

Jager, M., Murienne, J., Clabaut, C., Deutsch, J., Le Guyader, H., Manuel, M., 2006. Homology of arthropod anterior appendages revealed by Hox gene expression in a sea spider. *Nature* 441, 506–508.

Janssen, R., Damen, W.G., 2006. The ten *Hox* genes of the millipede *Glomeris marginata*. *Dev. Genes Evol.* 216, 451–465.

Jockusch, E.L., Williams, T.A., Nagy, L.M., 2004. The evolution of patterning of serially homologous appendages in insects. *Dev. Genes Evol.* 214, 324–338.

Johnson, F.B., Parker, E., Krasnow, M.A., 1995. Extradenticle protein is a selective cofactor for the *Drosophila* homeotics: Role of the homeodomain and YPWM amino acid motif in the interaction. *Proc. Natl. Acad. Sci. U. S. A.* 92, 739–743.

Jürgens, G., 1984. Mutations affecting the pattern of the larval cuticle in *Drosophila melanogaster*. *Dev. Genes Evol.* 193, 283–295.

Kaufman, T.C., 1978. Cytogenetic analysis of chromosome 3 in *Drosophila melanogaster*: Isolation and characterization of four new alleles of the *proboscipedia* (*pb*) locus. *Genetics* 90, 579–596.

Kitzmann, P., Schwirz, J., Schmitt-Engel, C., Bucher, G., 2013. RNAi phenotypes are influenced by the genetic background of the injected strain. *BMC Genomics* 14, 5-2164–14-5.

Kurant, E., Pai, C.Y., Sharf, R., Halachmi, N., Sun, Y.H., Salzberg, A., 1998. *dorsotonals*/*homothorax*, the *Drosophila* homologue of *meis1*, interacts with *extradenticle* in patterning of the embryonic PNS. *Development* 125, 1037–1048.

LaRonde-LeBlanc, N.A., Wolberger, C., 2003. Structure of HoxA9 and Pbx1 bound to DNA: Hox hexapeptide and DNA recognition anterior to posterior. *Genes Dev.* 17, 2060–2072.

Lu, Q., Knoepfler, P.S., Scheele, J., Wright, D.D., Kamps, M.P., 1995. Both Pbx1 and E2A-Pbx1 bind the DNA motif ATCAATCAA cooperatively with the products of multiple murine *Hox* genes, some of which are themselves oncogenes. *Mol. Cell. Biol.* 15, 3786–3795.

Mann, R.S., Chan, S.K., 1996. Extra specificity from extradenticle: The partnership between HOX and PBX/EXD homeodomain proteins. *Trends Genet.* 12, 258–262.

Manton, S. M. (1977). The Arthropoda: Habits, Functional Morphology and Evolution. Oxford: Clarendon Press.

Manuel, M., Jager, M., Murienne, J., Clabaut, C., Le Guyader, H., 2006. Hox genes in sea spiders (Pycnogonida) and the homology of arthropod head segments. *Dev. Genes Evol.* 216, 481–491.

McGinnis, W., Garber, R.L., Wirz, J., Kuroiwa, A., Gehring, W.J., 1984. A homologous protein-coding sequence in *Drosophila* homeotic genes and its conservation in other metazoans. *Cell* 37, 403–408.

Mito, T., Ronco, M., Uda, T., Nakamura, T., Ohuchi, H., Noji, S., 2008. Divergent and conserved roles of *extradenticle* in body segmentation and appendage formation, respectively, in the cricket *Gryllus bimaculatus*. *Dev. Biol.* 313, 67–79.

Mittmann, B., Scholtz, G., 2003. Development of the nervous system in the "head" of *Limulus polyphemus* (Chelicerata: Xiphosura): Morphological evidence for a correspondence between the segments of the chelicerae and of the (first) antennae of Mandibulata. *Dev. Genes Evol.* 213, 9–17.

Moczek, A.P., Rose, D.J., 2009. Differential recruitment of limb patterning genes during development and diversification of beetle horns. *Proc. Natl. Acad. Sci. U. S. A.* 106, 8992–8997.

Neuteboom, S.T., Peltenburg, L.T., van Dijk, M.A., Murre, C., 1995. The hexapeptide LFPWMR in Hoxb-8 is required for cooperative DNA binding with Pbx1 and Pbx2 proteins. *Proc. Natl. Acad. Sci. U. S. A.* 92, 9166–9170.

Ohde, T., Yaginuma, T., Niimi, T., 2013. Insect morphological diversification through the modification of wing serial homologs. *Science* 340, 495–498.

Pai, C.Y., Kuo, T.S., Jaw, T.J., Kurant, E., Chen, C.T., Bessarab, D.A., Salzberg, A., Sun, Y.H., 1998. The Homothorax homeoprotein activates the nuclear localization of another homeoprotein, Extradenticle, and suppresses eye development in *Drosophila*. *Genes Dev.* 12, 435–446.

Pattatucci, A.M., Otteson, D.C., Kaufman, T.C., 1991. A functional and structural analysis of the *Sex combs reduced* locus of *Drosophila melanogaster*. *Genetics* 129, 423–441.

Peifer, M., Wieschaus, E., 1990. Mutations in the *Drosophila* gene *extradenticle* affect the way specific homeo domain proteins regulate segmental identity. *Genes Dev.* 4, 1209–1223.

Percival-Smith, A., Weber, J., Gilfoyle, E., Wilson, P., 1997. Genetic characterization of the role of the two HOX proteins, Proboscipedia and Sex combs reduced, in determination of adult antennal, tarsal, maxillary palp and proboscis identities in *Drosophila melanogaster*. *Development* 124, 5049–5062.

Phelan, M.L., Rambaldi, I., Featherstone, M.S., 1995. Cooperative interactions between HOX and PBX proteins mediated by a conserved peptide motif. *Mol. Cell. Biol.* 15, 3989–3997.

Posnien, N., Bucher, G., 2010. Formation of the insect head involves lateral contribution of the intercalary segment, which depends on *Tc-labial* function. *Dev. Biol.* 338, 107–116.

Posnien, N., Schinko, J., Grossmann, D., Shippy, T.D., Konopova, B., Bucher, G., 2009. RNAi in the red flour beetle (*Tribolium*). *Cold Spring Harb Protoc.* 2009, pdb.prot5256.

Pultz, M.A., Diederich, R.J., Cribbs, D.L., Kaufman, T.C., 1988. The *proboscipedia* locus of the *Antennapedia* complex: A molecular and genetic analysis. *Genes Dev.* 2, 901–920.

Rauskolb, C., Smith, K.M., Peifer, M., Wieschaus, E., 1995. *extradenticle* determines segmental identities throughout drosophila development. *Development* 121, 3663–3673.

Rauskolb, C., Peifer, M., Wieschaus, E., 1993. *extradenticle*, a regulator of homeotic gene activity, is a homolog of the homeobox-containing human proto-oncogene *pbx1*. *Cell* 74, 1101–1112.

Rieckhof, G.E., Casares, F., Ryoo, H.D., Abu-Shaar, M., Mann, R.S., 1997. Nuclear translocation of Extradenticle requires Homothorax, which encodes an Extradenticle-related homeodomain protein. *Cell* 91, 171–183.

Ronco, M., Uda, T., Mito, T., Minelli, A., Noji, S., Klingler, M., 2008. Antenna and all gnathal appendages are similarly transformed by *homothorax* knock-down in the cricket *Gryllus bimaculatus*. *Dev. Biol.* 313, 80–92.

Ryoo, H.D., Mann, R.S., 1999. The control of trunk Hox specificity and activity by Extradenticle. *Genes Dev.* 13, 1704–1716.

Ryoo, H.D., Marty, T., Casares, F., Affolter, M., Mann, R.S., 1999. Regulation of Hox target genes by a DNA bound Homothorax/Hox/Extradenticle complex. *Development* 126, 5137–5148.

Sambrani, N., Hudry, B., Maurel-Zaffran, C., Zouaz, A., Mishra, R., Merabet, S., Graba, Y., 2013. Distinct molecular strategies for Hox-mediated limb suppression in *Drosophila*: From cooperativity to dispensability/antagonism in TALE partnership. *PLoS Genet.* 9, e1003307.

Scott, M.P., Weiner, A.J., 1984. Structural relationships among genes that control development: Sequence homology between the *Antennapedia*, *Ultrabithorax*, and *fushi tarazu* loci of *Drosophila*. *Proc. Natl. Acad. Sci. U. S. A.* 81, 4115–4119.

Sharma, P.P., Schwager, E.E., Extavour, C.G., Giribet, G., 2012. *Hox* gene expression in the harvestman *Phalangium opilio* reveals divergent patterning of the chelicerate opisthosoma. *Evol. Dev.* 14, 450–463.

Shippy, T.D., Tomoyasu, Y., Nie, W., Brown, S.J., Denell, R.E., 2008. Do *teashirt* family genes specify trunk identity? Insights from the single *tiptop/teashirt* homolog of *Tribolium castaneum*. *Dev. Genes Evol.* 218, 141–152.

Slattery, M., Ma, L., Negre, N., White, K.P., Mann, R.S., 2011. Genome-wide tissue-specific occupancy of the Hox protein Ultrabithorax and Hox cofactor Homothorax in *Drosophila*. *PLoS One* 6, e14686.

Slattery, M., Riley, T., Liu, P., Abe, N., Gomez-Alcala, P., Dror, I., Zhou, T., Rohs, R., Honig, B., Bussemaker, H.J., Mann, R.S., 2011. Cofactor binding evokes latent differences in DNA binding specificity between Hox proteins. *Cell* 147, 1270–1282.

Snodgrass, R.E., 1935. Principles of Insect Morphology. Cornell University Press, Ithaca.

Sokoloff, A., 1972. The Biology of Tribolium, Volume 1. Clarendon Press, Oxford.

Struhl, G., 1982. Genes controlling segmental specification in the *Drosophila* thorax. *Proc. Natl. Acad. Sci. U. S. A.* 79, 7380-7384.

Struhl, G., 1981. A homoeotic mutation transforming leg to antenna in *Drosophila*. *Nature* 292, 635–638.

Tomoyasu, Y., Wheeler, S.R., Denell, R.E., 2005. *Ultrabithorax* is required for membranous wing identity in the beetle *Tribolium castaneum*. *Nature* 433, 643–647.

Tomoyasu, Y., Denell, R.E., 2004. Larval RNAi in *Tribolium* (Coleoptera) for analyzing adult development. *Dev. Genes Evol.* 214, 575–578.

Trautwein, M.D., Wiegmann, B.M., Beutel, R., Kjer, K.M., Yeates, D.K., 2012. Advances in insect phylogeny at the dawn of the postgenomic era. *Annu. Rev. Entomol.* 57, 449–468.

Van der Meer, J., 1977. Optical clean and permanent whole mount preparation for phase-contrast microscopy of cuticular structures of insect larvae. *Dros. Inf. Serv* 52, 160.

van Dijk, M.A., Peltenburg, L.T., Murre, C., 1995. Hox gene products modulate the DNA binding activity of Pbx1 and Pbx2. *Mech. Dev.* 52, 99–108.

van Dijk, M.A., Murre, C., 1994. *extradenticle* raises the DNA binding specificity of homeotic selector gene products. *Cell* 78, 617–624.

Wasik, B.R., Rose, D.J., Moczek, A.P., 2010. Beetle horns are regulated by the *Hox* gene, *Sex combs reduced*, in a species- and sex-specific manner. *Evol. Dev.* 12, 353–362.

Wu, J., Cohen, S.M., 2000. Proximal distal axis formation in the *Drosophila* leg: Distinct functions of *teashirt* and *homothorax* in the proximal leg. *Mech. Dev.* 94, 47–56.

Yao, L.C., 1999. A common mechanism for antenna-to-leg transformation in *Drosophila*: Suppression of *homothorax* transcription by four HOM-C genes. *Dev. Biol.* 211, 268–276.

Tables

Table 1. Developmental genes investigated in this study. The GenBank accession numbers that were used to design primers to clone these genes are provided. Abbreviation: LG, linkage group.

Gene name	Symbol	Protein class	LG	GenBank
homothorax	*hth*	TALE class homeobox TXF	7	NM_001039400
extradenticle	*exd*	TALE class homeobox TXF	10	NM_001039412
labial	*lab*	homeobox TXF	2	NM_001114290
Deformed	*Dfd*	homeobox TXF	2	NM_001039421
proboscipedia	*pb*	homeobox TXF	2	NM_001114335
Sex combs reduced	*Scr*	homeobox TXF	2	NM_001039434
Antennapedia	*Antp*	homeobox TXF	2	NM_001039416
Ultrabithorax	*Ubx*	homeobox TXF	2	NM_001039408
abdominal-A	*abd-A*	homeobox TXF	2	NM_001039429
Abdominal-B	*Abd-B*	homeobox TXF	2	NM_001039430

Table 2. Results of larval RNAi. For the for single *Hox* RNAi experiments, the size and concentration used in RNAi experiments of two non-overlapping dsRNA fragments is provided. For double or triple knockdown *Hox* RNAi experiments, the size and concentration of all *Hox* dsRNAs used in the experiment are provided. Mildly affected specimens exhibited morphological defects, such as fusions between appendage segments, but did not exhibit

homeoses. Moderately affected specimens exhibited homeotic transformations of appendages and sclerites, but did not exhibit ectopic structures. Severely affected specimens exhibited homeoses, which included the appearance of ectopic ventral appendages and wings on segments that normally lack these structures. Abbreviation: bp, base pairs.

dsRNA sequence	dsRNA size (bp)	Concentration (μg/μl)	Number scored	Phenotypic penetrance			
				Unaffected	Mild	Moderate	Severe
GFP	600	1.00	65	90.77%	9.23%	0.00%	0.00%
hth	174	1.00	177	0.00%	8.19%	90.06%	1.75%
exd	236	1.00	43	0.00%	4.65%	95.35%	0.00%
lab	372	1.00	94	100.00%	0.00%	0.00%	0.00%
Dfd	373, 622	1.00, 0.60	106	10.38%	89.62%	0.00%	0.00%
pb	372, 624	1.00, 3.00	99	0.00%	0.00%	100.00%	0.00%
Scr	333, 422	1.00, 0.60	51	3.92%	23.53%	49.02%	23.53%
Antp	333, 624	1.00, 2.70	24	0.00%	100.00%	0.00%	0.00%
Ubx	522, 232	1.00, 0.70	36	0.00%	0.00%	44.44%	55.56%
abd-A	372, 486	1.00, 1.00	39	2.56%	10.26%	87.18%	0.00%
Abd-B	373, 522	1.00, 1.00	97	1.03%	15.46%	83.51%	0.00%
Dfd, *pb*	373, 372	0.50, 0.50	35	8.57%	0.00%	91.43%	0.00%
Dfd, *Scr*	373, 333	0.50, 0.50	37	0.00%	89.19%	10.81%	0.00%
pb, *Scr*	372, 333	0.50, 0.50	93	1.08%	2.15%	96.77%	0.00%
Dfd, *pb*, *Scr*	373, 372, 333	0.33, 0.33, 0.33	39	5.13%	2.56%	92.31%	0.00%
Scr, *Antp*	333, 333	0.50, 0.50	54	1.85%	18.52%	79.63%	0.00%
Antp, *Ubx*	333, 522	0.50, 0.50	26	0.00%	0.00%	53.85%	46.15%
Scr, *Antp*, *Ubx*	333, 333, 522	0.33, 0.33, 0.33	45	0.00%	0.00%	51.11%	48.89%

Figure 1. *T. castaneum* mouthpart phenotypes resulting from larval RNAi. Affected mouthpart elements are labeled in red. In cases where a mouthpart element is homeotically transformed to the identity of a different appendage, the element is labeled with the homeotic identity in italics. (A–B) Wild-type maxillae, labium (A) and mandible (B) morphologies are recovered in *GFP* RNAi treatments. Black arrowheads point to the distal sensory fields on the maxillary and labial palps. *Dfd* RNAi affects both mandible (C) and maxilla (D) morphology, but does not alter the identity of these appendages. Red arrowhead points to deformed lateral edge of mandible. (E) *pb* RNAi results in transformations of both the maxillary and labial palps to leg identity (compare to leg morphologies in Fig. 2). (F) *Scr* RNAi results in transformation of the distal labial palpomere to distal maxillary palpomere identity. (G) Double RNAi knockdowns of *Dfd* and *Scr* dsRNA resulted in a combination of the phenotypes produced in *Dfd* RNAi (D) and *Scr* RNAi (F) specimens. (H) Double RNAi knockdowns of *pb* and *Scr* resulted in a transformation of the maxillary palps to legs and the labial palps to a mixed identity (red arrowheads; see text). (I) Double RNAi knockdowns of *Dfd* and *pb* result in transformation of the maxillary palps to antennae and the labial palps to legs. (J) Head of *Dfd* and *pb* RNAi double knockdown specimen. (K) *Dfd*, *pb*, and *Scr* RNAi triple knockdowns resulted in transformation of the maxillary palps to antenna and the labial palps to adopt a mixed identity (red arrowheads; see text). (L) Head of *Dfd*, *pb*, and *Scr* RNAi triple knockdown specimen. (M–N) *hth* RNAi specimens. N shows a severely affected specimen. (O–P) *exd* RNAi specimens. P shows a severely affected specimen. Both *hth* and *exd* RNAi result in transformations of proximal palpomeres to more distal identity, and cause fusions between and losses of mouthpart elements. Abbreviations: ant, antenna; cd, condyle; crd, cardo; dt, distal tooth; gal, galea; il, incisor lobe; lac, lacinia; lig, ligula; lp, labial palpomere; mnt, mentum; mp, maxillary palpomere; plf,

palpifer; plf; paliger; pmt, prementum; stp, basal sclerite of stipes; tth, tooth. See figure two for abbreviations of leg anatomy.

Figure 1.

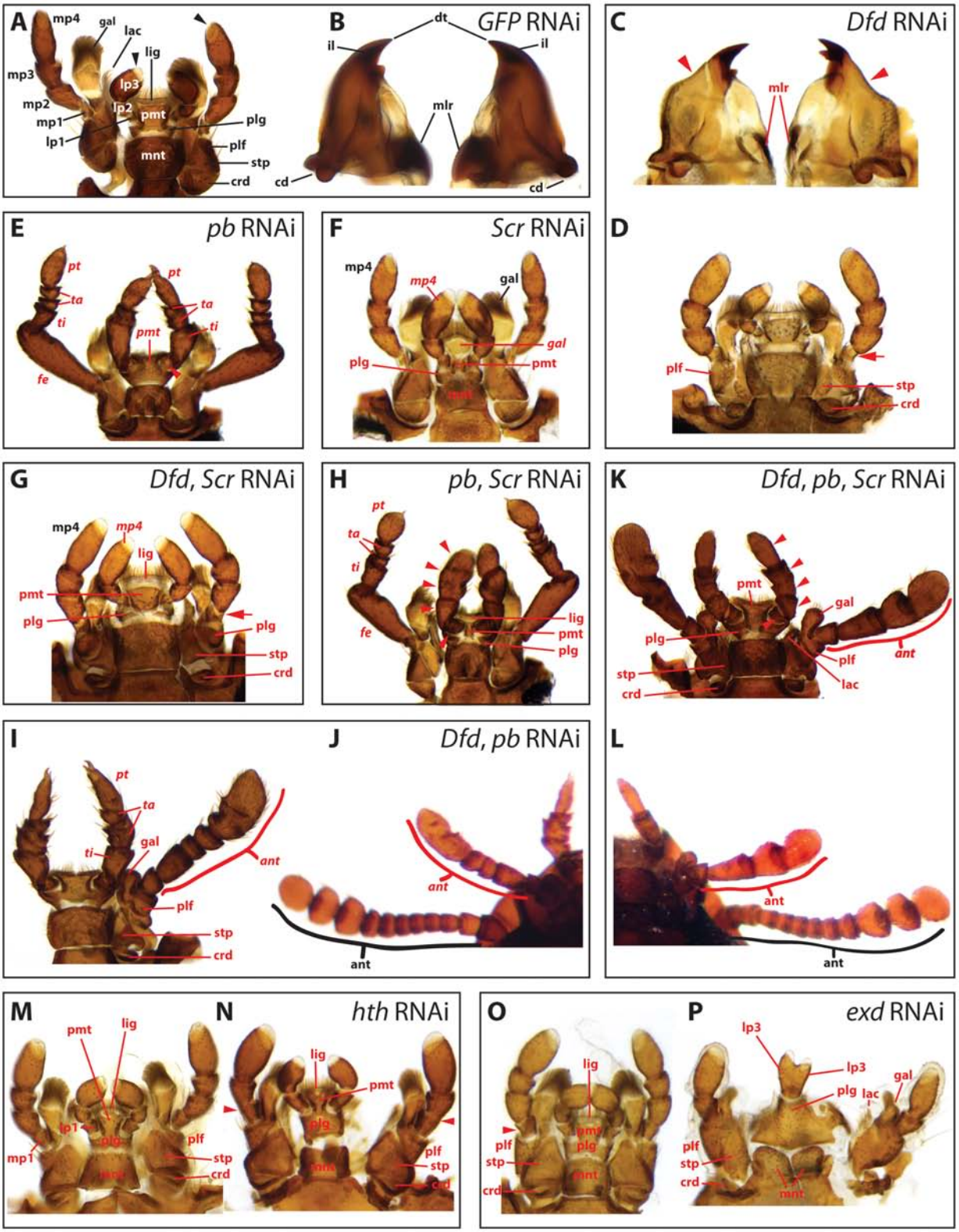
A
mp4
gal
lac
lig
mp3
lp3
mp2
lp2
pmt
mp1
plg
lp1
plf
mnt
stp
crd
cd
B
GFP RNAi
dt
il
il
mlr
cd
C
Dfd RNAi
mlr
D
plf
stp
crd
E
pb RNAi
pt
pt
ta
ta
ti
ti
pmt
fe
F
Scr RNAi
mp4
mp4
gal
gal
plg
pmt
mnt
G
Dfd, Scr RNAi
mp4
mp4
lig
pmt
plg
plg
stp
crd
H
pb, Scr RNAi
pt
ta
ti
fe
lig
pmt
plg
K
Dfd, pb, Scr RNAi
pmt
gal
plg
ant
plf
lac
stp
crd
I
J
Dfd, pb RNAi
pt
ta
gal
ti
ant
plf
stp
crd
ant
ant
L
ant
M
N
hth RNAi
pmt
lig
lp1
plg
plf
mp1
stp
crd
lig
pmt
plg
plf
stp
O
P
exd RNAi
lp3
lig
lp3
plg
lac
gal
plf
stp
crd
pmt
plg
plf
stp
crd
mnt

Figure 2. *T. castaneum* leg phenotypes resulting from larval RNAi. Affected leg elements are labeled in red. Italic symbols represent segmental transformations of leg podomeres. (A) Wild-type morphology exhibited by *GFP* RNAi specimens. Asterisk denotes the proximal concave slope of the dorsal femur, specific to the prothoracic leg. (B) *Scr* RNAi causes a transformation of the prothoracic tibia toward mesothoracic tibia identity and causes the coxa to adopt a rectangular shape. (C) *Antp* RNAi does not affect leg morphology or identity. (D) *Ubx* RNAi results in both the mesothoracic and metathoracic coxae to adopt a rectangular shape, and the femurs of these legs to approach prothoracic femur morphology. The tibia and tarsus of the metathoracic leg are transformed to mesothoracic identity. (E–F) *hth* and *exd* RNAi result in transformations of proximal leg podomeres to more distal identity. Note the tibial spur on the trochanter (E). Abbreviations: c, coxa; fe, femur; pt, pretarsus; t, tarsomere; ti, tibia; tr, trochanter; sp, tibial spur; T1, prothoracic leg; T2, mesothoracic leg; T3, metathoracic leg.

Figure 2.

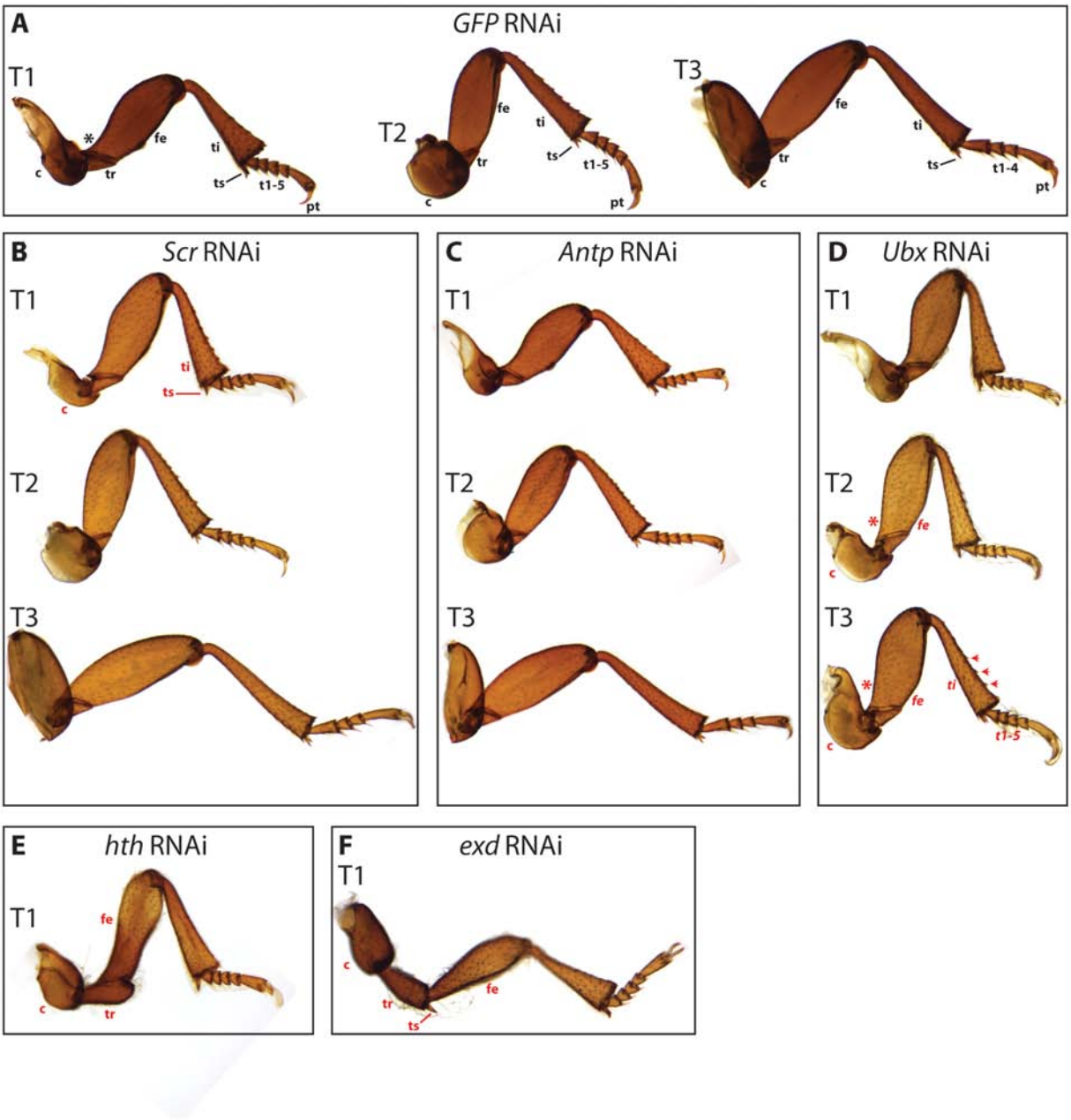
A
GFP RNAi
T1
T2
T3
fe
ti
tr
c
ts
t1-5
t1-4
pt
B
Scr RNAi
C
Antp RNAi
D
Ubx RNAi
E
hth RNAi
F
exd RNAi

Figure 3. Scanning electron micrographs and *Hox* expression profiles of legs. Homeotically transformed elements are labeled in red. (A) Wild-type prothoracic leg. (B) Subapical tibial setae are found along the dorsal (white arrowheads) and ventral (black arrowheads) edges of the wild-type prothoracic distal tibia. Note the robust medial spur (arrow). (C) Subapical tibial setae are found along the dorsal edge (arrowheads) of the wild-type mesothoracic leg. Note the slender tibial spur (arrow). (D) Wild-type metathoracic distal tibia lack subapical setae. Note the slender medial spur (arrow). (E) Mesothoracic leg of an *hth* RNAi specimen. Note the cuticular sculpting pattern that resembles distal tibia cuticle (compare to C). (*E*) Magnification of boxed region in E. Note the presence of ectopic apical setae, normally found along distal edge of tibia. (F) Distal tibia of *Scr* RNAi specimen. Note the slender medial tibial spur. (G) Distal tibia of *Ubx* RNAi specimen. Note the presence of subapical setae (red arrowheads). (H–K) Pupal *Hox* expression profiles. *rsp18* was amplified from each cDNA sample as a positive control and a 235 base pair *rsp18* fragment can be seen at the bottom of each lane. (H) Expression profile of thoracic *Hox* genes from cDNA prepared from whole bodies of *T. castaneum* pupae. A 422 base pair fragment of *Scr*, a 483 base pair fragment of *Antp*, and a 648 base pair fragment of *Ubx* were detected. Expression profiles of *Scr* (I), *Antp* (J), and (*Ubx*) in cDNA prepared from prothoracic, mesothoracic, or metathoracic pupal legs. Hash mark to the left in J denotes 483 bp. Hash mark to the left in K denotes 648 bp. Abbreviations: bp, base pairs; T1, prothoracic leg; T2, mesothoracic leg; T3, metathoracic leg.

Figure 3.

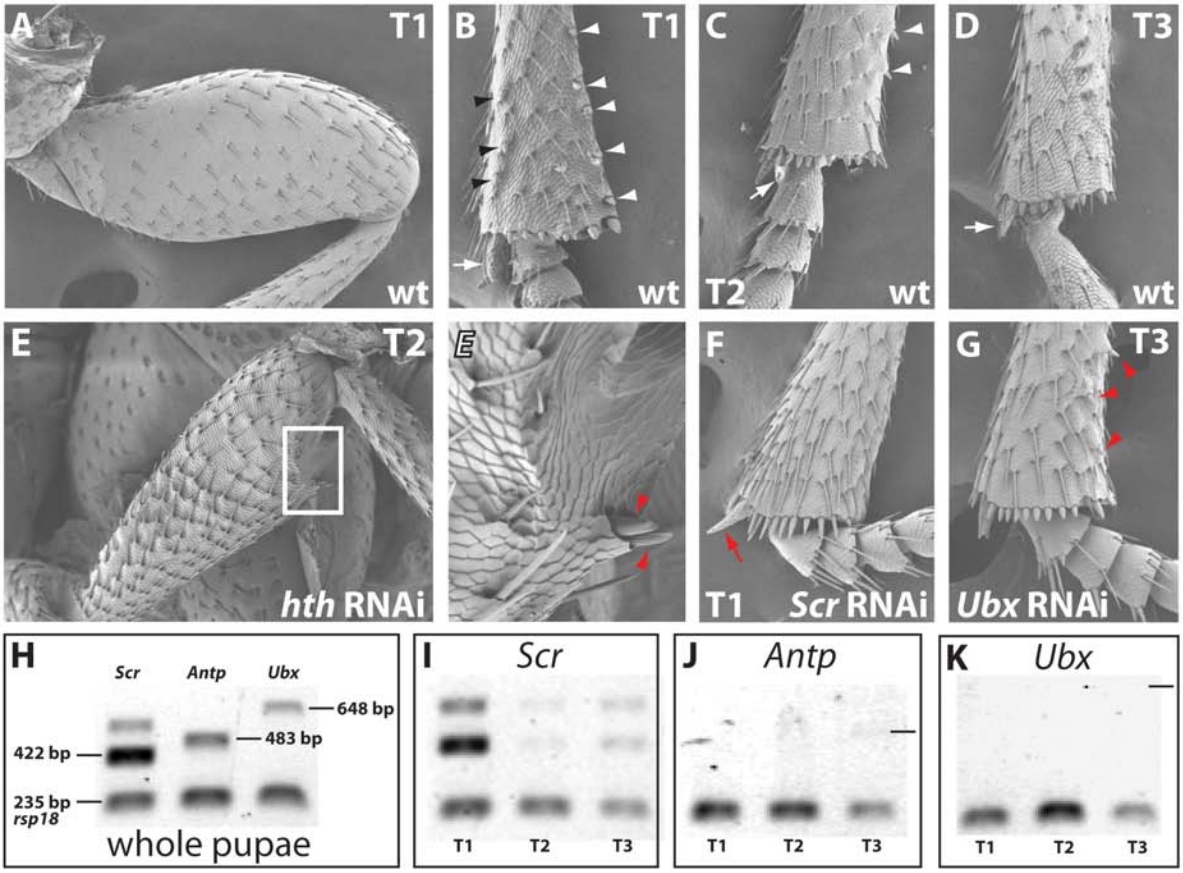
A
T1
wt
B
T1
wt
C
T2
wt
D
T3
wt
E
T2
hth RNAi
E
F
T1
Scr RNAi
G
T3
Ubx RNAi
H
Scr
Antp
Ubx
648 bp
483 bp
422 bp
235 bp
rsp18
whole pupae
I
Scr
T1
T2
T3
J
Antp
T1
T2
T3
K
Ubx
T1
T2
T3

Figure 4. *T. castaneum* thoracic sclerite phenotypes resulting from larval RNAi. Affected elements are labeled in red. Homeotically transformed structures are labeled with the homeotic identity in italics. (A–D) Dorsal views are in top panels and ventral views are in lower panels. (A) Thorax of *GFP* RNAi specimen. (B) *Scr* RNAi results in the development of ectopic elytra on the prothorax. (C) *Antp* RNAi results in loss of the scutoscutellar ridge of the mesonotum (top panel) and a transformation of the mesosternellum to prosternellum (bottom panel). (D) *Ubx* RNAi results in transformation of the metathorax and first abdominal segment to mesothoracic identity. The metathoracic sternite is transformed to mesothoracic sternite (*ms2*) and the membranous wing is transformed to elytron (*el2*). Ectopic elytra (*el3*) and a leg (*L3*) are present on the first abdominal segment. (E–F) Left panels are dorsal views and right panels are ventral views. (E) *hth* RNAi. Ectopic elytron tissue is present on the prothorax, the mesonotum lacks ridges, and the ventral sternites are reduced. (F) *exd* RNAi results in phenotypes similar to *hth* RNAi. Legs have been removed to view sternites. Abbreviations: A, abdominal segment; elytra, el; epimeron, ep; L, leg; ml, mesosternellum; mr, medial ridge; ms, mesothoracic sternite; msn, mesonotum; mt, metathoracic sternite; mtn, metanotum; mw, membranous wing; ps, prosternal process; pts, prothoracic sternite; ptt, prothoracic tergite; sr, scutoscutellar ridge.

Figure 4.

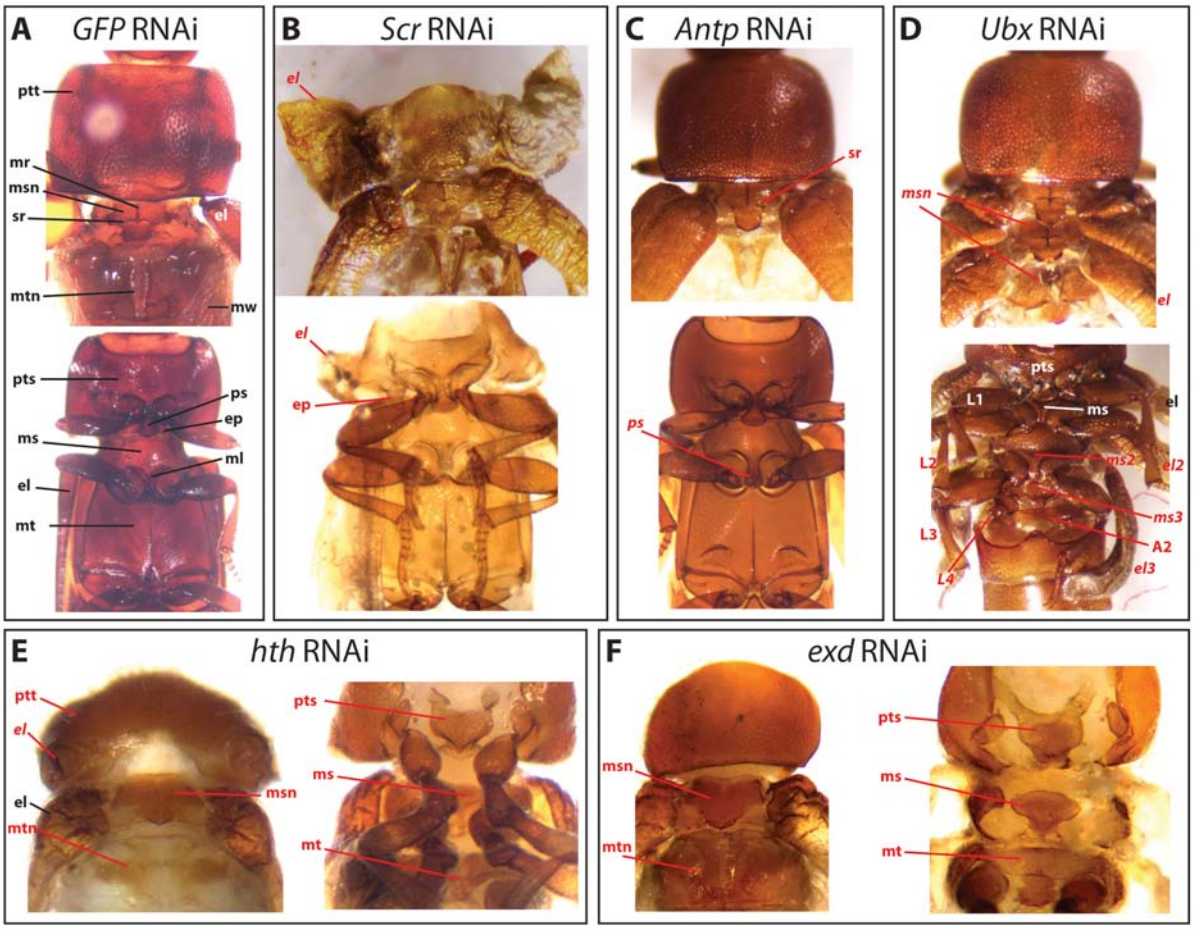
A GFP RNAi
ptt
mr
msn
sr
el
mtn
mw
pts
ps
ep
ms
ml
el
mt
B Scr RNAi
el
el
ep
C Antp RNAi
sr
ps
D Ubx RNAi
msn
el
pts
L1
ms
el
L2
ms2
el2
ms3
L3
A2
el3
L4
E hth RNAi
ptt
el
el
mtn
msn
pts
ms
mt
F exd RNAi
msn
mtn
pts
ms
mt

Figure 5. *T. castaneum* abdominal phenotypes resulting from larval RNAi. Affected elements are labeled in red. Homeotically transformed structures are labeled with the homeotic identity in italics. (A) Abdomens of *GFP* RNAi specimens exhibit wild-type morphology. (B) *abd-A* RNAi causes homeotic transformations of segments 4–7 to more anterior abdominal segment identity. (C–D) *Abd-B* RNAi results in transformation of abdominal segments 7–9 to more anterior abdominal segment identity. (D) The female genitalia became heavily sclerotized. (E) The male aedeagus becomes bipronged and sclerotized. (F) *Ubx* RNAi results in exposure and sclerotization of the first and second abdominal segments. (G–J) *hth* and *exd* RNAi results in exposure and sclerotization of the first two abdominal segments, transformation of the third abdominal segment to more posterior abdomen identity (note the loss of the intercoxal process), and transformations of posterior abdominal segments to more anterior abdominal identity. Abbreviation: ip, intercoxal process.

Figure 5.

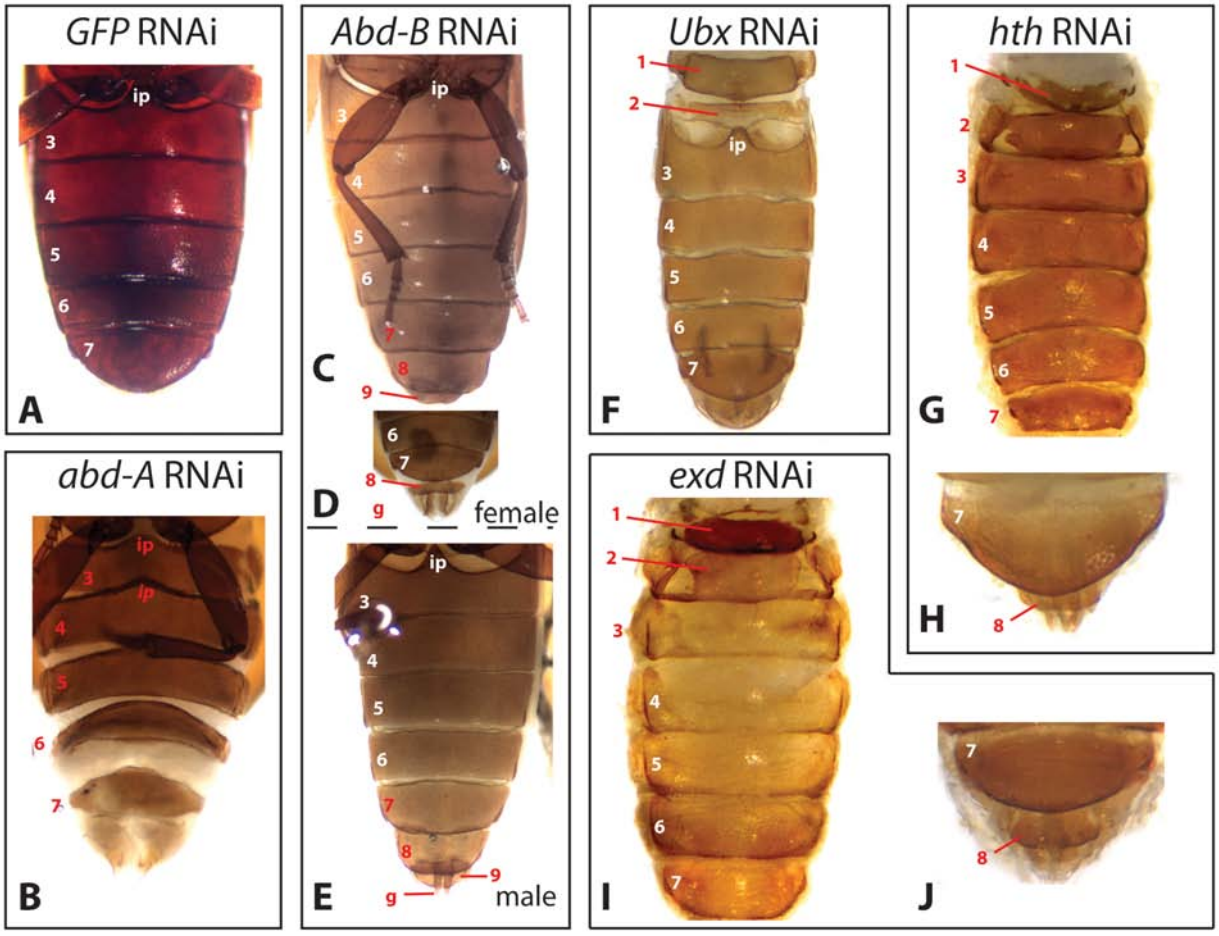
GFP RNAi
ip
3
4
5
6
7
A
Abd-B RNAi
ip
3
4
5
6
7
8
9
C
6
7
8
g
female
D
ip
3
4
5
6
7
8
9
g
male
E
Ubx RNAi
1
2
ip
3
4
5
6
7
F
hth RNAi
1
2
3
4
5
6
7
G
7
8
H
abd-A RNAi
ip
3
ip
4
5
6
7
B
exd RNAi
1
2
3
4
5
6
7
I
7
8
J

Supplementary Figure 1. Results of *T. brevicornis hth* and *exd* RNAi. Top panels show mouthparts and bottom panels shows dorsal thoraces. (A) Results of *GFP* RNAi. (B–C) Results of *hth* (B) and *exd* (C) RNAi. Arrowheads point to ectopic elytra tissue on the prothorax. Abbreviations are as in Figure 1.

Supplementary Figure 1.

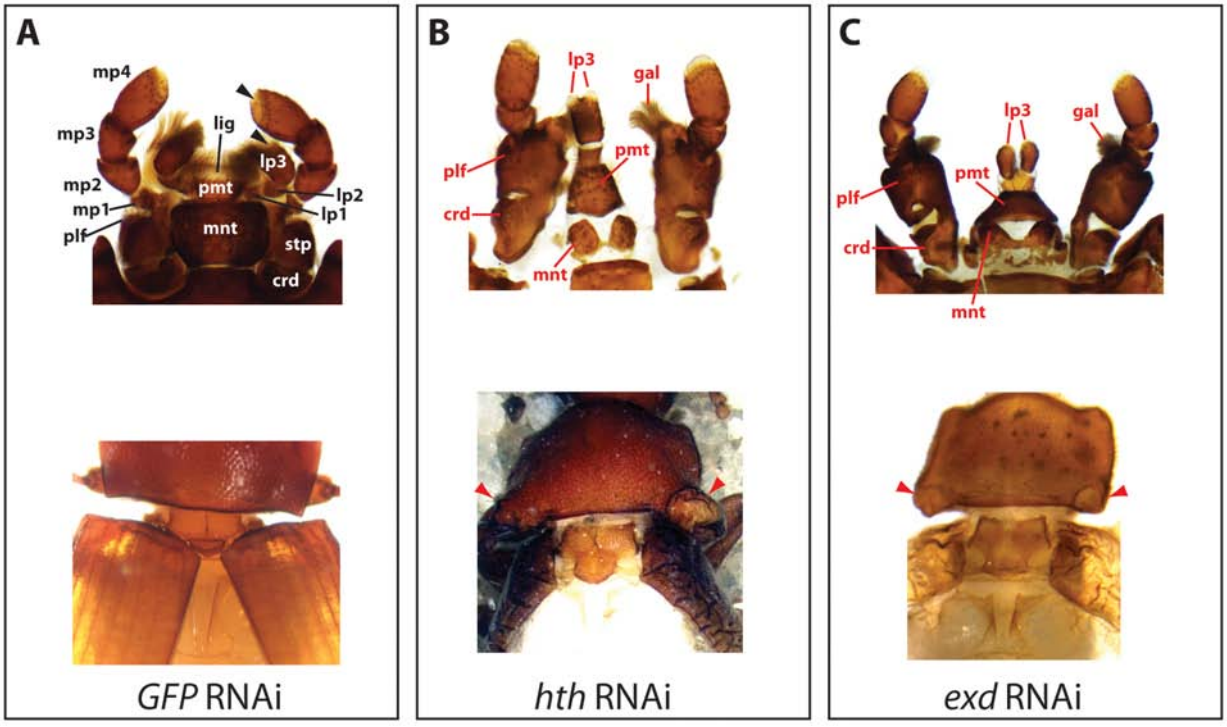

Chapter 3.

All trunk segments exhibit distinct ventral morphologies in the tardigrade *Hypsibius dujardini*

Introduction

The phylum Tardigrada is composed of microscopic invertebrate animals known for their remarkable ability to survive hostile environments, including extremes in temperature, pressure, salinity, radiation, and even the vacuum of outer space (Horwikawa et al., 2006; Jönsson et al., 2008; Møbjerg et al., 2013; Seki et al., 1998). Tardigrada is an ancient lineage, with a fossil record extending back to the Cambrian period (Maas and Waloszek, 2001). Extant tardigrade species inhabit marine, freshwater, and terrestrial habitats (Brusca and Brusca, 2003; Kinchin, 1994). Roughly 1030 extant species of tardigrades have been described; they are placed in three classes, the Heterotardigrada, Mesotardigrada, and Eutardigrada. The class Mesotardigrada was erected based on a single specimen named *Thermozodium esakii*, which has been lost, and no further specimens have been found, casting doubt on the existence of this class (Guil and Giribit, 2011). The class Heterotardigrada includes two orders, the Arthrotardigrada and the Echiniscoidea, which include 40.5% of described tardigrade species (Guil and Giribit, 2011). Eutardigrada are composed of the Apochela and the Parachela, and include 59.5% of described tardigrade species.

The body plan of Tardigrada includes a head and four trunk segments (Brusca and Brusca, 2003; Kinchin, 1994; Manton, 1977; Nielsen, 2001). Each trunk segment houses a pair

of lobopodal legs and leg morphology is very similar between segments. Tardigrada shares a body plan composed of segments and ventral appendages with the phyla Onychophora and Arthropoda. These characters are interpreted as synapomorphies, uniting these three phyla in the superphylum Panarthropoda (Brusca and Brusca, 2003; Budd, 1996; Budd, 2001a, b; Dewel and Dewel, 1996; Nielsen, 2001). Surprisingly, the first taxonomically well-sampled multigene molecular analyses of Metazoa failed to support monopholy of Panarthropoda, instead suggesting a closer affinity between Tardigrada and the roundworm phylum Nematoda (Dunn et al., 2008; Philippe et al., 2005). This result was likely an artifact due to long-branch attraction (Budd and Telford, 2009). A more recent taxonomically well-sampled phylogenomic analysis recovered a highly supported monophyletic Panarthropoda, with Arthropoda and Onychophora forming a clade that is the sister taxon of Tardigrada (Campbell et al., 2011).

Besides the first segment that likely had eyes of some sort, the body plan of the panarthropod ancestor is thought to have been constructed of homonomous (i.e., very similar) body segments, which each housed a pair of lobopodal (i.e., unjointed) appendages (Budd, 2001a, b; Budd and Telford, 2009; Grenier, 1997; Ma et al., 2009; Manton, 1977; Shubin et al., 1997; Snodgrass, 1935). Arthropoda is by far the most speciose animal phylum (Grimaldi and Engel, 2005), and much of the evolutionary success of arthropods can be attributed to the evolution of distinct (i.e., heteronomous) segmental morphologies and tagmosis patterns (Carroll, 2001) in this lineage. To a much lesser degree, the onychophoran body plan also exhibits distinct segmental morphologies and tagmosis patterns. This lineage exhibits a head composed of three segments, each housing a morphologically and functionally distinct pair of appendages, and homonomous trunk segments, each housing a pair of legs (Brusca and Brusca, 2003).

The fossil record suggests distinct segmental morphologies and tagmosis patterns evolved independently in the onychophoran and arthropod lineages (Eriksson et al., 2010; Ma et al., 2009). However, during development, very similar patterning processes differentiate the anterior four segments of both onychophorans and arthropods. For example, the genes *six3* and *orthodenticle* (*otx*) are expressed in the ocular segment, the anterior most segment, and are thought to both play roles in specifying this segment during embryogenesis in both Onychophora and Arthropoda (Eriksson et al., 2013; Posnien et al., 2009; Steinmetz et al., 2010). In both phyla, *six3* is expressed in the anterior most part of the ocular segment, anterior to the region that gives rise to the eyes, while *otx* is expressed in the developing eyes and the cells surrounding the eyes. A conserved regulatory code involving *Hox* genes specifies more posterior segments in both phyla (Eriksson et al., 2010; Hughes and Kaufman, 2002; Jager et al., 2006; Janssen and Damen, 2006; Manuel et al., 2006; Sharma et al., 2012). The second segment lacks *Hox* gene expression, and the morphology of this segment represents the default state that emerges in the absence of *Hox* genes (Brown et al., 2002). The anterior most expression boundaries of the *Hox* genes *labial* (*lab*) and *proboscipedia* (*pb*) align with the anterior boundary of the third segment, while the anterior boundary of *Deformed* (*Dfd*) aligns with the anterior boundary of the fourth segment. Expression of *Dfd* differentiates the third and fourth segments in both phyla. These conserved expression patterns suggest that the developmental mechanisms that differentiate the anterior segments already existed in the ancestor of Onychophora and Arthropoda. Why would the ancestor of these two phyla, which lacked obvious morphological distinctions between segments, already possess the developmental machinery to produce morphologically distinct anterior segments?

It is possible that the *Hox* genes originally patterned organ systems, such as the muscular and nervous system, that exhibited distinct segmental patterns, but that are not preserved in fossils. Tardigrada are the only extant lineage of panarthropodans that retain the heteronomous segmental body plan architecture of the panarthropod ancestor. The discovery of hidden segmental diversity in tardigrades would support a panarthropod ancestor that exhibited subtle morphological distinctions of the anterior segments. To test for segmental diversity in Tardigrada, we stained the nervous system of *Hypsibius dujardini* with a β-tubulin antibody and the muscle system with phalloidin, then analyzed the segmental structure of these systems with confocal microscopy. Our results demonstrate that each trunk segment of *H. dujardini* exhibits unique muscle patterns and the ventral ganglion of the fourth trunk segment is morphologically distinct from the other trunk ganglia. These results suggest that internal morphological aspects of the anterior segments were already differentiated in the panarthropodan ancestor. The activity of conserved mechanisms that differentiate anterior segments in Onychophora and Arthropoda is sufficient to explain the development of segmental diversity in Tardigrada.

Materials and methods

Choice of tardigrade species

The eutardigrade species *Hypsibius dujardini* was chosen for this study. This species is an ideal system for investigating the tardigrade body plan and the developmental mechanisms producing it, for several reasons. First, *H. dujardini* is easily cultured, providing unlimited access to embryos for experimentation (Gabriel et al., 2007). Second, the feasibility of

embryonic studies of gene expression (Gabriel and Goldstein, 2007) and gene function through RNAi (Tenlen et al., 2013) has been demonstrated for this species. Lastly, a *H. dujardini* genome sequencing project is in progress (Goldstein, pers. comm.), which will facilitate future developmental genetic studies.

Maintaining tardigrade cultures

Our line of *H. dujardini* was originally collected from a benthic pond sample in Darcy Lever, Bolton, Lancashire, England (Gabriel et al., 2007), and has been maintained in culture since 1987. For this study, tardigrade cultures were maintained in 60 mm polystyrene petri dishes in 12.5 ml of Poland Springs brand water. Tardigrades were fed a diet of *Chlorococcum sp*. algae. *Chlorococcum sp*. cultures were grown in a 250 ml Erlenmeyer flask, in 100 ml of modified Bold's basal medium (Bold, 1949; McManus and Lewis, 2011), on a C1 Platform Shaker (New Brunswick Scientific) set to speed 20, using a desk lamp as a light source. 1 ml of algal solution was added to each culture. Cultures were inspected weekly, and fresh water was added to the cultures to offset evaporation. Subcultures were prepared at least once a month and parent cultures were allowed to expire. We have maintained our *H. dujardini* cultures for over 3 years with this method.

Specimen relaxation and fixation

A mixture of juvenile and reproductively mature *H. dujardini* specimens was collected for this study. Tardigrades tend to contract their muscles during the fixation process, making it difficult to interpret anatomy. To avoid this issue, specimens were relaxed in carbonated water for 1 hour before fixation. At the end of this hour, the bodies of specimens appeared turgid and

the appendages were completely extended. Specimens were fixed in 4% EM Grade Paraformaldehyde (Electron Microscopy Sciences) in PB-Triton (1X phosphate-buffered saline, 0.1% Triton X-100, pH 7.4) for 15 minutes at room temperature. Specimens were used immediately for staining of the muscle or nervous systems, as described below.

Anti β-tubulin immunostaining

We stained the nervous system of *H. dujardini* using a monoclonal anti β-tubulin antibody (Chu and Klymkowsky, 1989; E7, Developmental Studies Hybridoma Bank), following a slightly modified version of a protocol previously used to stain α-tubulin in a different tardigrade species (Zantke et al., 2008). Fixation was followed by three 5 minute and four 30 minute rinses in PB-Triton. At this point, the specimens were in a 1.5 ml microcentrifuge tube filled with 1 ml of PB-Triton. Specimens were then permeabilized by sonicating them for 25 seconds with an FS30 sonicater (Fisher Scientific) filled with 850 ml of water. This was followed by three 10 minute and four 30 minute washes in PB-Triton with 0.2% Bovine Serum Albumin and two 30 minute washes in PB-Triton with 5% normal goat serum (NGS). Specimens were then incubated at 4° C overnight in a 1:100 dilution of β-tubulin antibody in PB-Triton+NGS. This incubation period was followed by three 5 minute and four 30 minute washes in PB-Triton. Specimens were then washed twice for 30 minutes in PB-Triton+NGS. This was followed by an overnight incubation at 4° C in a 1:200 dilution of a goat anti-mouse Cy3 conjugated secondary antibody (Jackson ImmunoResearch). This incubation period was followed by three 5 minute and six 30 minute washes in PB-Triton.

Phalloidin staining

We stained muscle cells with Oregon Green 488 phalloidin (Molecular Probes), which binds actin filaments, following a slightly modified version of the protocol used by Halberg et al. (2009). Fixation was followed by four 15 minute and an overnight wash in PB-Triton with 0.1% NaN_3. Specimens were then incubated at room temperature for 27 hrs in a 1:40 dilution of phalloidin in PB-Triton with 0.1% NaN_3. Following phalloidin incubation, specimens were rinsed 3 times for 5 minutes in PB-Triton.

Specimen preparation, imaging, and analysis

Before mounting on slides, specimens were taken through a glycerol series, which included 1 hour washes in 5%, 10%, 20%, and 40% glycerol in PB-Triton. Specimens were then mounted on slides in Fluoromount-G (SouthernBiotech) with 1.5 µg/ml 4', 6-diamidino-2-phenylindole (DAPI) added to counterstain nuclei. Differential interference contrast (DIC) micrographs were taken on a Zeiss Axioskop or a Nikon A1R Spectral Confocal Microscope. Z-series of phalloidin (N=8) and anti β-tubulin (N=3) stained specimens were taken on a Nikon A1R Spectral Confocal Microscope. Figi (Abràmoff et al., 2004; Rasband, 1997–2012; Schindelin et al., 2012; Schneider et al., 2012) was used for image analysis and processing. The merge function in Figi was used to produce images showing data from multiple confocal channels. Depth coded images were produced using the Temporal-Color Code function in Figi. Maximum projection images were produced using the maximum intensity option of the Z Project function in Figi. Contrast and brightness of whole images were adjusted in Adobe Photoshop CS4.

Results

Like other tardigrades, *H. dujardini* possess a head and four trunk segments. A pair of ventral legs is found in each trunk segment (Fig. 1A). A series of claws attach to the distal tip of each leg (Fig. 1D). The head lacks legs, but has an internal pharyngeal apparatus (Fig. 1A–B) suggested to be derived from an ancestral pair of head appendages (Halberg et al., 2009; Nielsen, 2001). The pharyngeal apparatus includes a muscular pharyngeal bulb and stylets that are used in feeding (Fig. 1B). The mouth is found at the very anterior end of the head (Fig. 1A). Below we describe the nervous and muscular systems of *H. dujardini*. We base our morphological nomenclature on that developed in previous investigations of different tardigrade species (Table 1).

Nervous system anatomy

The *H. dujardini* nervous system is composed of an anterior brain, a pair of ventral nerve cords, and a peripheral nervous system composed of many smaller nerves. In DAPI stained specimens, two bilaterally symmetrical pairs of brain lobes, outer lobes and inner lobes, were detected, along with a ventral lobe that was not paired (Fig. 2). In anti β-tubulin stained specimens, two nerves, the outer connective and the inner connective, could be seen extending from both the right and left anterior of the first trunk ganglion into the brain (Fig. 3C–E). Paired anterior, dorsal, and posterior clusters of intense β-tubulin expression were detected in the brain (Fig. 3D–E). These clusters were associated with low cell body numbers as detected by DAPI staining (data not shown), suggesting they may represent collections of axons innervating sensory fields. The outer connective extends dorsally to the dorsal cluster near the eye. The

inner connective extends to the posterior cluster of the inner brain lobe (Fig. 3C–D). Anti β-tubulin immunostaining also revealed connectives extending from the first trunk ganglion to the ventral lobe (Fig. 3C, E). Several nerves extend posteriorly from the brain along the sides of the pharyngeal bulb (Fig. 3C–E). No evidence of a subesophogeal ganglion or a stomatogastric ganglion was found.

Four ganglia are found along the ventral nerve cords, one for each trunk segment (Fig. 3A). Each ganglion includes a single dense cluster of cell bodies. Within each ganglion, the ventral nerve cords swell to roughly three times the width of the connectives between the ganglia. The ventral nerve cords are connected by commissures that extend across the cell clusters of each ganglion (Fig. 3A, C–D, G). We did not detect commissures outside the ganglia. Nerves extend from each ganglion into the legs of the segment in which the ganglion is found. The first three ganglia are wider than the fourth ganglion (Fig. 3A, G). For example, in the specimen shown in Fig. 3A, from ganglion 1 to 4, the maximum widths of the ganglia measured 12.4 µm, 12.8 µm, 13.4 µm, and 8.0 µm, respectively.

β-tubulin expression was also detected in the stomach of the *H. dujardini* specimens. DAPI stained nuclei within the stomach had roughly two times the diameter of somatic *H. dujardini* nuclei found outside the stomach (N=7 nuclei in stomach, average diameter=4.28 µm, standard deviation=0.80; N=7 somatic nuclei, average diameter=2.09, standard deviation=0.32). Expression of tubulin in the stomach has not been reported for other tardigrade species. It is possible that this difference is due to the different tubulin antibody used in this study (anti β-tubulin) compared to previous studies (anti α-tubulin) (Mayer et al., 2013; Persson et al., 2012; Zantke et al., 2008). However, given that the anti β-tubulin antibody reacts with β-tubulin in

Chylamydomonas (Developmental Studies Hybridoma Bank), which are algae, it seems likely that the cells observed in the stomach are algal gut contents.

General muscle anatomy

The most conspicuous aspect of the anterior muscle system of *H. dujardini* is the pharyngeal apparatus, which includes a large muscular pharynx, a ventral muscle strand and a dorsal muscle strand that both extend from the base of the left stylet to the base of the right stylet, and muscles that extend posteriorly from either stylet, and form sheet muscles connecting to the dorsal pharyngeal bulb (Fig. 4A, C–D). Two pairs of longitudinal dorsal muscle strands extend from anterior to the pharyngeal bulb along the dorsum to the posterior end (Fig. 4E–F). One strand of each pair extends to the very distal tip of the fourth leg, while the other strand of each pair extends to the base of the fourth leg. Ventrally, muscle strands extend longitudinally from anterior of either side of the pharyngeal bulb to the distal tip of the fourth legs (Fig. 4E–F). These ventral longitudinal muscle strands widen in the trunk region, run directly above the base of the first three legs, and terminate in the fourth leg, where they each form a sheet muscle along the posterior edge of the leg. Three pairs of muscle strands extend from the sides of the ventral part of the body in a dorsoanterior direction, align outside the outer muscle strands, and continue to extend anteriorly (Fig. 4F). Several thin dorsoventral muscle strands extend along the body wall and intersect the inner or outer muscle strands of either pair of dorsal longitudinal muscle strands (Fig. 4E–F). Muscle strands extend from the legs to the ventral median attachment sites and dorsally along the body wall to the dorsal muscle strands (Fig. 4E; see below).

Ventral median attachment sites

Seven ventral median muscle attachment sites are found in *H. dujardini* and other tardigrade species (Fig. 5; Halberg et al., 2009; Schmidt-Rhaesa and Kulessa, 2007). Muscles attaching at the ventral median attachment sites extend to the base of the legs or into the legs, run along the ventral muscle strands, run dorsally to the dorsal muscle strands, extend dorsoanteriorly, or extend anteriorly along the ventral muscle bands. We analyzed the structures of these attachment sites in seven phalloidin-stained *H. dujardini* specimens to look for consistent differences between segments. All ventral median attachment sites were bilaterally symmetrical and morphology of these sites was consistent between specimens. Because each attachment site is bilaterally symmetrical, below we provide anatomical details, in roughly anteroposterior order, for one half of each attachment site.

The first ventral median attachment site includes six muscle pairs. None make contact medially (Fig. 4B; Fig. 5A). A muscle strand extends anteriorly. Next, two thin muscle strands extend into the first leg and a thin muscle strand extends across the body into the contralateral first leg. These are followed by two thick muscle strands that extend to the base of the second leg. The second ventral median attachment site includes three pairs of muscles, all of which make contact medially. The anterior-most muscle strand of the second attachment site extends into the ipsilateral first leg, where it forms a sheet muscle along the posterior wall of the leg (Fig. 4B–C; Fig. 5B, left). Next, a muscle strand extends dorsally along the body wall, bifurcating close to the attachment site. The posterior-most muscle of the second attachment site extends posteriorly to the base of the ipsilateral second leg.

The third ventral median attachment site includes five muscle pairs. None make contact medially (Fig. 4C; Fig. 5C). The anterior-most muscle strand of the third attachment site extends

dorsoanteriorly along the ventral muscle strands. This muscle is followed by a muscle strand that extends into the ipsilateral second leg. Two thin muscle strands extend dorsally from the third attachment site along the body wall. These are followed by a muscle strand that extends to the base of the ipsilateral third leg.

The architecture of ventral median attachment site 4 is like that of attachment site 2 (Fig. 4B–C; Fig. 5B, right). In this case, the anterior-most muscle of the attachment site runs into the second leg and the posterior-most muscle strand runs to the base of third leg. Ventral median attachment site 5 is similar to attachment site 3 (Fig. 4B–C; Fig. 5D). In this case, the posterior-most muscle strand extends from attachment site 5 laterally into the third leg. However, no posteriorly directed muscle strands are present, unlike in attachment site 3.

Two pairs of muscle strands, all of which make contact medially, are present at ventral median attachment site 6 (Fig. 4B–C; Fig. 5E). The anterior muscle strand of attachment site 6 extends laterally into the ipsilateral third leg and forms a sheet muscle along the posterior of the leg. A posterior muscle splits into two muscle strands that run dorsally along the body wall. Four muscle pairs extend from ventral median attachment site 7. None make contact medially (Fig. 4B–C; Fig. 5F). The anterior-most muscle strand extends dorsoanteriorly to the outermost ipsilateral dorsal muscle strand. It is followed by two thin muscle strands that extend dorsally along the body wall. Finally a muscle strand extends to the base of the posterior-most ipsilateral leg.

Leg muscles

The first three pairs of legs share similar muscle anatomy, which differs from the muscle anatomy of the fourth leg pair. Laterally, a single muscle attaches distally to the base of the

claws in the legs of the first three pairs and extends to the inner strand of the dorsal longitudinal muscles (Fig. 6A). Although the arrangement of muscles is the same in the first three pairs of legs, the distally connected muscle strand is much wider at the distal end in the second and third leg pairs than in the first leg pair. In the specimen shown in Fig. 6A, at their widest point, the muscle strands of the second and third leg both measure 2.1 μm, while the corresponding muscle strand in the first leg only measures 1.0 μm at its widest point. We found no distinction in muscle architecture in the medial regions of the first three leg pairs (Fig. 6B). The similarities observed here between leg pairs two and three compared to the first leg pair are consistent with the pattern reported for the leg muscles of two other tardigrade species, *Milnesium tardigradum* and an unidentified *Hypsibius* species (Schmidt-Rhaesa and Kulessa, 2007). The presence of muscle sheets in the posterior of legs distinguishes *H. dujardini* from the unidentified *Hypsibius* species studied by Schmidt-Rhaesa and Kulessa (2007). Because the legs of the *Hypsibius* species in the previous study lacked muscle sheets found in our species (Fig. 6B, D), we conclude that it was not *H. dujardini.*

Discussion

The tardigrade nervous system and its relationship to that of Arthropoda

Evolutionary interpretations of several aspects of tardigrade nervous system morphology have been quite contentious. Testing the various hypotheses that have been presented is critical for reconstructing the ancestral panarthropodan body plan and the developmental mechanisms that produced it. Investigations of both heterotardigrade (Dewel and Dewel, 1996; Kristensen

and Higgins, 1984a, b) and eutardigrade (Mayer et al., 2013; Persson et al., 2012; Zantke et al., 2008; this study) brain morphology have been performed, although high-resolution technology has only been used in studies of brain anatomy of eutardigrade species. In general, there is agreement that the tardigrade nervous system includes a brain and a pair of ventral nerve cords, but disagreement remains about the number of lobes composing the brain, whether all the lobes are paired, and the existence of a subesophogeal ganglion.

Most studies of both eutardigrade and heterotardigrade species have detected three brain lobes (Dewel and Dewel, 1996; Persson et al., 2012; Kristensen and Higgins, 1984a, b; Mayer et al., 2013; Nielsen, 2001; this study). However, Zantke et al. (2008) detected only two brain lobes in the eutardigrade species *Macrobiotus hufelandi*. On the other hand, Mayer et al. (2013) detected three lobes in *Macrobiotus harmsworthi*, suggesting that a three-lobed brain is plesiomorphic for Tardigrada. All the above studies agree on the existence of paired inner and outer brain lobes. However, of the studies that report a ventral brain lobe, there is disagreement on whether this lobe is paired (*Halobiotus crispae*, Persson et al., 2012; *Echiniscus viridissimus*, Dewel and Dewel, 1996) or a single structure (Mayer et al., 2013). In this respect, our results agree with the conclusion of Mayer et al. (2013) that the ventral lobe is an unpaired structure. However, it is possible that the ventral lobe of *H. dujardini*, and other tardigrades, originates from paired *anlagen* during development.

Three evolutionary interpretations of the tardigrade brain lobes have been presented; all attempt in some way to homologize the tardigrade brain with the arthropod brain. The tripartite brain of arthropods includes the protocerebrum, deuterocerebrum, and tritocerebrum. These three brain lobes are thought to have evolved from the ganglia present in the first three segments of an arthropod ancestor (Scholtz and Edgecomb, 2006). In the "tripartite" hypothesis of

tardigrade brain composition, the three lobes of the tardigrade brain are directly homologous with the three segments of the arthropod brain with the inner lobe of the tardigrade brain homologized with the protocerebrum, the outer lobe with the deuterocerebrum, and the ventral lobe with the tritocerebrum (Kristensen, 1983; Nielsen, 2001). The implication of this hypothesis is that the tardigrade head is composed of parts of at least three ancestral segments. The "protocerebral" hypothesis suggests that the tardigrade brain is composed of just a single segment that aligns with the protocerebral segment of arthropods (Mayer et al., 2013; Zantke et al., 2008). The "fusion" hypothesis suggests that the entirety of the tardigrade brain aligns with just the protocerebrum of arthropods, but that both the arthropod protocerebrum and the tardigrade brain comprise nervous tissue of three ancestral anterior segments (Dewel and Dewel, 1996).

We reject the "fusion" hypothesis since current agreement in the literature, based on morphology and surveys of gene expression, is that the arthropod brain is composed of nervous tissue of three segments, with the protocerebrum representing nervous tissue of the anterior-most segment. Since most biologists are only concerned with the relationship of the tardigrade brain to the arthropod brain, the "fusion" hypothesis of Dewel and Dewel (1996) suggesting that the protocerebrum of the ancestor of arthropods and tardigrades was composed of three cryptic segments is irrelevant to most discussions.

Criticism of the "tripartite" hypothesis centers on the assumption that each lobe of a tardigrade brain represents a ganglion. However, each segment of the arthropod brain is composed of several parts, so there is no reason to expect that the tri-lobed tardigrade brain is composed of multiple segments, rather than a single segment with multiple parts (Zantke et al., 2008). There is no other direct evidence that the tardigrade brain lobes represent distinct ganglia

homologous to trunk ganglia. In the trunk, the ganglia are composed of dense clusters of cells, presumably the perikarya of neurons, with thick bands of β-tubulin expression along their ventrolateral edges, which presumably represent the axons of the neurons composing the ganglia (Fig 3). However, the brain lobes of *H. dujardini* lack thick bands of β-tubulin expression. The regions of the brain that exhibit the highest levels of β-tubulin expression, the anterior, dorsal, and posterior clusters, are in regions of very low cell body density. This does not match the pattern expected if the brain lobes are homologous to ganglia. Differences in what these same researchers recognize as a ganglion likely also explain the contradictory reports of presence (Kristensen and Higgins, 1984a, b; Persson et al., 2012) or absence (Mayer et al., 2013; Zantke et al., 2008; this study) of a subesophogeal ganglion among tardigrade species. In our view, sufficient evidence has not been presented by Kristensen and Higgins (1984a, b) or Persson et al. (2012) to buttress their claims of the existence of a subesophogeal ganglion in tardigrades.

Investigations of segmentation genes could provide a solution to the composition of the tardigrade head. Gabriel and Goldstein (2007) reported a stripe of expression of the segmentation gene *engrailed* (*en*) in the posterior of each body segment during *H. dujardini* embryogenesis. However, no extra stripes of *en* expression were detected in the head, even though a stripe of *en* expression is found within each segment of the arthropod head. Zantke et al. (2008) presented this as evidence of a tardigrade head composed of a single segment. On the other hand, a tardigrade head composed of multiple segments could have evolved by the loss of the *en* stripes that ancestrally demarcated the boundaries between these segments.

Molecular phylogenies contradict an important assumption of the "tripartite" hypothesis. Earlier reconstructions of the tardigrade brain were based on the assumption that tardigrades were the sister phylum of Arthropoda (Dewel and Dewel, 1996; Budd, 1996). However, recent

molecular analyses consistently recover a sister relationship between Arthropoda and Onychophora (Dunn et al., 2008; Campbell et al., 2011). Results of a *Hox* gene expression study in the onychophoran *Euperipatoides kanangrensis* suggested that the first three segments of Onychophora align directly with the protocerebral, deuterocerebral, and tritocerebral segments of Arthropoda (Eriksson et al. 2010). Based on brain development and anatomy of the onychophoran species *Euperipatoides rowelli* and *Epiperipatus isthmicola*, Mayer et al. (2010) suggested that the onychophoran brain is composed of nervous tissue of the anterior two segments, and is thus bipartite. Mayer et al. (2010) concluded that the tritocerebrum is a synapomorphy of Arthropoda, and therefore cannot be part of the tardigrade brain, in discordance with the "tripartite" hypothesis. However, it is possible that the simplicity of the onychophoran brain is secondarily derived, which would allow the ancestral panarthropodan to possess a brain composed of parts of three anterior segments.

As with results of embryonic *en* expression, lack of evidence of segmentation can always be interpreted as reflecting the highly derived nature of a multi-segmented head, rather than taken as evidence against the existence of a head composed of multiple segments. Mayer et al. (2013) used what they identified as a stomatogastric ganglion to align and count segments. In arthropods, the stomatogastric ganglion is generally agreed to be part of the third segment and sits above and behind the foregut (Bitsch and Bitsch, 2010; Scholtz and Edgecomb, 2006). Mayer et al. (2013) reported a structure above the second trunk ganglion of *M. harmsworthi* that they suggested was homologous to the arthropod stomatogastric ganglion. If there finding prove true, than the second trunk segment would be homologous with the tritocerebral segment of arthropods; the first trunk segment would be homologous to the deuterocerebral segment; and the tardigrade head would be homologous with the arthropod protocerebrum. This result supports

the "protocerebral" hypothesis. We did not discover a structure that resembles the stomatogastric ganglion in *H. dujardini*, and it has not been reported for any other tardigrade species, casting doubt on whether or not the structure discovered by Mayer et al. (2013) is truly homologous to the arthropod stomatogastric ganglion. However, given that the "tripartite" hypotheses is based on an incorrect inference of a sister group relationship between Arthropoda and Tardigrada, and that neither segment development (Gabriel and Goldstein, 2007) nor anatomy of the muscular system (this study) support a multi-segmented composition of the head, the most parsimonious explanation is that the tardigrade head and associated brain are directly homologous to the ocular segment and protocerebrum of arthropods.

Problems also emerge when trying to determine homologies of the segmented ventral nervous systems among panarthropodans. Both tardigrades and arthropods (Scholtz, 2002) have clearly identifiable rope ladder-like nervous systems, with paired ventral nerve cords connecting ganglia, found one to each segment posterior to the brain. Although ventral commissures connecting the nerve cords in the ganglia were not detected in the tardigrade *M. hufelandi* (Zantke et al., 2008), vental commissures were detected in *M. harmsworthi* (Mayer et al., 2013), *H. crispae* (Persson et al., 2012), and *H. dujardini* (this study). Based on the phylogeny of tardigrades (Guil and Giribet, 2011), it appears that ventral commissures are plesiomorphic for Tardigrada. Unlike tardigrades and arthropods, onychophorans lack ganglia along the trunk (Mayer and Whittington, 2009). Mayer and Whittington (2009) suggested that the ganglia of tardigrades and arthropods are homologous. This suggests that ganglia were lost in the onychophoran lineage, based on the sister group relationship of Onychophora and Arthropoda suggested by a recent molecular analysis (Campbell et al., 2011). It is possible that the ganglia of tardigrades and arthropods evolved independently (Mayer and Whittington, 2009). However,

with the amount of variation in nervous system architecture outside of Panarthropoda, it is difficult to polarize evolutionary changes within. For example, among non-panarthropodan ecdysozoans, the Nematoda have dorsal and ventral nerve cords that lack ganglia (Brusca and Brusca, 2003), while the Kinorhyncha have segmental ganglia, but lack transverse commissures (Persson et al., 2012). Investigations of developmental patterning could help resolve the segmental composition of the tardigrade head (see below and Fig. 7) and whether or not ganglia are homologous between tardigrades and arthropods.

Distinct segmental identities in H. dujardini

Segmental patterns were detected for the nervous system using an anti β-tubulin antibody; phalloidin was used to investigate muscle anatomy. The tardigrade body plan has a head and four trunk segments, with segmentally repeated muscle and nervous system patterns (Halberg et al., 2009; Mayer et al., 2013; Persson et al., 2011; Schmidt-Rhaesa and Kulessa, 2007; Zantke et al., 2008). Although the trunk segments are considered homonomous, our fine-scale analysis of the nervous system using anti β-tubulin and muscles using phalloidin reveal that each segment is morphologically unique. Based on muscle and nervous system anatomy, we detected five segments, each exhibiting a distinct morphological identity. The head segment is the most distinct, with the presence of the brain and pharyngeal apparatus, and absence of external legs. Interestingly, the stylets and stylet glands of the pharyngeal apparatus have been proposed to be homologous to the claws and claw glands of tardigrade legs, suggesting that the stylets and associated structures may be derived from ancestral legs of the head (Nielsen, 2001). This is supported by the fact that only leg muscles and stylet muscles exhibit cross-striation

patters in the tardigrade species *Halobiotus crispae* (Halberg et al., 2009). We did not investigate whether these two muscle types are striated in *H. dujardini*.

Each of the trunk segments of *H. dujardini* has a ventral ganglion. The first three trunk ganglia are noticeably wider than the fourth ganglion. Based on the distinct morphology of the fourth ganglion, we suggest that it has a unique segmental identity. A similar conclusion can be drawn from results reported for the tardigrade species *Halobiotus crispae* (Persson et al., 2012), which is in the family Hypsibiidae with *H. dujardini*. In this species, the first three trunk ganglia each have two transverse commissures, while the fourth trunk ganglion has only one transverse commissure, suggesting that the fourth ganglion also has a distinct segmental identity in this species.

The ventral median muscle attachment sites of *H. dujardini* also present an intriguing pattern. Attachment sites 1, 5, 6, and 7 have unique morphologies. Site 2 and 4 have an identical muscle arrangement. The anterior part of ventral attachment site 5 is identical to the anterior of ventral attachment site 3. In our model, attachment site 1 is part of the first trunk segment, attachment sites 2 and 3 are parts of the second trunk segment, attachment sites 4 and 5 are parts of the third trunk segment, and attachment sites 6 and 7 are parts of the fourth trunk segment. Based on muscle anatomy in the legs, we detected three distinct leg identities. Appendage pairs one and four have distinct morphologies, while appendage pairs two and three are identical. In Arthropoda and Onychophora, conserved mechanisms appear to specify anterior segment identities (Eriksson et al., 2010; Eriksson et al., 2013; Steinmetz et al., 2010). We propose that these same mechanisms specify the distinct segmental morphologies seen in *H. dujardini* (Fig. 7B), and that these segmental specification mechanisms are ancestral for Panarthropoda.

Conclusions

Although tardigrades are thought to have homonomous trunk segments, our investigation of nervous system and muscle system anatomy suggest that each trunk segment has a unique morphology. Moreover, we identified three distinct leg identities. These results suggest that the muscle system and nervous system may have already evolved distinct segmental morphologies in the panarthropodan ancestor, long before the evolution of conspicuously different segment morphologies and tagmatization patterns found within arthropodan and onychophoran body plans. Possibly the developmental mechanisms differentiating the anterior segments of both onychophorans and arthropods were responsible for differentiation of the nervous system and muscular system in the anterior segments of the panarthropod ancestor. This would explain the high similarity of these mechanisms between Onychophora and Arthropoda, even though the ancestor of these phyla is not thought to have exhibited conspicuous morphological differences between anterior segments beyond the presence of an eye and possibly a morphologically distinct appendage pair on the ocular segment (Janssen et al., 2010; Ma et al., 2009). Functional and expression studies of genes underlying segmental diversity in the onychophoran and arthropodan body plans in *H. dujardini* would illuminate ancestral anterior segment patterning mechanisms and whether these genes underlie the production of segmental differentiation in tardigrades.

References

Abràmoff, M.D., Magalhães, P.J., Ram, S.J., 2004. Image processing with ImageJ. *Biophoton Int*. 11, 36–42.

Bitsch, J., Bitsch, C., 2010. The tritocerebrum and the clypeolabrum in mandibulate arthropods: Segmental interpretations. *Acta Zoologica* 91, 249–266.

Bold, H.C., 1949. The morphology of *Chlamydomonas chlamydogama*, sp. nov. *Bulletin of the Torrey Botanical Club* 101–108.

Brown, S.J., Shippy, T.D., Beeman, R.W., Denell, R.E., 2002. *Tribolium Hox* genes repress antennal development in the gnathos and trunk. *Mol. Phylogenet. Evol.* 24, 384–387.

Brusca, R.C., Brusca, G.J., 2003. Invertebrates 2nd ed. Sinaur Associates, Sunderland MA.

Budd, G.E., Telford, M.J., 2009. The origin and evolution of arthropods. *Nature* 457, 812–817.

Budd, G.E., 2001. Tardigrades as 'stem-group arthropods': The evidence from the Cambrian fauna. *Zoologischer Anzeiger-A Journal of Comparative Zoology* 240, 265–279.

Budd, G.E., 1996. The morphology of *Opabinia regalis* and the reconstruction of the arthropod stem-group. *Lethaia* 29, 1–14.

Budd, G.E., 2001. Why are arthropods segmented? *Evol. Dev.* 3, 332–342.

Campbell, L.I., Rota-Stabelli, O., Edgecombe, G.D., Marchioro, T., Longhorn, S.J., Telford, M.J., Philippe, H., Rebecchi, L., Peterson, K.J., Pisani, D., 2011. MicroRNAs and

phylogenomics resolve the relationships of Tardigrada and suggest that velvet worms are the sister group of Arthropoda. *Proc. Natl. Acad. Sci. U. S. A.* 108, 15920–15924.

Carroll, S.B., 2001. Chance and necessity: The evolution of morphological complexity and diversity. *Nature* 409, 1102–1109.

Chu, D.T., Klymkowsky, M.W., 1989. The appearance of acetylated alpha-tubulin during early development and cellular differentiation in *Xenopus*. *Dev. Biol.* 136, 104–117.

Dewel, R.A., Dewel, W.C., 1996. The brain of *Echiniscus viridissimus* Peterfi, 1956 (Heterotardigrada): A key to understanding the phylogenetic position of tardigrades and the evolution of the arthropod head. *Zool. J. Linn. Soc.* 116, 35–49.

Dunn, C.W., Hejnol, A., Matus, D.Q., Pang, K., Browne, W.E., Smith, S.A., Seaver, E., Rouse, G.W., Obst, M., Edgecombe, G.D., Sorensen, M.V., Haddock, S.H., Schmidt-Rhaesa, A., Okusu, A., Kristensen, R.M., Wheeler, W.C., Martindale, M.Q., Giribet, G., 2008. Broad phylogenomic sampling improves resolution of the animal tree of life. *Nature* 452, 745–749.

Eriksson, B.J., Samadi, L., Schmid, A., 2013. The expression pattern of the genes *engrailed*, *pax6*, *otd* and *six3* with special respect to head and eye development in *Euperipatoides kanangrensis* Reid 1996 (Onychophora: Peripatopsidae). *Dev. Genes Evol.* 1–10.

Eriksson, B.J., Tait, N.N., Budd, G.E., Janssen, R., Akam, M., 2010. Head patterning and *Hox* gene expression in an onychophoran and its implications for the arthropod head problem. *Dev. Genes Evol.* 220, 117–122.

Gabriel, W.N., Goldstein, B., 2007. Segmental expression of *pax3/7* and *engrailed* homologs in tardigrade development. *Dev. Genes Evol.* 217, 421–433.

Gabriel, W.N., McNuff, R., Patel, S.K., Gregory, T.R., Jeck, W.R., Jones, C.D., Goldstein, B., 2007. The tardigrade *Hypsibius dujardini*, a new model for studying the evolution of development. *Dev. Biol.* 312, 545–559.

Grenier, J.K., Garber, T.L., Warren, R., Whitington, P.M., Carroll, S., 1997. Evolution of the entire arthropod *Hox* gene set predated the origin and radiation of the onychophoran/arthropod clade. *Current Biology* 7, 547–553.

Grimaldi, D., Engel, M.S., 2005. Evolution of the Insects. Cambridge University Press, Cambridge.

Guil, N., Giribet, G., 2012. A comprehensive molecular phylogeny of tardigrades—adding genes and taxa to a poorly resolved phylum - level phylogeny. *Cladistics* 28, 21–49.

Halberg, K.A., Persson, D., Mobjerg, N., Wanninger, A., Kristensen, R.M., 2009. Myoanatomy of the marine tardigrade *Halobiotus crispae* (Eutardigrada: Hypsibiidae). *J. Morphol.* 270, 996–1013.

Horikawa, D.D., Sakashita, T., Katagiri, C., Watanabe, M., Kikawada, T., Nakahara, Y., Hamada, N., Wada, S., Funayama, T., Higashi, S., Kobayashi, Y., Okuda, T., Kuwabara, M., 2006. Radiation tolerance in the tardigrade *Milnesium tardigradum*. *Int. J. Radiat. Biol.* 82, 843–848.

Hughes, C.L., Kaufman, T.C., 2002. *Hox* genes and the evolution of the arthropod body plan. *Evol. Dev.* 4, 459–499.

Jager, M., Murienne, J., Clabaut, C., Deutsch, J., Le Guyader, H., Manuel, M., 2006. Homology of arthropod anterior appendages revealed by *Hox* gene expression in a sea spider. *Nature* 441, 506–508.

Janssen, R., Damen, W.G., 2006. The ten *Hox* genes of the millipede *Glomeris marginata*. *Dev. Genes Evol.* 216, 451–465.

Jonsson, K.I., Rabbow, E., Schill, R.O., Harms-Ringdahl, M., Rettberg, P., 2008. Tardigrades survive exposure to space in low earth orbit. *Curr. Biol.* 18, R729–R731.

Kinchin, I.A., 1994. The Biology of Tardigrades. Portland Press Limited, London.

Kristensen, R.M., Higgins, R.P., 1984. A new family of Arthrotardigrada (Tardigrada: Heterotardigrada) from the Atlantic coast of Florida, USA. *Trans. Am. Microsc. Soc.* 295–311.

Kristensen, R.M., Higgins, R.P., 1984. Revision of Styraconyx (Tardigrada: Halechiniscidae) with descriptions of two new species from Disko Bay, West Greenland. *Smithson. Contrib. Zool.* 391, 1–40.

Kristensen, R.M., 1983. The first record of cyclomorphosis in Tardigrada based on a new genus and species from arctic meiobenthos1. *J. Zool. Syst. Evol. Res.* 20, 249–270.

Ma, X., Hou, X., Bergstrom, J., 2009. Morphology of *Luolishania longicruris* (Lower Cambrian, Chengjiang Lagerstatte, SW China) and the phylogenetic relationships within lobopodians. *Arthropod Struct. Dev.* 38, 271–291.

Maas, A., Waloszek, D., 2001. Cambrian derivatives of the early arthropod stem lineage, pentastomids, tardigrades and lobopodians an 'Orsten'Perspective. *Zoologischer Anzeiger-A Journal of Comparative Zoology* 240, 451–459.

Manton, S.M., 1977. The Arthropoda: Habits, Functional Morphology and Evolution. Clarendon Press, Oxford.

Manuel, M., Jager, M., Murienne, J., Clabaut, C., Le Guyader, H., 2006. *Hox* genes in sea spiders (Pycnogonida) and the homology of arthropod head segments. *Dev. Genes Evol.* 216, 481–491.

Mayer, G., Kauschke, S., Rudiger, J., Stevenson, P.A., 2013. Neural markers reveal a one-segmented head in tardigrades (water bears). *PLoS One* 8, e59090.

Mayer, G., Whitington, P.M., 2009. Neural development in Onychophora (velvet worms) suggests a step-wise evolution of segmentation in the nervous system of Panarthropoda. *Dev. Biol.* 335, 263–275.

Mayer, G., Whitington, P.M., Sunnucks, P., Pfluger, H.J., 2010. A revision of brain composition in Onychophora (velvet worms) suggests that the tritocerebrum evolved in arthropods. *BMC Evol. Biol.* 10, 255-2148-10-255.

McManus, H.A., Lewis, L.A., 2011. Molecular phylogenetic relationships in the freshwater family Hydrodictyaceae (Sphaeropleales, Chlorophyceae), with an emphasis on pediastrum duplex1. *J. Phycol.* 47, 152–163.

Mobjerg, N., Halberg, K.A., Jorgensen, A., Persson, D., Bjorn, M., Ramlov, H., Kristensen, R.M., 2011. Survival in extreme environments - on the current knowledge of adaptations in tardigrades. *Acta Physiol. (Oxf)* 202, 409–420.

Nielsen, C., 2001. Animal Evolution: Interrelationships of the Animal Phyla. Oxford University Press, New York.

Persson, D.K., Halberg, K.A., Jorgensen, A., Mobjerg, N., Kristensen, R.M., 2012. Neuroanatomy of *Halobiotus crispae* (Eutardigrada: Hypsibiidae): tardigrade brain structure supports the clade Panarthropoda. *J. Morphol.* 273, 1227–1245.

Philippe, H., Lartillot, N., Brinkmann, H., 2005. Multigene analyses of bilaterian animals corroborate the monophyly of Ecdysozoa, Lophotrochozoa, and Protostomia. *Mol. Biol. Evol.* 22, 1246–1253.

Posnien, N., Bashasab, F., Bucher, G., 2009. The insect upper lip (labrum) is a nonsegmental appendage-like structure. *Evol. Dev.* 11, 480–488.

Rasband, W.S., 1997–2012. ImageJ, U.S. National Institutes of Health, Bethesda, Maryland, USA,imagej.nih.gov/ij/

Schmidt-Rhaesa, A., Kulessa, J., 2007. Muscular architecture of *Milnesium tardigradum* and *Hypsibius sp.*(Eutardigrada, Tardigrada) with some data on *Ramazottius oberhaeuseri*. *Zoomorphology* 126, 265–281.

Schneider, C.A., Rasband, W.S., Eliceiri, K.W., 2012. NIH image to ImageJ: 25 years of image analysis. *Nat Methods* 9, 671–675.

Scholtz, G., 2002. The Articulata hypothesis- or what is a segment? *Org. Divers. Evol.* 2, 197–215

Scholtz, G., Edgecombe, G.D., 2006. The evolution of arthropod heads: Reconciling morphological, developmental and palaeontological evidence. *Dev. Genes Evol.* 216, 395–415.

Seki, K., Toyoshima, M., 1998. Preserving tardigrades under pressure. *Nature* 395, 853–854.

Sharma, P.P., Schwager, E.E., Extavour, C.G., Giribet, G., 2012. *Hox* gene expression in the harvestman *Phalangium opilio* reveals divergent patterning of the chelicerate opisthosoma. *Evol. Dev.* 14, 450–463.

Shubin, N., Tabin, C., Carroll, S., 1997. Fossils, genes and the evolution of animal limbs. *Nature* 388, 639–648.

Snodgrass, R.E., 1935. Principles of Insect Morphology. Cornell University Press, Ithaca.

Tenlen, J.R., McCaskill, S., Goldstein, B., 2012. RNA interference can be used to disrupt gene function in tardigrades. *Dev. Genes Evol.* 1–11.

Zantke, J., Wolff, C., Scholtz, G., 2008. Three-dimensional reconstruction of the central nervous system of *Macrobiotus hufelandi* (Eutardigrada, Parachela): implications for the phylogeneticposition of Tardigrada. *Zoomorphology* 127, 21–36.

Table

Table 1. List of anatomical terms used in this study that are based on presumed homology with structures named in previous studies. The source of these terms and the species investigated in these previous studies is provided. The order of species corresponds to the order of the studies. Semicolons separate species used in different studies.

Structure	System	Study	Species
anterior cluster	nervous	Zantke et al., 2008	*Macrobiotus hufelandi*
connectives	nervous	Mayer et al. 2013	*Macrobiotus harmsworthi*
dorsal cluster	nervous	Zantke et al., 2008	*Macrobiotus hufelandi*
inner connective	nervous	Mayer et al. 2013; Persson et al., 2012; Zantke et al., 2008	*Macrobiotus harmsworthi*; *Halobiotus crispae*; *Macrobiotus hufelandi*
inner lobe	nervous	Persson et al., 2012	*Halobiotus crispae*
outer connective	nervous	Mayer et al. 2013	*Macrobiotus harmsworthi*
outer lobe	nervous	Persson et al., 2012	*Halobiotus crispae*
posterior cluster	nervous	Zantke et al., 2008	*Macrobiotus hufelandi*
dorsal longitudinal muscles	muscle	Halberg et al., 2009; Schmidt-Rhaesa and Kulessa, 2007	*Halobiotus crispae*; *Hypsibius* sp. and *Milnesium tardigradum*
sheet mucles	muscle	Halberg et al., 2009	*Halobiotus crispae*
ventral longitudinal muscles	muscle	Halberg et al., 2009; Schmidt-Rhaesa and Kulessa, 2007	*Halobiotus crispae*; *Hypsibius* sp. and *Milnesium tardigradum*
ventral median attachment sites	muscle	Halberg et al., 2009; Schmidt-Rhaesa and Kulessa, 2007	*Halobiotus crispae*; *Hypsibius* sp. and *Milnesium tardigradum*

Figure 1. General anatomy of *H. dujardini*. Scale bars equal 25 μm. (A) DIC micrograph showing ventrolateral view of the left side of an adult *H. dujardini* specimen. The body plan includes a head and four trunk segments, each with a pair of legs (left legs are in focus). Dashed line delineates the boundary between the head segment and the first trunk segment. (B) Light micrograph of an adult laying eggs in its exuvia during molting. (C) DIC micrograph of the ventral head of an adult *H. dujardini* specimen showing pharyngeal apparatus. (D) DIC micrograph of the leg claws of the anterior three right legs. Abbreviations: bu, buccal tube; c, claws; l, leg; ph, pharyngeal bulb; so, stomach; st, stylet.

Figure 1.

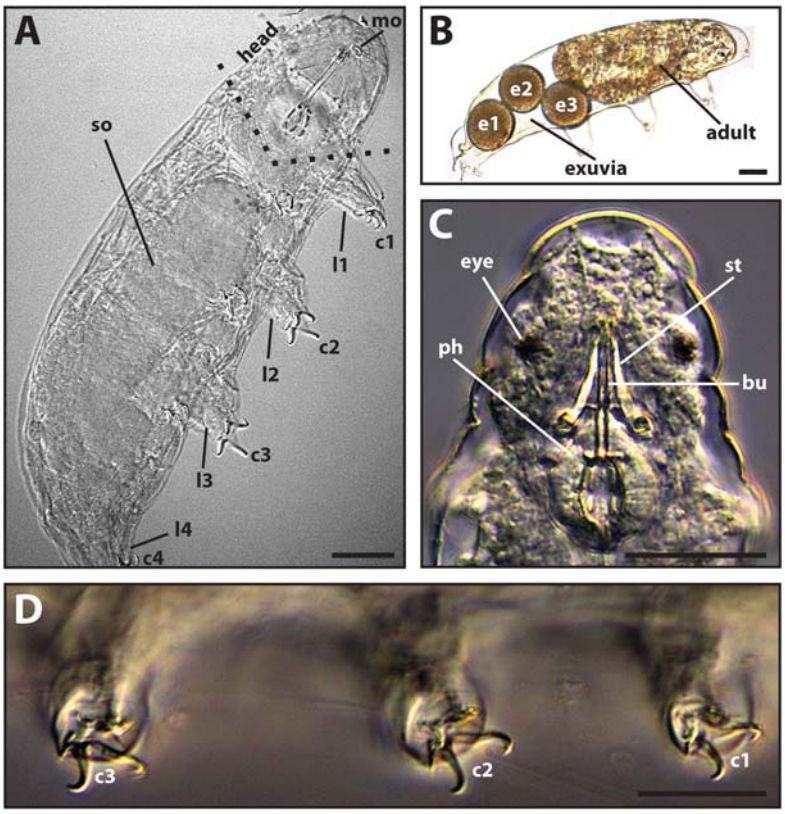
A
head
mo
so
c1
l1
c2
l2
c3
l3
l4
c4
B
e2
e3
e1
adult
exuvia
C
eye
st
ph
bu
D
c3
c2
c1

Figure 2. Laser confocal microscopy sections showing brain anatomy of a DAPI-stained head of a *H. dujardini* specimen. Anterior is to the top. The dorsoventral position of each section is shown in the bottom right of each panel. Scale bars equal 25 μm. (A) Grooves can be seen that run through the ventral surface of the ventral brain lobe (arrowheads) and outer brain lobes (arrows). (B) Grooves are not seen in a deeper section of either the ventral or outer brain lobes (C) The pharyngeal apparatus is found in the head cavity dorsal to the ventral lobe. Abbreviations: bu, buccal tube; g, ganglion; il, inner brain lobe; l, leg; ol, outer brain lobe; ph, pharyngeal bulb; st, stylet; vl, ventral lateral lobe.

Figure 2.

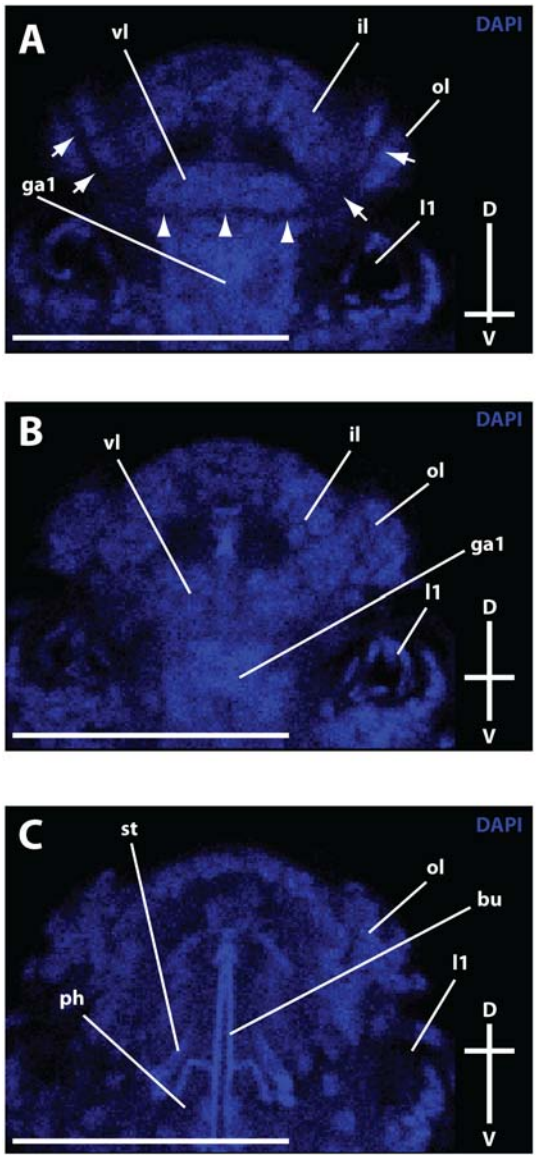
A
vl
il
DAPI
ol
ga1
l1
D
V
B
vl
il
DAPI
ol
ga1
l1
D
V
C
st
DAPI
ol
bu
l1
ph
D
V

Figure 3. Nervous system of *H. dujardini*. Anti β-tubulin immunolabeling is shown in A, C–G. DAPI counterstaining is shown in A, D–G. Scale bars equal 25 μm. (A) Ventrolateral view of a maximum projection; anterior is to the left. Each body segment includes a ventral ganglion. The intense β-tubulin expression in the stomach likely reflects exogenous gut contents. (B) DIC micrograph of the head of a *H. dujardini* specimen. (C) Depth-coded maximum-projection of confocal Z-series of specimen shown in B. Connectives labeled extend to the ventral lobe. Nerves extending posteriorly from the brain around the pharyngeal bulb are labeled. (D–E) Individual slices of the Z-series used to produce C. The Z positions of the slices are illustrated in the top right corners of both panels. (D) The right anterior cluster and posteriorly directed nerves can be seen. (E) Connectives extending anteriorly from the first ganglion to the ventral lobe are labeled. (F) Maximum projection of the ganglion and a leg of the third trunk segment. This is a magnification of specimen show in A. Arrowheads point to nerves extending from the third trunk ganglion into the left third leg. Intense expression of β-tubulin can be seen in the claw gland. (G) Maximum projection of the second, third, and anterior fourth segments of the same specimen as shown in B–E. Ganglia 2 and 3 are similar in morphology, but differ from ganglion 4 in terms of size. Inset shows β-tubulin staining of the second ganglia showing a ventral commissure. Abbreviations: ac, anterior cluster; br, brain; bu, buccal tube; cg, claw gland; cn, connective; co, commissure; dc, dorsal cluster; ga, ganglion; il, inner lobe; l, leg; mo, mouth; ol, outer lobe; pc, posterior cluster; ph, pharyngeal bulb; pn, posterior nerves; so, stomach; st, stylet.

Figure 3.

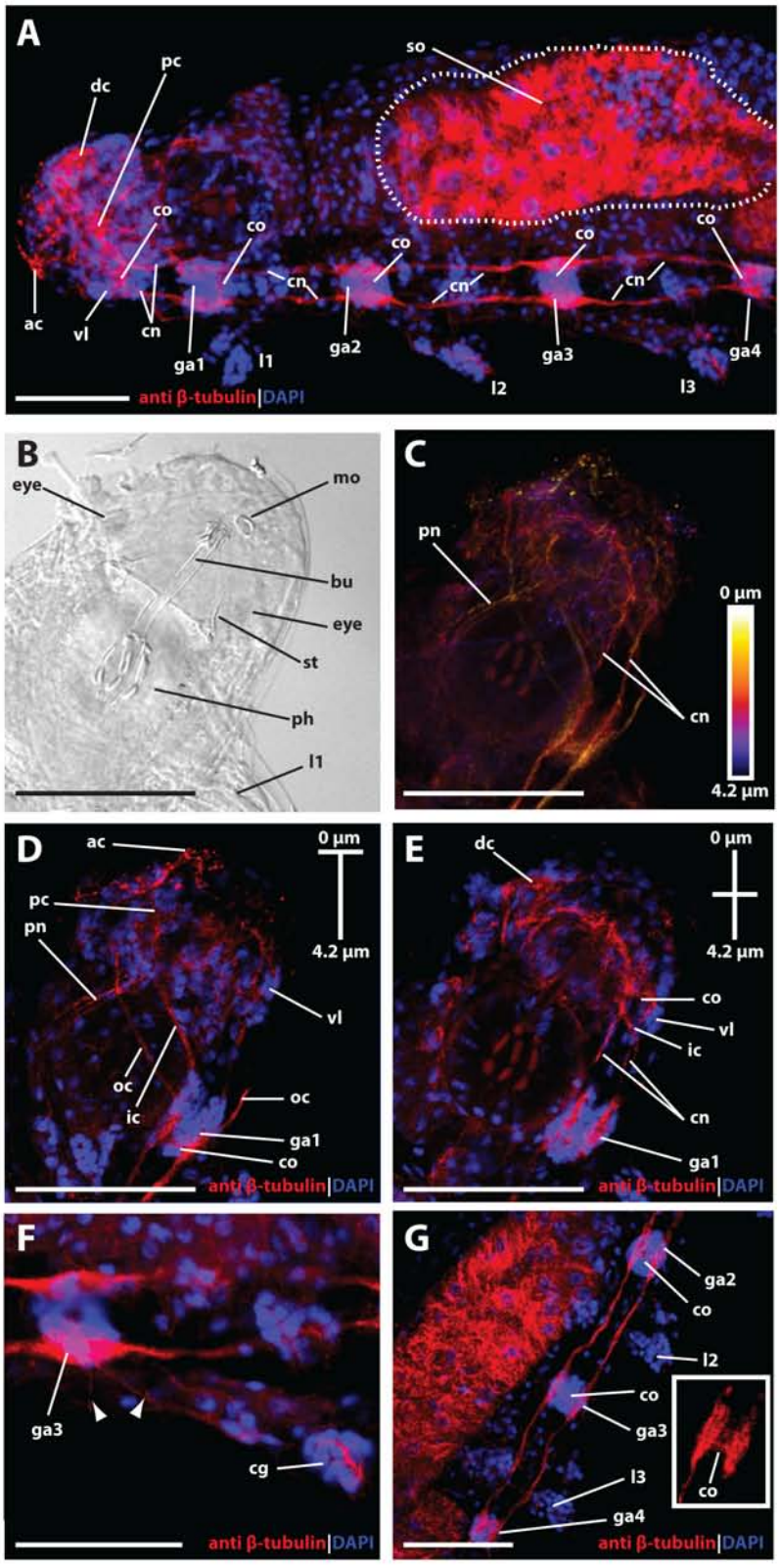
A
so
pc
dc
co
co
co
co
co
co
cn
cn
cn
ac
vl
cn
ga1
l1
ga2
ga3
ga4
l2
l3
anti β-tubulin|DAPI
B
eye
mo
bu
eye
st
ph
l1
C
pn
0 µm
cn
4.2 µm
D
ac
0 µm
pc
pn
4.2 µm
vl
oc
ic
oc
ga1
co
anti β-tubulin|DAPI
E
dc
0 µm
4.2 µm
co
vl
ic
cn
ga1
anti β-tubulin|DAPI
F
ga3
cg
anti β-tubulin|DAPI
G
ga2
co
l2
co
ga3
co
l3
ga4
anti β-tubulin|DAPI

Figure 4. General muscle anatomy in *H. dujardini* as revealed by phalloidin staining. Scale bars equal 25 μm. (A–D) Ventral view. Anterior is to the top. (A) Depth coded maximum-projection of confocal Z-series. (B–D) Slices of Z series used to produce A. Position in the Z series is illustrated in the bottom right corners. Ventral median attachment sites are numbered. (B) Ventral attachment site 1 is ventral to the pharyngeal bulb. (C) Muscle strands on the left and right sides of the even attachment sites make contact medially. (D) The dorsal muscle strand that connects the left and right stylet bases and the sheet muscles connected to the pharynx can be seen. (E–F) Anterior is to the right, and the position in the Z series is illustrated in the bottom right corners. Arrows point to ends of dorsal longitudinal muscles. (E) Ventrolateral view of left side. (F) Ventromedial view of left side. Arrowheads point to ends of ventral longitudinal muscles. Abbreviations: dl, dorsal longitudinal muscle; dv, dorsoventral muscles; l, leg; ph, pharyngeal bulb; sh, sheet muscle; sm, stylet muscle; vl, ventral longitudinal muscle.

Figure 4.

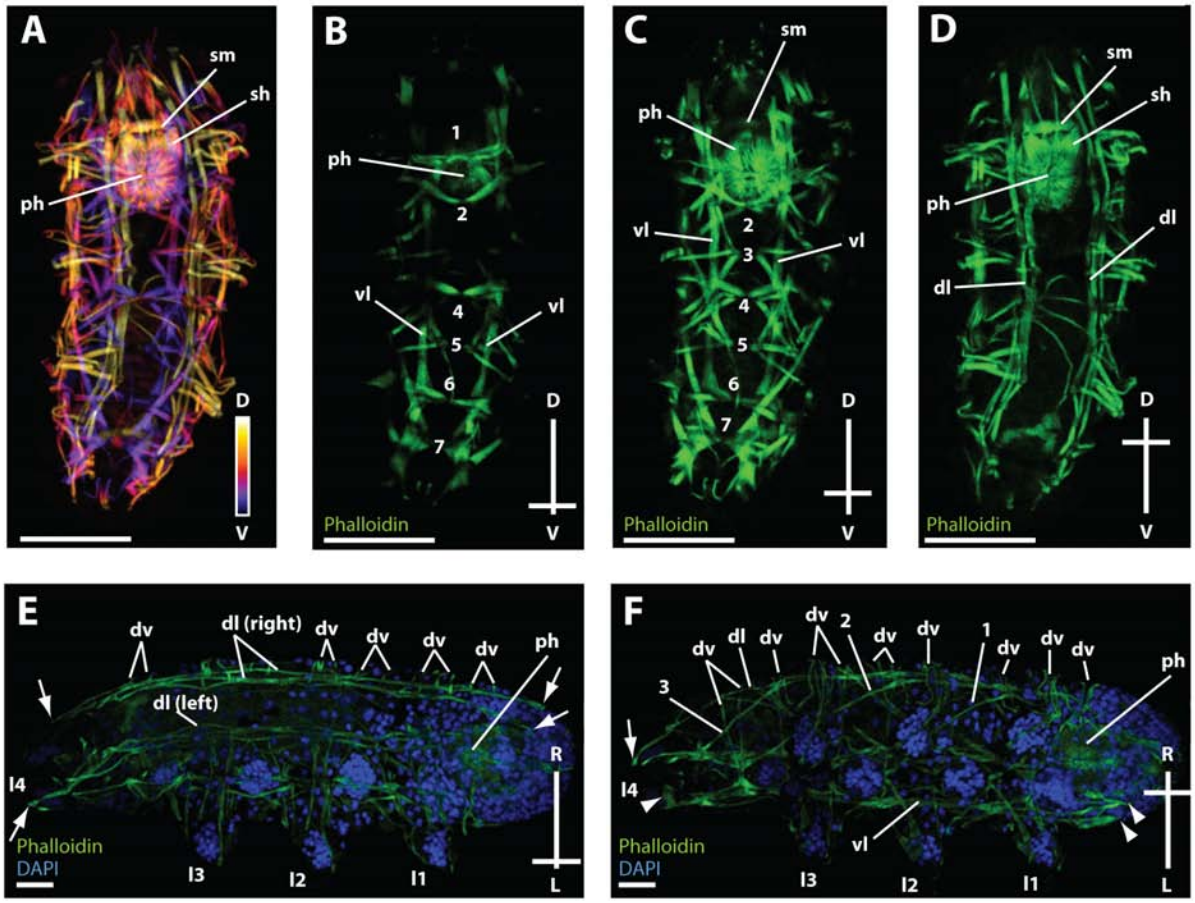
A
sm
sh
ph
D
V
B
1
ph
2
vl
vl
4
5
6
7
D
Phalloidin
V
C
sm
ph
vl
2
3
vl
4
5
6
7
D
Phalloidin
V
D
sm
sh
ph
dl
dl
D
Phalloidin
V
E
dv
dl (right)
dv
dv
dv
dv
ph
dl (left)
R
l4
Phalloidin
DAPI
l3
l2
l1
L
F
dv
dl
dv
dv
2
dv
dv
1
dv
dv
dv
ph
3
R
l4
vl
Phalloidin
DAPI
l3
l2
l1
L

Figure 5. Models of ventral median attachment site morphology based on phalloidin staining. In all models, anterior is to the top. The anteroposterior number of the attachment site that each model depicts is shown in the bottom left of each panel. The muscle strands are labeled in terms of their direction of extension and relative sizes of the strands are depicted. (B) Attachment sites 2 and 4 show the same pattern. The left side of the model represents attachment site 2 and the right side represents attachment site 4. Abbreviations: a, towards the anterior; d, dorsal along body wall; da, dorsoanterior to the dorsal longitudinal muscle strands; l, to a leg.

Figure 5.

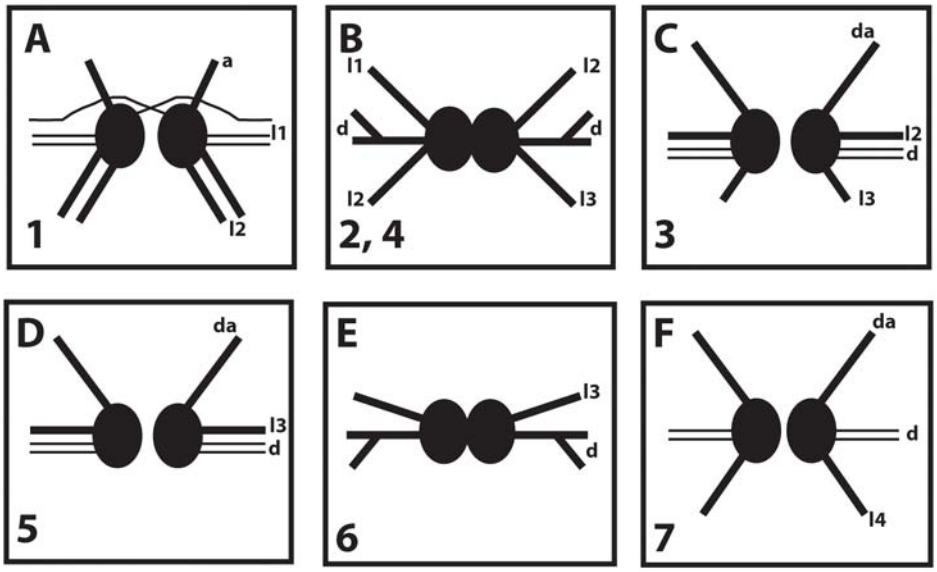

Figure 6. Ventrolateral view of *H. dujardini* specimen showing leg muscle anatomy as revealed by phalloidin staining. Anterior is to the right. Muscles extending into the leg are labeled according to their origination site outside of the leg. Scale bars equal 25 μm. (A) Maximum projection of the lateral muscles of the left three anterior-most legs. (B) Maximum projection of the medial muscles of the left three anterior legs. Ventral median attachment sites are numbered. (C) Maximum projection of the lateral muscles of the posterior-most legs. The outer strand of the right dorsal muscle (OD) extends to the distal point of the posterior leg. (D) Maximum projection of the medial muscles of the posterior-most legs. Abbreviations: do, dorsal muscle strands; ga, ganglion; ip, connects with inner strand of the right dorsal muscle strands; l, leg; op, connects with outer strand of right dorsal muscle strands; p, connects with leg muscles from a posterior leg; sh, sheet muscle v, connects to ventral median attachment site.

Figure 6.

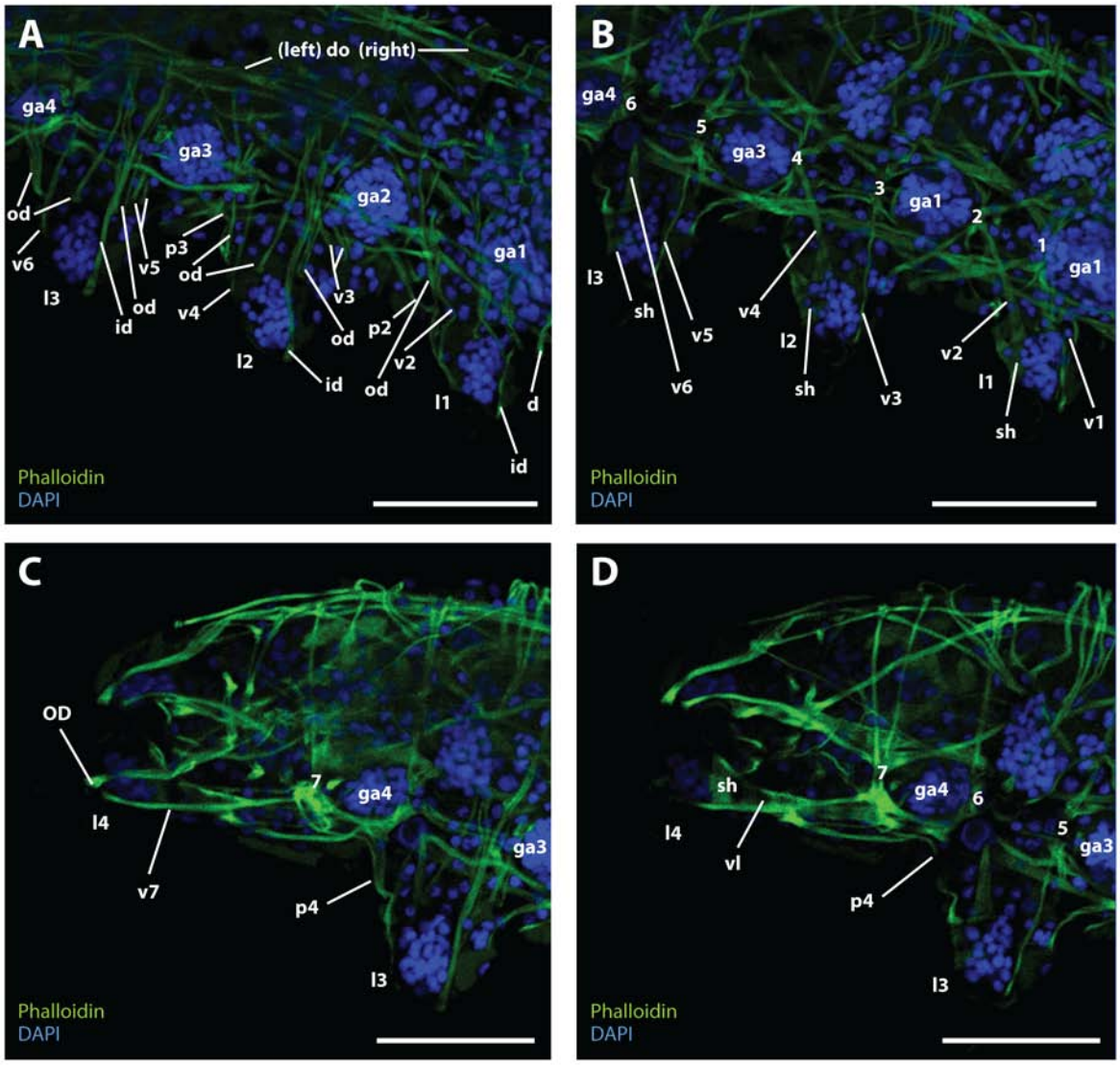
A
(left) do (right)
ga4
ga3
ga2
ga1
od
v6
v5
p3
od
l3
od
id
v4
v3
od
p2
v2
l2
id
od
l1
d
id
Phalloidin
DAPI
B
ga4
6
5
ga3
4
3
ga1
2
1
ga1
l3
sh
v5
v6
v4
l2
sh
v3
v2
l1
sh
v1
Phalloidin
DAPI
C
OD
7
ga4
l4
ga3
v7
p4
l3
Phalloidin
DAPI
D
sh
7
ga4
6
l4
5
ga3
vl
p4
l3
Phalloidin
DAPI

Figure 7. The body plan of *H. dujardini* includes five distinct segment morphologies. (A) A model of the body plan of *H. dujardini* based on results of the investigations of ventral nervous and muscle systems presented here. Dashed lines demarcate the hypothesized boundaries between segments. Nervous system structures are depicted in red. A ganglion is shown in each trunk segment. Different shapes of ganglia represent distinct morphologies. Muscle system structures are depicted in green. Symbols in the legs represent patterns of leg musculature. Ventral median attachment sites are modeled as in Figure 5. (B) Expression domains of anterior segment identity specification genes that are conserved between Onychophora and Arthropoda are depicted. These domains of expression are consistent with the pattern of segment morphologies seen in *H. dujardini*. It is hypothesized that the first three segments of the tardigrade body plan are directly homologous with the first three segments of Arthropoda/Onychophora and that expression of each *Hox* gene extends to the very posterior. The identity of the first segment, the head, is specified by *six3* and *otx*. *Hox* genes are not expressed in the anterior two segments. The identity of the first trunk segment emerges because of a lack of *Hox* expression and lack of expression of head identity specification genes. Either *lab* or *pb*, or a combination of these factors, specifies the muscle anatomy found in the legs of segments two and three, and the anatomy of the ventral median attachment sites of the second segment. *Dfd* specifies the unique morphology of ventral median attachment site 5 found in segment 3. One or more of the remaining seven *Hox* genes specify the unique morphologies of the ventral median attachment sites found in segment 4, the unique appendage muscles found in the fourth pair of legs, and the unique morphology of the fourth trunk ganglion. Abbreviations: H, head segment; ph, pharyngeal bulb; T, trunk segment.

Figure 7.

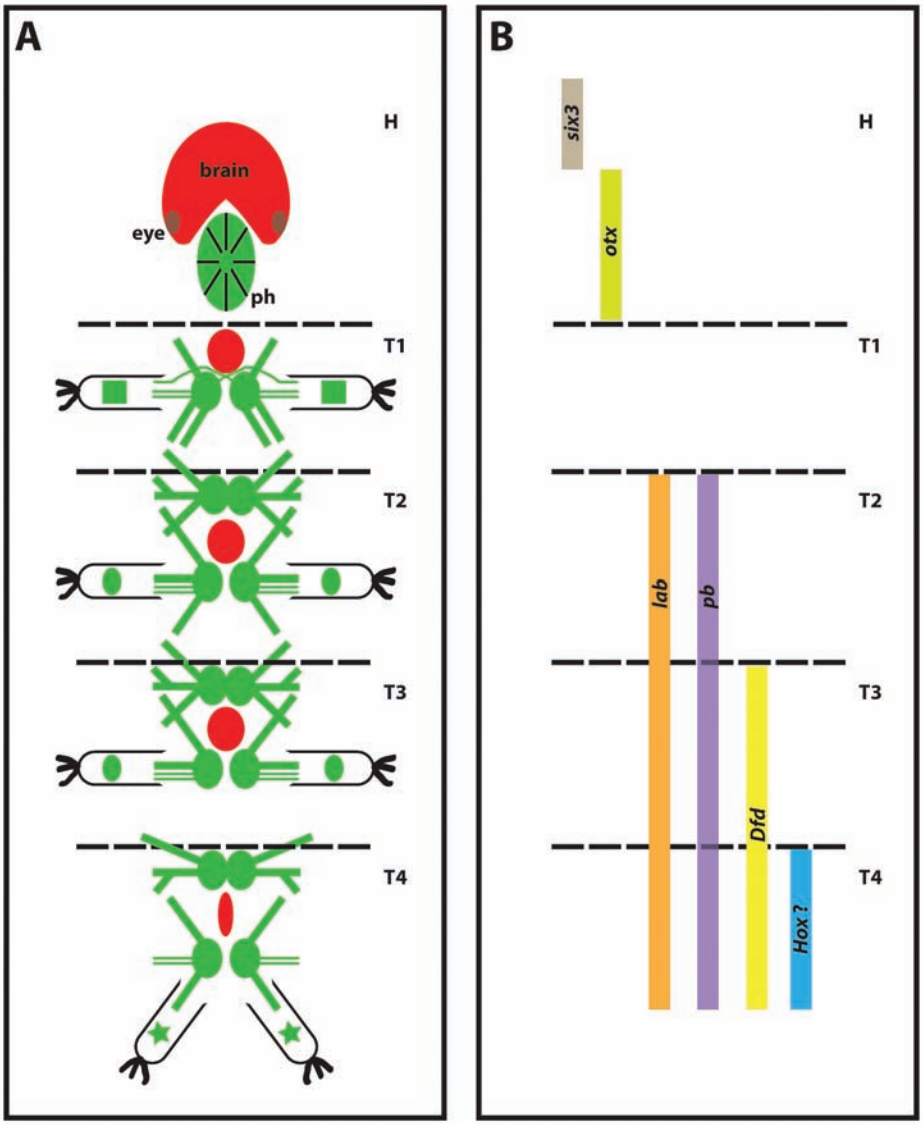

Chapter 4.

Distal-less specifies legs and stylets in the tardigrade *Hypsibius dujardini*

Introduction

The superphylum Panarthropoda includes the phylum Arthropoda, its sister phylum Onychophora, and the phylum Tardigrada (Budd and Telford, 2009; Campbell et al., 2011; Nielsen, 2001). These phyla have very ancient origins, and had diverged from each other by the Cambrian period (Budd and Telford, 2009; Mass and Waloszek, 2001). A body plan characteristic uniting these phyla is the presence of segmentally iterated paired ventral appendages. Ancestral panarthropods are thought to have had unjointed (i.e., lobopodal) leg-like appendages on all segments; these appendages are not thought to have exhibited clear patterns of morphological regionalization along the proximodistal axis (Budd, 2001; Budd and Telford, 2009; Grenier, 1997; Hou et al., 2004; Manton, 1977; Shubin et al., 1997; Snodgrass, 1935). Lobopodal appendages are retained in the extant Onychophora and Tardigrada. The appendages of tardigrades and onychophorans lack appendage joints, and like the appendages of hypothesized ancestral panarthropodans, there is little structural evidence of proximodistal appendage regionalization, beyond the presence of claws on the distal tips of legs.

Stem-group arthropods exhibited elongate multi-jointed appendages (Legg et al., 2012), and this is likely the evolutionary ground state of the arthropod appendage. In extant arthropods, a variety of appendages are found along the anteroposterior axis, including antennae (chelicerae in spiders and other chelicerates), gnathal appendages, legs, and genitalia. These appendages are

composed of segments, called podomeres, which are separated by joints. In extant arthropods, different podomeres within a single appendage often exhibit extremely distinct morphologies, which contribute to the functional performance of the appendage. The evolution of appendage joints and anteroposteriorly regionalized appendage morphologies likely contributed to the incredible evolutionary success of this phylum. Illuminating the developmental genetic changes that coincided with the evolution of these appendage features in the arthropod lineage would provide valuable insight into the origin of the arthropod appendage and the evolution of appendage morphologies within Panarthropoda.

In developing arthropod legs, the leg gap genes, *Distal-less* (*Dll*), *dachshund* (*dac*), and *extradenticle*/*homothorax* (*exd*/*hth*), are expressed in the distal, intermediate, and proximal appendages domains, respectively, with very little overlap between their expression domains (Abzhanov and Kaufman, 2000; Barnett and Thomas, 2013; Dong et al. 2001, Prpic et al. 2003, Prpic and Damen 2004; Prpic and Tautz, 2003; Rauskolb 2001; Sewell et al., 2008; Sharma et al., 2012). These genes code for transcription factors that act as master regulators of appendage morphology (Casares and Mann, 2001; Cohen et al., 1989; González-Crespo and Morata, 1995; González-Crespo and Morata, 1996; Kato et al., 2011; Mardon et al., 1994; Pechmann, et al., 2011; Rauskolb et al., 1995; Schoppmeier and Damen, 2001; Sharma et al., 2013). The regionalized pattern of leg gap gene expression initiates a cascade of gene regulatory interactions, leading to increased regionalization of gene expression along the proximodistal axis (Kojima, 2004; Rauskolb, 2001). Ultimately, this lays the groundwork for morphological regionalization and initiation of the Notch pathway, which specifies joint development between podomeres (Kojima, 2004; Prpic and Damen, 2008; Prpic and Damen, 2009; Rauskolb 2001).

Appendages that have secondarily evolved a reduced number of podomeres and associated joints, such as the spider chelicerae and the mandibles of myriopods, crustaceans, and insects are associated with loss of expression of a leg gap gene; the spider chelicerae lack *dac* expression (Abzanhov and Kaufman, 2000; Prpic and Damen, 2004) and arthropod mandibles exhibit reduced *Dll* expression (Abzanhov and Kaufman, 2000; Panganiban et al., 1994; Popadić et al., 1996; Popadić et al., 1998; Prpic and Tautz, 2003). These results support the hypothesized requirement of antagonistic leg gap gene expression domains for the development of multi-jointed arthropod appendages with leg-like morphology (Prpic and Damen, 2004). Therefore, it is reasonable to conclude that the evolution of antagonistic leg gap gene expression domains in developing appendages was a key step in the evolution of arthropod jointed appendages. However, arthropod-like expression patterns of the leg gap genes are found in the developing appendages of the onychophoran *Euperipatoides kanangrensis* (Janssen et al., 2010), suggesting that regionalized expression patterns of these genes predate the emergence of the jointed arthropod appendage.

How can this discordance between the evolution of regionalized expression patterns of developmental genes and the evolution of regionalized appendage morphology be explained? Recently, it has been suggested the leg gap genes were part of an anterior neurectodermal-patterning network in the bilaterian ancestor that was later co-opted for appendage patterning (Lemons et al., 2010). This suggestion is based on the fact that the leg gap genes are expressed in an anteroposterior pattern in the neurectoderm of both *Drosophila melanogaster* and the appendageless hemichordate *Saccoglossus kowalevskii* that mirrors the proximodistal expression pattern of these genes in both arthropod and onychophoran appendages. In this scenario, the regionalized expression patterns of the leg gap genes in Onychophora could merely reflect an ancestral role of these genes in patterning a morphologically regionalized brain. Unfortunately, it is

not currently possible to test the function of genes in Onychophora, which would provide insight into the developmental significance of the expression pattern of the leg gap genes in this phylum.

Studies of tardigrade appendage patterning would provide a clearer picture of appendage patterning in the panarthropod ancestor and illuminate the genetic changes that enabled the evolution of joints and regionalized appendage morphologies in the arthropod lineage. The tardigrade species *Hypsibius dujardini* is particularly suited for developmental investigations. This species is easily reared in the lab, an embryonic staging series is available, and embryonic gene functions can be investigated with RNA interference (RNAi) (Gabriel et al., 2007; Tenlen et al., 2013). Also, a genomic sequencing project is in progress (Bob Goldstein, pers. comm.), which will facilitate developmental studies.

Here, an investigation of the expression pattern and function of the leg gap gene *Dll* is presented. This study includes the first successful detection of embryonic gene expression in tardigrades utilizing the *in situ* hybridization technique. A developmental analysis of *Dll* presents an ideal starting point to unravel tardigrade appendage patterning, because clear predications of *Dll* expression and function can be made based on previous studies. First, *Dll* is expressed in developing appendages across Bilateria (Panganiban et al., 1997), so *Dll* is the gene that can most confidently be predicted to play a role in tardigrade appendage development. Secondly, if the leg gap gene network that patterns arthropod and onychophoran appendages is ancestral for Panarthropoda (Lemons et al., 2011; Janssen et al., 2010), then *Dll* should only be expressed in the distal domain of developing *H. dujardini* limb buds. Finally, as in arthropods (Angelini et al., 2009; Angelini et al., 2012a; Angelini et al., 2012b; Kato et al., 2011; Pechmann et al., 2011; Schoppmeier and Damen, 2001; Sharma et al., 2013), *Dll* RNAi should lead to truncation of *H. dujardini* appendages.

Material and methods

Maintaining tardigrade cultures

Chapter 3 describes methods of culturing *H. dujardini* used in this study.

Molecular cloning of H. dujardini Dll

Embryonic cDNA was produced from mixed-stage embryos. Embryos were placed in 10 µl of Trizol reagent in the cap of a 1.5 ml microcentrifuge tube and sheared under a dissecting microscope with a 25 gauge needle. The cap was placed back on the tube, which was filled with 90 µl of Trizol reagent, and centrifuged briefly. At this stage, cDNA production proceeded as in described in chapter 1.

A 139 base pair *Dll* fragment was targeted in embryonic cDNA using nested degenerate PCR. Degenerate PCR primers were designed to recognize sites that code for conserved amino acid sequences at the ends of the Dll homeodomain. The sequences of the primary PCR primers were forward-GCGAGTGAACGGCAARGGCAARAARATNMG (translation: RVNGKGKKMR) and reverse-GGACCGCCGGTTCTGAAACCADATYTTNAC (translation: VKIWFQNRRS). The sequences of the secondary PCR primers were forward-CAAAAAGAT-GCGGAAACCCMGNACNATHTA (translation: KKMRKPRTIY) and reverse-GGTTCTGGA-ACCAGATTTTAACYTGNGTYTG (translation: QTQVKIWFQN). This fragment was cloned and sequenced as described in chapter 1. 3' RACE PCR was then used to amplify a larger fragment of *H. dujardini Dll* from embryonic cDNA. The forward primers used in the 3' RACE PCR were designed based on the sequence of the initial *H. dujardini Dll* clone. The sequences of the primary PCR primers were forward-GAAACCCCGAACGATTTATTCC and reverse-

[AAGGATCCGTCGACATCGATAAACTAGGGA]TTTTTTTTT (adapter sequence is bracketed). The sequences of the secondary PCR primers were forward-GATATCGTTCCACT-TGTCTGCGAT and reverse-AAGGATCCGTCGACATCGAT. This fragment was also cloned and sequenced as described in chapter 1.

Phylogenetic analysis

A maximum likelihood phylogenetic approach was used to confirm the identity of the prospective *H. dujardini Dll* sequence. First, the amino acid translation of the prospective *H. dujardini Dll* sequence was predicted using the 'Translate DNA to Protein' function in Mesquite (Maddison and Maddison, 2011). This sequence was aligned with twenty Dll protein sequences chosen to span metazoan diversity using the MUSCLE algorithm (Edgar, 2004). Identification and alignment of Dll homeodomains with homeodomains of other metazoan transcription factors was based on alignments from Ryan et al. (2007) (Table 1). ProtTest (Abascal et al., 2005), implementing the Akaike Information Criterion framework, selected LG+G as the model of protein evolution that best fit the homeodomain alignment. This model was implemented in a RAxML (Starnatakis, 2006) maximum likelihood analysis of the alignment. 500 bootstrap replicates were performed in this analysis. The tree was rooted based on Ryan et al. (2007).

In situ hybridization

In this study, an *in situ* hybridization protocol for tardigrades was developed, and the first *H. dujardini* mRNA gene expression data were collected. Briefly, sense and anti-sense digoxigenin-labeled probes were synthesized from the 3' RACE *H. dujardini Dll* clone. Embryos were permeabilized for 1 hour at room temperature (RT) in a solution of 50 mg/ml

chitinase and 15 mg/ml chymotrpysin in 50 mM potassium phosphate buffer (pH 6.0). This was followed by three 5-minute washes is DEPC treated 0.5X PBTw (0.5X phosphate buffer saline, 0.1% Tween20). Embryos were fixed for 30 minutes in formaldehyde solution (4% formaldehyde, 33% heptane, 0.1% Tween20, in 0.5X PBTw). Embryos were then rinsed with five 5-minute washes in 0.5X PBTw. An acetylation step was performed to reduce background. First, embryos were washed twice with 1% triethanolamine in 0.5X PBTw. Embryos were then acetylated with two 5-minutes washes in 0.25% acetic anhydride in 1% triethanolamine in PBTw. Acetylation was followed by three 5-minutes washes in 0.5X PBTw. For prehybridization, embryos were washed twice at RT for 20 minutes in hybridization buffer (50% formaldehyde, 5X SSC, 50 µg/µl heparin, 0.1% CHAPS, 1X Denhardt's solution, 100 µg/ml yeast RNA, 0.1% Tween20, in DEPC H_2O), followed by a 2-hour wash at 60° C in hybridization buffer that had been preheated to 60° C. 0.5 µg/ml solutions of sense strand and anti-sense strand *Dll* probes in Hybe buffer were heated to 80C. 1 µl of boiled and sheared salmon sperm was added to the probes immediately before hybridization. Hybridization was performed for 16 hours at 60°C. Embryos were then washed five times quickly and five times for 20 minutes in plain Hybe buffer (50% formaldehyde, 5X SSC, 0.1% Tween20). Next, embryos were washed five times quickly and for 30 minutes in 2X SSC, 0.1% CHAPS and twice quickly in 0.5X PBTw. Embryos were then washed twice for 30 minutes in 1X SSC, 0.1% CHAPS. Embryos were washed with blocking solution for two hours, followed by a 16-hour incubation in 1:1,500 anti-DIG antibody in blocking solution. Next, embryos were washed five times quickly, followed by five 10-minute rinses in 0.5X PBTw. Embryos were then washed several times in AP developing solution (100 mM Tris HCl, 100 mM NaCl, 50 mM M $MgCl_2$, 0.1% Tween20). BPIC/NBT Plus solution (Southern Biotech 0302-01) was used for probe detection. Embryos

were washed with 0.5X PBTw to stop the staining reaction. A more detailed description of the *in situ* protocol for *H. dujardini* is provided in the Appendix to this chapter.

RNA interference

A 523-base pair fragment of *Dll* was amplified from the 3' RACE *Dll* clone using forward-taatacgactcactatagggAGAATCCCAACGGCGGCACT and reverse-taatacgactca-ctatagggGGTGTGATGGTAGCCCTGATGATG primers, which had T7 RNA polymerase recognition sites added to the 5' ends (lower case sequence). This fragment was used as template for dsRNA synthesis, using a T7 RiboMax Express RNAi System (Promega), following the manufacturers protocol. The sodium acetate/ethanol method was used to precipitate dsRNA, which was then resuspended in nuclease free water. The RNAi protocol followed that of Tenlen et al. (2013). Adult females that lacked visible embryos in their abdomens were collected and anesthetized in levamisole diluted to 10 μM in spring water. Anesthetized females were placed in Halocarbon oil on a microscope slide and injected with dsRNA. Injection of *GFP* dsRNA acted as a negative control. Following injection, females were kept separately in spring water and monitored daily. Any embryos laid were collected and monitored. If an embryo had not hatched by 5 days post-laying, it was considered unviable. These embryos were scored for morphological defects. Hatchlings were scored for morphological and behavioral defects.

Specimen imaging

Embryos were imaged on slides in either BCIP/NBT PLUS solution (Southern Biotech) during the *in situ* hybridization development step or in Fluoromount-G mounting solution (SouthernBiotech) after termination of development of the *in situ* hybridization signal.

Differential interference contrast (DIC) micrographs of embryos were taken on a Ziess Axioskop compound microscope with an Olympus digital camera using Magnafire imaging software. Light micrographs of embryos were taken with the same set up as the DIC micrographs, or on a Nikon Eclipse 800 compound microscope with a Diagnostic Instruments SPOT2 camera using Metamorph v 6.3r7 (Molecular Devices) software. The brightness and contrast of images were adjusted in Adobe Photoshop CS4.

Results and discussion

Phylogenetic analysis confirms identity of H. dujardini *Dll sequence*

The homeodomain is a highly conserved DNA binding domain uniting a class of transcriptions factors found across Eukaryota (Gehring et al., 1994). *In vivo*, this domain forms a helix-turn-helix motif (Billeter et al., 1990; Otting et al., 1988; Qian et al., 1989). These transcription factors are encoded by homeobox genes, which play important roles in animal development, including proximodistal axis patterning. The genes form two distinct, but evolutionarily related, subclasses: the typical homeobox genes, which include *Dll* and the *Hox* genes, and the TALE-class homeobox genes, which include *exd*/*hth* (Bürglin, 1998). The transcription factors coded by the typical homeobox genes include a 60-amino acid-long homeodomain. On the other hand, the homeodomain of TALE-class homeodomain transcription factors includes an additional 3 amino acids in the region linking the two helices (Bertolino et al., 1995). Between families of homeodomain proteins, very little conservation of amino acid sequences is found outside of the homeodomain, and it is not clear which, if any, non-homeodomain regions are homologous between families.

A phylogenetic analysis of typical homeodomain sequences was used to verify the identity of the prospective *H. dujardini* Dll sequence. *Dll* orthologs are found in genomes across Bilateria and Cnidaria (Panganiban et al., 1997; Ryan et al., 2007). The prospective *H. dujardini* Dll sequence fell within a well-supported clade (100% bootstrap support) that included all Dll sequences and excluded all non-Dll sequences (Fig. 1B). Little support was found for phylogenetic relationships within the Dll clade, and the topology of the Dll clade did not closely match the taxonomic relationships of the species from which the Dll sequences were derived (compare phylogeny in Fig. 1A to 1B). The low support for relationships within the Dll clade is likely the result of the low number of phylogenetically informative sites in the Dll homeodomain alignment, highlighting the extreme conservation of the Dll homeodomain across Bilateria and Cnidaria (Fig. 1; Table 1). In sum, results of the phylogenetic analysis presented here provide conclusive evidence that the prospective *H. dujardini Dll* sequence represents a *Dll* ortholog of *H. dujardini*.

Dll *is expressed across the developing limb buds in* H. dujardini

Dll expression was characterized using *in-situ* hybridization at four embryonic periods: 27 hours post laying (hpl), 45 hpl, 55 hpl, and 65 hpl. By 27 hpl, elongation of the embryo has concluded and a complete anteroposterior axis is present (Gabriel et al., 2007), but limb buds are not yet visible. At this stage, *Dll* expression was detected in cells at the surface of the embryo, but was not detected in interior embryonic cells (Fig. 2A). This is surprising, given that this pattern of *Dll* expression has not been reported for Onychophora or Arthropoda. The role that *Dll* is playing at this stage is impossible to predict, because the tissues to which the *Dll* expressing cells and non-*Dll* expressing cells give rise are not currently known. However, it has

been speculated that the exterior cells at the *H. dujardini* elongation stage give rise to ectodermal tissues, while the internal cells give rise to endomesodermal derivatives (Gabriel et al., 2007), suggesting that *Dll* may play an early role in ectodermal specification.

In arthropods, a single example exists for a requirement of *Dll* prior to appendage formation. In the spider *Achaearanea tepidariorum*, *Dll* is expressed before anteroposterior segmentation, and is required for normal segmentation of the head (Pechmann et al., 2011). Specifically, *Dll* is required for specification of the first leg-bearing segment (legs are on head segments in spiders); therefore, *Dll* RNAi causes deletion of this segment in this species. *Dll* RNAi does not result in the loss of the first leg-bearing segment in the spider *Cupiennius salei* (Schoppmeier and Damen, 2001), the harvestman *Phalangium opilio* (Sharma et al., 2013), the spider mite *Tetranychus urticae* or non-chelicerate arthropods (Angelini and Kaufman, 2004; Kato et al., 2011; Ohde et al., 2009), suggesting that the segmentation function of *Dll* evolved in the lineage leading to *A. tepidariorum*. Therefore, it is unlikely that the early expression of *Dll* in *H. dujardini* is evolutionarily related to *Dll* expression in arthropods or onychophorans. Either early expression of *Dll* was lost in the lineage leading to Onychophora and Arthropoda, or it represents a derived function of *Dll* in *H. dujardini* and possibly Tardigrada as a whole.

Limb buds first become evident at ~45 hpl, although claws have yet to appear. At this stage, *Dll* expression was detected across the developing limb bud (Fig. 2B–C). This expression pattern was maintained through ~65 hpl, the latest stage examined, at which point claws have developed (Fig. 2D). These results differ from previous reports of *Dll* expression in the developing appendages of Onychophora (Janssen et al., 2010) and Arthropoda (reviewed in Angelini et al., 2005), where a large domain of *Dll* expression is only seen in the distal region of embryonic appendages. These results present the possibility that regionalized expression

patterns of the leg gap genes, including *Dll*, evolved in the lineage leading to Onychophora and Arthropoda after the divergence of this lineage from Tardigrada. On the other hand, it is also possible that regionalized expression of these genes was present during ancestral panarthropod appendage development, but was subsequently lost during evolution within the tardigrade lineage. Without a suitable outgroup for comparison, it is not possible to distinguish between these two possibilities. The results presented here suggest that regionalized expression of the leg gap genes is not a requirement for development of lobopodal appendages. Future studies are needed to investigate whether *exd*/*hth* and *dac* lack regionalized expression during leg development in *H. dujardini*.

Dll *expression in the head supports homology between stylet apparatus and legs*

Ancestral panarthropods are thought to have had appendages on every segment, including the ocular segment that houses the eyes. Most Cambrian lobopods exhibit this body plan architecture (Hou et al., 2004; Lamsdell et al., 2013) and the Onychophora retain an unambiguous frontal appendage on the ocular segment (Eriksson et al., 2006). Based on fossil evidence, stem-group arthropods are known to have had a pair of appendages on the ocular segment, although the fate of this appendage in crown group arthropods is highly debated (Scholtz and Edgecomb, 2006). However, no clear appendage pair is present on the ocular segment of tardigrades. What was the fate of the ocular appendage in this lineage?

One interesting hypothesis proposes that the legs of the tardigrade ocular segment became internalized and evolved into the stylet apparatus (Nielsen, 2001). Several morphological features support this hypothesis. First, both the stylets of the stylet apparatus and the claws are non-cellular glandular secretions; second, striated muscles are only found in the

muscles of the stylet apparatus and the legs; and finally, microtubles are only found in the cells of muscle attachment sites in the leg and epidermal cells at the base of the stylets where the stylet muscles attach (Halberg et al., 2009). As acknowledged by Halberg et al. (2009), similarities between the muscle systems of the stylet apparatus and the legs could have evolved independently due to similarities in functional requirements of the stylets and legs. However, further support for serial homology of the stylet apparatus and legs is provided by *Dll* expression. Expression of this gene was detected at the base of the developing stylets in a late stage embryo (Fig. 3), as predicted if the stylets are homologous to claws. Caution should be given to conclusions about serial homology based on expression patterns of a single gene. Additional data to test the serial homology hypothesis could be acquired through investigations of expression patterns of other appendage patterning genes.

Dll *RNAi elevated mortality during* H. dujardini *embryogenesis*

Of 63 specimens scored from *GFP* RNAi treatments, only 1.59% died during embryogenesis (Table 2). Maternal injection of *Dll* dsRNA resulted in an increase in embryo lethality (Table 2). Of twenty-eight embryos scored, 21.43% died in 1 µg/µl *Dll* dsRNA treatments (z-test, p=0.0005). In five of these embryos, embryogenesis terminated early in development after only a few cell divisions. A sixth embryo developed normally, and lacked any obvious morphological defects, but failed to hatch. In 1.5 µg/µl *Dll* dsRNA treatments, of 103 embryos scored, 8.74% died (z-test, p=0.0302). Eight of these embryos appeared normal, while in one embryo, embryogenesis terminated prior to elongation. The cause of increased lethality associated with *Dll* RNAi is unclear. All embryos that hatched possessed wild-type legs and walked normally. Based on these results, it is impossible to interpret the function of *Dll* in *H.*

dujardini appendage development. Investigations implementing confocal microscopy analyses of morphology might make it possible to detect subtle morphological defects associated with *Dll* RNAi that are not apparent with light microscopy.

Conclusion

This study presented the first *in situ* hybridization gene expression data for the phylum Tardigrada. The *in situ* hybridization protocol developed for this study (Appendix) complements an existing RNAi protocol for *H. dujardini* (Tenlen et al., 2013), making developmental genetic studies feasible for this species. Results of the investigation of the role of *Dll* in appendage patterning presented here suggest that the evolution of appendage patterning in Panarthropoda was much more dynamic then previously appreciated. For example, unlike previously described for Onychophora or Arthropoda, *Dll* is expressed across the developing limb bud in *H. dujardini*. This suggests that the *Dll* expression domain retracted to the very distal appendage region in the lineage leading to Onychophora and Arthropoda, or expanded to encompass the entire proximodistal appendage axis in the tardigrade lineage. A suitable outgroup is not available to distinguish between these two possibilities. However, it seems likely, given *Dll* is expressed in embryonic legs of *H. dujardini*, that *Dll* played an appendage patterning role in the panarthropod ancestor. Investigations of the expression patterns and functions of *exd*/*hth* and *dachshund* in *H. dujardini* appendage development would further illuminate the roles of the leg gap genes in appendage development in the panarthropod ancestor.

References

Abascal, F., Zardoya, R., Posada, D., 2005. ProtTest: Selection of best-fit models of protein evolution. *Bioinformatics* 21, 2104–2105.

Abzhanov, A., Kaufman, T.C., 2000. Homologs of *Drosophila* appendage genes in the patterning of arthropod limbs. *Dev. Biol.* 227, 673–689.

Angelini, D.R., Kaufman, T.C., 2005. Insect appendages and comparative ontogenetics. *Dev. Biol.* 286, 57–77.

Angelini, D.R., Kaufman, T.C., 2004. Functional analyses in the hemipteran *Oncopeltus fasciatus* reveal conserved and derived aspects of appendage patterning in insects. *Dev. Biol.* 271, 306–321.

Angelini, D.R., Smith, F.W., Aspiras, A.C., Kikuchi, M., Jockusch, E.L., 2012. Patterning of the adult mandibulate mouthparts in the red flour beetle, *Tribolium castaneum*. *Genetics* 190, 639–654.

Angelini, D.R., Smith, F.W., Jockusch, E.L., 2012. Extent with modification: Leg patterning in the beetle *Tribolium castaneum* and the evolution of serial homologs. *G3 (Bethesda)* 2, 235–248.

Angelini, D.R., Kikuchi, M., Jockusch, E.L., 2009. Genetic patterning in the adult capitate antenna of the beetle *Tribolium castaneum*. *Dev. Biol.* 327, 240–251.

Barnett, A.A., Thomas, R.H., 2013. The expression of limb gap genes in the mite *Archegozetes longisetosus* reveals differential patterning mechanisms in chelicerates. *Evol. Dev.* 15, 280–292.

Bertolino, E., Reimund, B., Wildt-Perinic, D., Clerc, R.G., 1995. A novel homeobox protein which recognizes a TGT core and functionally interferes with a retinoid-responsive motif. *J. Biol. Chem.* 270, 31178–31188.

Billeter, M., Qian, Y., Otting, G., Muller, M., Gehring, W.J., Wuthrich, K., 1990. Determination of the three-dimensional structure of the Antennapedia homeodomain from drosophila in solution by 1H nuclear magnetic resonance spectroscopy. *J. Mol. Biol.* 214, 183–197.

Budd, G.E., Telford, M.J., 2009. The origin and evolution of arthropods. *Nature* 457, 812–817.

Budd, G.E., 2001. Why are arthropods segmented? *Evol. Dev.* 3, 332–342.

Burglin, T.R., 1998. The PBC domain contains a MEINOX domain: Coevolution of Hox and TALE homeobox genes? *Dev. Genes Evol.* 208, 113–116.

Campbell, L.I., Rota-Stabelli, O., Edgecombe, G.D., Marchioro, T., Longhorn, S.J., Telford, M.J., Philippe, H., Rebecchi, L., Peterson, K.J., Pisani, D., 2011. MicroRNAs and phylogenomics resolve the relationships of tardigrada and suggest that velvet worms are the sister group of arthropoda. *Proc. Natl. Acad. Sci. U. S. A.* 108, 15920–15924.

Casares, F., Mann, R.S., 2001. The ground state of the ventral appendage in *Drosophila*. *Science* 293, 1477–1480.

Cohen, S.M., Bronner, G., Kuttner, F., Jurgens, G., Jackle, H., 1989. *Distal-less* encodes a homoeodomain protein required for limb development in *Drosophila*. *Nature* 338, 432–434.

Dong, P.D., Chu, J., Panganiban, G., 2001. Proximodistal domain specification and interactions in developing *Drosophila* appendages. *Development* 128, 2365–2372.

Dunn, C.W., Hejnol, A., Matus, D.Q., Pang, K., Browne, W.E., Smith, S.A., Seaver, E., Rouse, G.W., Obst, M., Edgecombe, G.D., Sorensen, M.V., Haddock, S.H., Schmidt-Rhaesa, A., Okusu, A., Kristensen, R.M., Wheeler, W.C., Martindale, M.Q., Giribet, G., 2008. Broad phylogenomic sampling improves resolution of the animal tree of life. *Nature* 452, 745–749.

Edgar, R.C., 2004. MUSCLE: Multiple sequence alignment with high accuracy and high throughput. *Nucleic Acids Res.* 32, 1792–1797.

Eriksson, B.J., Tait, N.N., Budd, G.E., Janssen, R., Akam, M., 2010. Head patterning and hox gene expression in an onychophoran and its implications for the arthropod head problem. *Dev. Genes Evol.* 220, 117–122.

Gabriel, W.N., Goldstein, B., 2007. Segmental expression of Pax3/7 and Engrailed homologs in tardigrade development. *Dev. Genes Evol.* 217, 421–433.

Gabriel, W.N., McNuff, R., Patel, S.K., Gregory, T.R., Jeck, W.R., Jones, C.D., Goldstein, B., 2007. The tardigrade *Hypsibius dujardini*, a new model for studying the evolution of development. *Dev. Biol.* 312, 545–559.

Gehring, W.J., Affolter, M., Burglin, T., 1994. Homeodomain proteins. *Annu. Rev. Biochem*. 63, 487–526.

González-Crespo, S., Morata, G., 1996. Genetic evidence for the subdivision of the arthropod limb into coxopodite and telopodite. *Development* 122, 3921–3928.

Gonzalez-Crespo, S., Morata, G., 1995. Control of *Drosophila* adult pattern by *extradenticle*. *Developmen*t 121, 2117–2125.

Grenier, J.K., Garber, T.L., Warren, R., Whitington, P.M., Carroll, S., 1997. Evolution of the entire arthropod *Hox* gene set predated the origin and radiation of the onychophoran/arthropod clade. *Current Biology* 7, 547–553.

Halberg, K.A., Persson, D., Mobjerg, N., Wanninger, A., Kristensen, R.M., 2009. Myoanatomy of the marine tardigrade *Halobiotus crispae* (eutardigrada: Hypsibiidae). *J. Morphol*. 270, 996–1013.

Hou, X., Aldridge, R., Bergstrom, J., Siveter, D.J, Siveter, D., Feng, X., 2004. The Cambrian Fossils of Chengjiang, China: The Flowering of Early Animal Life. Wiley-Blackwell, Hoboken.

Janssen, R., Eriksson, B.J., Budd, G.E., Akam, M., Prpic, N.M., 2010. Gene expression patterns in an onychophoran reveal that regionalization predates limb segmentation in pan-arthropods. *Evol. Dev.* 12, 363–372.

Kato, Y., Shiga, Y., Kobayashi, K., Tokishita, S., Yamagata, H., Iguchi, T., Watanabe, H., 2011. Development of an RNA interference method in the cladoceran crustacean *Daphnia magna*. *Dev. Genes Evol.* 220, 337–345.

Khila, A., Grbic, M., 2007. Gene silencing in the spider mite *Tetranychus urticae*: dsRNA and siRNA parental silencing of the *Distal-less* gene. *Dev. Genes Evol.* 217, 241–251.

Kojima, T., 2004. The mechanism of *Drosophila* leg development along the proximodistal axis. *Dev. Growth Differ.* 46, 115–129.

Lamsdell, J.C., Stein, M., Selden, P.A., 2013. *Kodymirus* and the case for convergence of raptorial appendages in Cambrian arthropods. *Naturwissenschaften*. DOI 10.1007/s00114-013-1081-y

Legg, D.A., Sutton, M.D., Edgecombe, G.D., Caron, J.B., 2012. Cambrian bivalved arthropod reveals origin of arthrodization. *Proc. Biol. Sci.* 279, 4699–4704.

Lemons, D., Fritzenwanker, J.H., Gerhart, J., Lowe, C.J., McGinnis, W., 2010. Co-option of an anteroposterior head axis patterning system for proximodistal patterning of appendages in early bilaterian evolution. *Dev. Biol.* 344, 358–362.

Maas, A., Waloszek, D., 2001. Cambrian derivatives of the early arthropod stem lineage, pentastomids, tardigrades and lobopodians an 'Orsten'Perspective. *Zoologischer Anzeiger*. 240, 451–459.

Maddison, W. P. and D.R. Maddison. 2011. Mesquite: a modular system for evolutionary analysis. Version 2.75 http://mesquiteproject.org

Manton, S. M., 1977. The Arthropoda: Habits, Functional Morphology and Evolution. Clarendon Press, Oxford.

Mardon, G., Solomon, N.M., Rubin, G.M., 1994. *Dachshund* encodes a nuclear protein required for normal eye and leg development in *Drosophila*. *Development* 120, 3473–3486.

Nielsen, C., 2001. Animal Evolution: Interrelationships of the Animal Phyla. Oxford University Press, New York.

Ohde, T., Masumoto, M., Yaginuma, T., Niimi, T., 2009. Embryonic RNAi analysis in the firebrat, *Thermobia domestica* [Zygentoma: Lepismatidae]: *Distal-less* is required to form caudal filament. *J. Insect Biotechnol. Sericology* 78, 99–105.

Otting, G., Qian, Y.Q., Muller, M., Affolter, M., Gehring, W., Wuthrich, K., 1988. Secondary structure determination for the Antennapedia homeodomain by nuclear magnetic resonance and evidence for a helix-turn-helix motif. *EMBO J.* 7, 4305–4309.

Panganiban, G., Nagy, L., Carroll, S.B., 1994. The role of the *Distal-less* gene in the development and evolution of insect limbs. *Current Biology* 4, 671–675.

Panganiban, G., Irvine, S.M., Lowe, C., Roehl, H., Corley, L.S., Sherbon, B., Grenier, J.K., Fallon, J.F., Kimble, J., Walker, M., Wray, G.A., Swalla, B.J., Martindale, M.Q., Carroll, S.B., 1997. The origin and evolution of animal appendages. *Proc. Natl. Acad. Sci. U. S. A.* 94, 5162–5166.

Pechmann, M., Khadjeh, S., Turetzek, N., McGregor, A.P., Damen, W.G., Prpic, N.M., 2011. Novel function of distal-less as a gap gene during spider segmentation. *PLoS Genet.* 7, e1002342.

Pechmann, M., Prpic, N.M., 2009. Appendage patterning in the south american bird spider *Acanthoscurria geniculata* (araneae: Mygalomorphae). *Dev. Genes Evol.* 219, 189–198.

Popadić, A., Panganiban, G., Rusch, D., Shear, W.A., Kaufman, T.C., 1998. Molecular evidence for the gnathobasic derivation of arthropod mandibles and for the appendicular origin of the labrum and other structures. *Dev. Genes Evol.* 208, 142–150.

Popadic, A., Rusch, D., Peterson, M., Rogers, B.T., Kaufman, T.C., 1996. Origin of the arthropod mandible. *Nature* 380*,* 395.

Prpic, M, Damen, W. G. M., Arthropod appendages: a prime example for the evolution of morphological diversity and innovation. In: Fusco, G., Minelli, M. (Ed.), Evolving Pathways: Key Themes in Evolutionary Developmental Biology, Cambridge University Press, Cambridge, 2008, pp. 381–398.

Prpic, N.M., Damen, W.G., 2009. *Notch*-mediated segmentation of the appendages is a molecular phylotypic trait of the arthropods. *Dev. Biol.* 326, 262–271.

Prpic, N.M., Damen, W.G., 2004. Expression patterns of leg genes in the mouthparts of the spider cupiennius salei (chelicerata: Arachnida). *Dev. Genes Evol.* 214, 296–302.

Prpic, N.M., Janssen, R., Wigand, B., Klingler, M., Damen, W.G., 2003. Gene expression in spider appendages reveals reversal of *exd*/*hth* spatial specificity, altered leg gap gene dynamics, and suggests divergent distal morphogen signaling. *Dev. Biol.* 264, 119–140.

Prpic, N.M., Tautz, D., 2003. The expression of the proximodistal axis patterning genes distal-less and dachshund in the appendages of *Glomeris marginata* (myriapoda: Diplopoda)

suggests a special role of these genes in patterning the head appendages. *Dev. Biol.* 260, 97–112.

Qian, Y.Q., Billeter, M., Otting, G., Muller, M., Gehring, W.J., Wuthrich, K., 1989. The structure of the Antennapedia homeodomain determined by NMR spectroscopy in solution: Comparison with prokaryotic repressors. *Cell* 59, 573–580.

Rauskolb, C., 2001. The establishment of segmentation in the *Drosophila* leg. *Development* 128, 4511–4521.

Rauskolb, C., Smith, K.M., Peifer, M., Wieschaus, E., 1995. Extradenticle determines segmental identities throughout *Drosophila* development. *Development* 121, 3663–3673.

Ryan, J.F., Mazza, M.E., Pang, K., Matus, D.Q., Baxevanis, A.D., Martindale, M.Q., Finnerty, J.R., 2007. Pre-bilaterian origins of the hox cluster and the hox code: Evidence from the sea anemone, *Nematostella vectensis*. *PLoS One* 2, e153.

Scholtz, G., Edgecombe, G.D., 2006. The evolution of arthropod heads: Reconciling morphological, developmental and palaeontological evidence. *Dev. Genes Evol.* 216, 395–415.

Schoppmeier, M., Damen, W.G., 2001. Double-stranded RNA interference in the spider *Cupiennius salei*: The role of *Distal-less* is evolutionarily conserved in arthropod appendage formation. *Dev. Genes Evol.* 211, 76–82.

Sewell, W., Williams, T., Cooley, J., Terry, M., Ho, R., Nagy, L., 2008. Evidence for a novel role for *Dachshund* in patterning the proximal arthropod leg. *Dev. Genes Evol.* 218, 293–305.

Sharma, P.P., Schwager, E.E., Giribet, G., Jockusch, E.L., Extavour, C.G., 2013. *Distal-less* and *Dachshund* pattern both plesiomorphic and apomorphic structures in chelicerates: RNA interference in the harvestman *Phalangium opilio* (opiliones). *Evol. Dev.* 15, 228–242.

Sharma, P.P., Schwager, E.E., Extavour, C.G., Giribet, G., 2012. Evolution of the chelicera: A *Dachshund* domain is retained in the deutocerebral appendage of opiliones (arthropoda, chelicerata). *Evol. Dev.* 14, 522–533.

Shubin, N., Tabin, C., Carroll, S., 1997. Fossils, genes and the evolution of animal limbs. *Nature* 388, 639–648.

Snodgrass, R.E., 1935. Principles of Insect Morphology. Cornell University Press, Ithaca.

Stamatakis, A., 2006. RAxML-VI-HPC: Maximum likelihood-based phylogenetic analyses with thousands of taxa and mixed models. *Bioinformatics* 22, 2688–2690.

Tenlen, J.R., McCaskill, S., Goldstein, B., 2012. RNA interference can be used to disrupt gene function in tardigrades. *Dev. Genes Evol*. 1–11.

Trautwein, M.D., Wiegmann, B.M., Beutel, R., Kjer, K.M., Yeates, D.K., 2012. Advances in insect phylogeny at the dawn of the postgenomic era. *Annu. Rev. Entomol.* 57, 449–468.

Tables

Table 1. Key to taxon abbreviations shown in Figure 1. GenBank accession numbers for the sequences used in the phylogenetic analysis are provided. Nev'DLL in Fig. 1A = Ne'DLL in Fig. 1B.

Abbreviation	Phylum	Species	Gene	Accession
Ag'DLL	Arthropoda	*Anopheles gambiae*	*Distal-less*	XP_308706
Am'DLL	Arthropoda	*Apis mellifera*	*Distal-less*	NP_001124509
Ba'DLL	Arthropoda	*Bicyclus anynana*	*Distal-less*	AAL69325
Bf'DLL	Chordata	*Branchiostoma floridae*	*Distal-less*	P53772
Bf'EVXA	Chordata	*Branchiostoma floridae*	*even-skipped A*	XP_002612703
Bf'HOX1	Chordata	*Branchiostoma floridae*	*Hox-1*	CAA84514
Ce'CE-43	Nematoda	*Caenorhabditis elegans*	*ceh-43*	NP_497904
Ci'DLXC	Chordata	*Ciona intestinalis*	*Distal-less C*	NP_001027821
Cs'DLL	Arthropoda	*Cupiennius salei*	*Distal-less*	CAC34380
Dm'DLL	Arthropoda	*Drosophila melanogaster*	*Distal-less*	NP_001137759
Dm'EVE	Arthropoda	*Drosophila melanogaster*	*even-skipped*	AAA28522
Dm'EXEX	Arthropoda	*Drosophila melanogaster*	*extra-extra*	NP_648164
Dm'LAB	Arthropoda	*Drosophila melanogaster*	*Labial*	NP_001246953
Dr'DL1A	Chordata	*Danio rerio*	*Distal-less 1a*	NP_571380
Ek'DLL	Onychophora	*Euperipatoides kanangrensis*	*Distal-less*	CAX63043
Gg'DLX1	Chordata	*Gallus gallus*	*Distal-less 1*	NP_001039307
Gm'DLL	Arthropoda	*Glomeris marginata*	*Distal-less*	CAD82905
Hs'DLX6	Chordata	*Homo sapiens*	*Distal-less 6*	P56179
Hs'HLXB9	Chordata	*Homo sapiens*	*motor neuron and pancreas homeobox 1*	AAD41467
Mm'DLX6	Chordata	*Mus musculus*	*Distal-less 6*	AAB94583
Ne'ANTHOX6	Cnidaria	*Nematostella vectensis*	*anthox6-ANTP*	ABB86465
Ne'DLL	Cnidaria	*Nematostella vectensis*	*Distal-less*	XP_001638618
Ne'EVX	Cnidaria	*Nematostella vectensis*	*even-skipped*	ABB86502
Ne'HLXB9	Cnidaria	*Nematostella vectensis*	*motor neuron and pancreas homeobox*	ACT36591
Of'DLL	Arthropoda	*Oncopeltus fasciatus*	*Distal-less*	AAS93631
Pd'DLX	Annelida	*Platynereis dumerilii*	*Distal-less*	CAJ38799
Ph'DLL	Arthropoda	*Parhyale hawaiensis*	*Distal-less*	ACT78885
Phc'DLL	Arthropoda	*Pediculus humanus*	*Distal-less*	XP_002423032
Sk'DLX1	Hemichordata	*Saccoglossus kowalevskii*	*Distal-less 1*	NP_001158371
Sp'DLX	Echinodermata	*Strongylocentrotus purpuratus*	*Distal-less*	NP_001123282
Tc'DLL	Arthropoda	*Tribolium castaneum*	*Distal-less*	NP_001034528

Table 2. Summary of *Dll* RNAi results. The number of adults injected and the number of embryos scored are provided. Embryos that failed to hatch after 5 days were considered dead.

dsRNA sequence sequence	dsRNA size (bp)	Concentration (µl)	Number injected (adults)	Number scored (embryos)	Embryonic lethality (%)
GFP	897	1.00	22	63	1.59
Dll	523	1.00	24	28	21.43
Dll	523	1.50	65	103	8.74

Figure 1. Phylogenetic analysis of metazoan Homeodomain proteins. (A) Alignment of Dll amino acid sequences used in the phylogenetic analysis. The homeodomain in labeled. The *H. dujardini* Dll sequence is boxed. To the left is a phylogenetic tree showing the relationships of the taxa (based on Campbell et al. 2011; Dunn et al., 2008; Trautwein et al., 2012). (B) Maximum likelihood phylogenetic tree obtained by analysis of Dll homeodomain sequences from a diverse set of metazoan phyla. *H. dujardini* Dll is boxed and its branch is labeled with an asterisk. Bootstrap supports of greater than 50% are shown. Non-Dll homeodomain sequences were used as outgroups. Taxa/gene abbreviations are available in Table 1.

Figure 1.

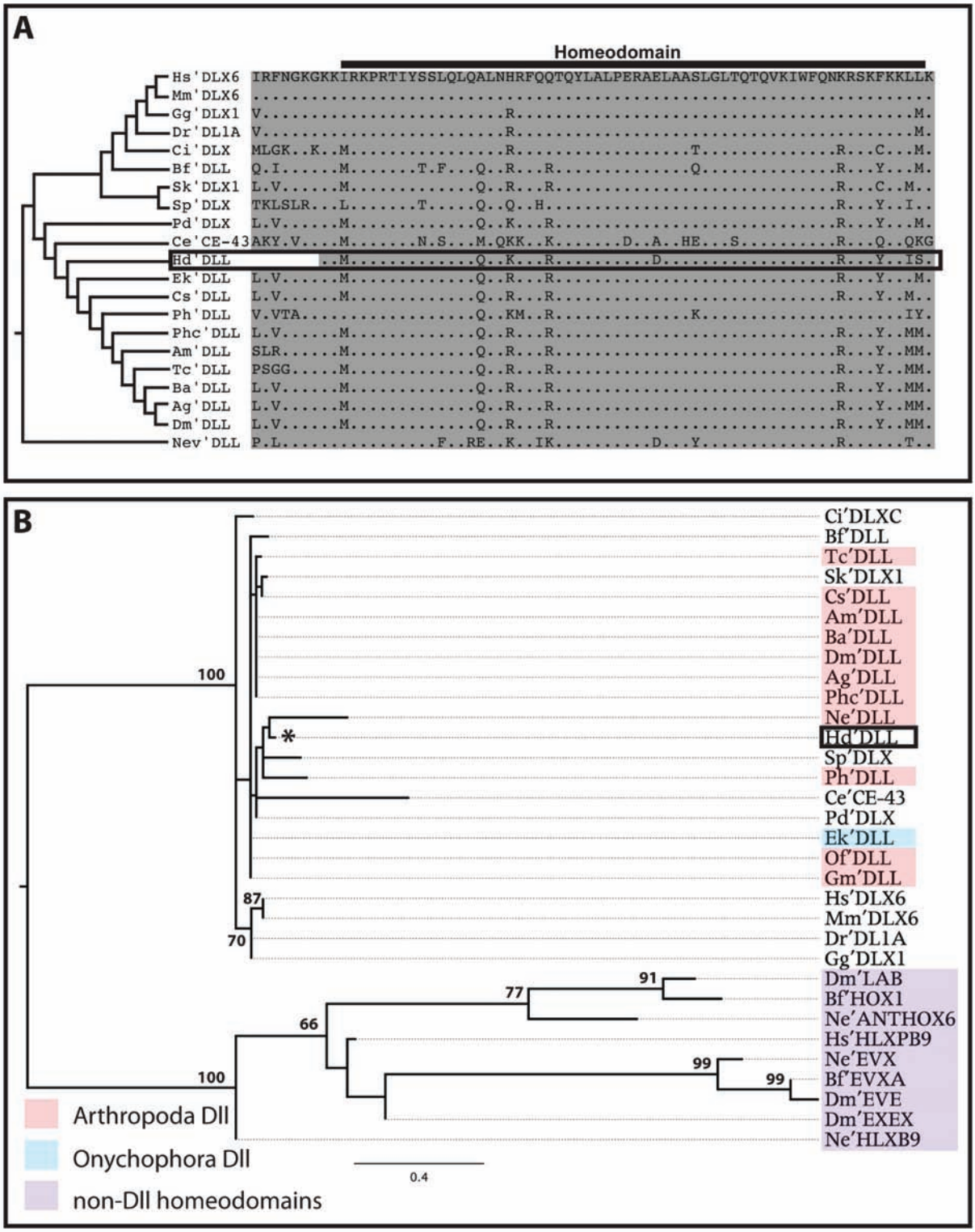
A
Homeodomain
Hs'DLX6 IRFNGKGKKIRKPRTIYSSLQLQALNHRFQQTQYLALPERAELAASLGLTQTQVKIWFQNKRSKFKKLLK
Mm'DLX6
Gg'DLX1
Dr'DL1A
Ci'DLX
Bf'DLL
Sk'DLX1
Sp'DLX
Pd'DLX
Ce'CE-43
Hd'DLL
Ek'DLL
Cs'DLL
Ph'DLL
Phc'DLL
Am'DLL
Tc'DLL
Ba'DLL
Ag'DLL
Dm'DLL
Nev'DLL
B
Ci′DLXC
Bf′DLL
Tc′DLL
Sk′DLX1
Cs′DLL
Am′DLL
Ba′DLL
Dm′DLL
Ag′DLL
Phc′DLL
Ne′DLL
Hd′DLL
Sp′DLX
Ph′DLL
Ce′CE-43
Pd′DLX
Ek′DLL
Of′DLL
Gm′DLL
Hs′DLX6
Mm′DLX6
Dr′DL1A
Gg′DLX1
Dm′LAB
Bf′HOX1
Ne′ANTHOX6
Hs′HLXPB9
Ne′EVX
Bf′EVXA
Dm′EVE
Dm′EXEX
Ne′HLXB9
100
87
70
91
77
66
99
99
100
*
Arthropoda Dll
Onychophora Dll
non-Dll homeodomains
0.4

Figure 2. *Dll* is expressed in the developing germ-band and appendages of *H. dujardini*. Legs are labeled 1–4 in B–C. (A) DIC micrograph showing ventral view of an embryo at 27 hours post-laying (hpl). *Dll* expression is detected in exterior embryonic cells, but is lacking in interior embryonic cells. (B–C) At 45 hpl, *Dll* is expressed across the developing leg buds. (B) DIC micrograph showing lateral view of an embryo. (C) Light micrograph showing lateral view of a different embryo. (D) DIC micrograph showing ventrolateral view of an embryo at 65 hpl. Claws are present on legs and *Dll* is expressed at high levels in the legs. Abbreviations: cl, claw; gb, germ-band; L, left; R, right.

Figure 2.

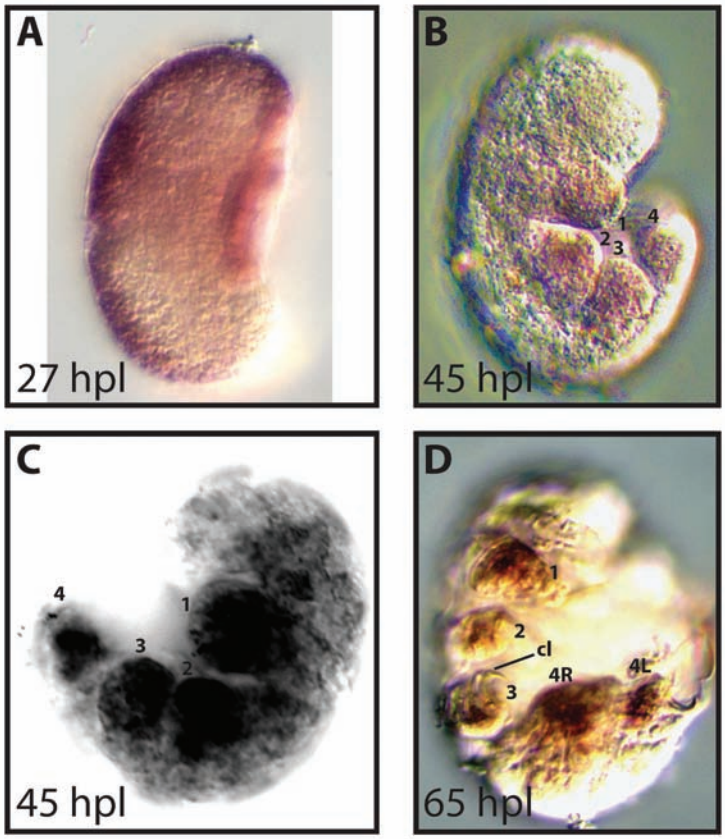

Figure 3. *Dll* is expressed at the base of the developing stylets. (A–D) Increasingly deep focal planes in a late stage embryo. Arrows point to domains of *Dll* expression. Abbreviations: bu, buccal tube; ph, pharyngeal bulb.

Figure 3.

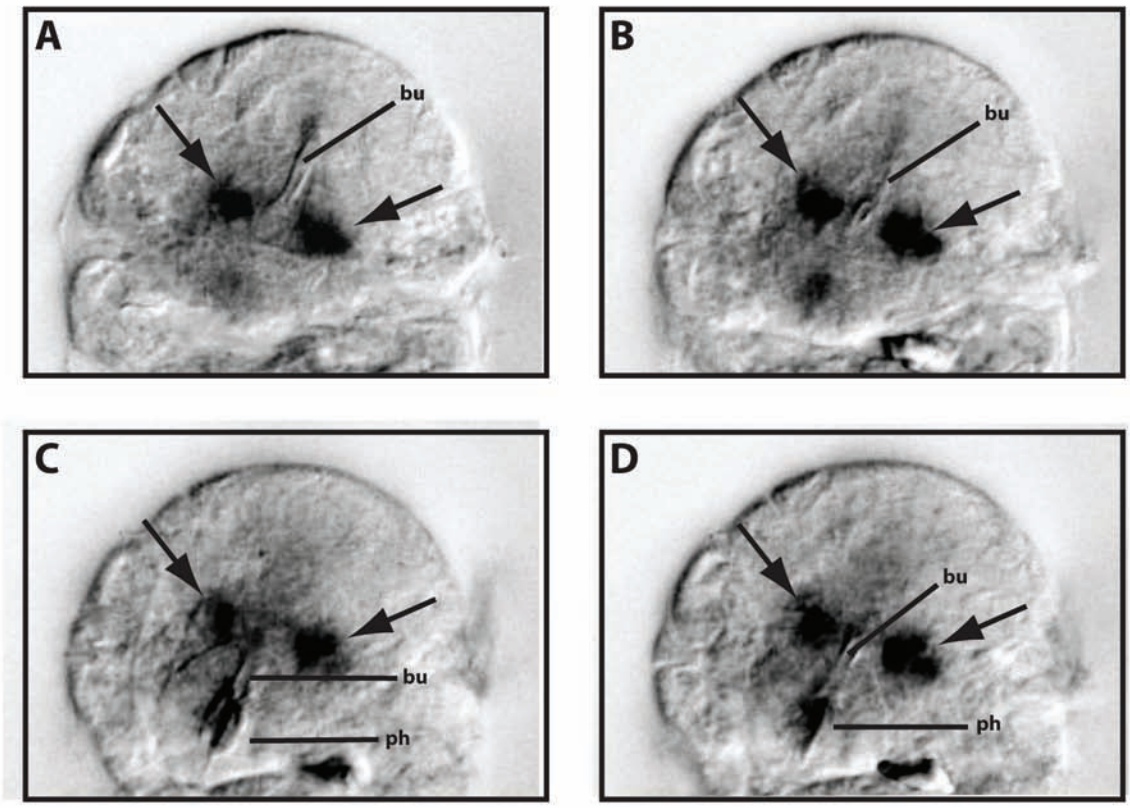

Appendix

Embryonic *in-situ* hybridization for the tardigrade *Hypsibius dujardini*

Introduction

Tardigrada is an enigmatic phylum of microscopic invertebrates known for their incredible ability to survive in extreme environments. Their phylogenetic position within Ecdysozoa relative to both the nematode *Caenorhabditis elegans* and the fruit fly *Drosophila melanogaster* makes them an important lineage to study in order to address questions about ecdysozoan body plan evolution. Here an *in-situ* hybridization protocol is presented for the tardigrade *H. dujardini.* This protocol is based on *in-situ* protocols for insects (Tomoysu et al., 2009), the nematode *Caenorhabditis elegans* (Seydoux and Fire, 1995), and a protocol for small embryos (Irvine, 2007). This protocol complements an RNA interference protocol (Tenlen et al., 2013), enabling developmental genetic investigations in this species.

Materials

Please consult appropriate Chemical Health and Safety datasheets for reagents below.

Reagents

pCR 4-TOPO vector (Invitrogen K4575-01)

RNAse Away (Sigma-Aldrich 83931)

DIG RNA labeling mix (Roche 11277073910)

0.5X PBTw

10X PBS	2.5 ml
10% Tween20	500 µl
DEPC H_2O	47 ml
Final volume	50 ml

Chymotrypsin/Chitinase solution (store at 4° C in the dark)

Chitinase (Sigma-Aldrich C6137)	50 mg
Chymotrypsin (Sigma-Aldrich C4129)	15 mg
50 mM potassium phospate buffer (pH 6.0)	1 ml
Final volume	~1 ml

Fixative Solution

Heptane	333.33 µl
16 % formaldehyde (Electron Microscopy Sciences 15700)	250 µl
10% Tween20	10 µl
0.5X PBTw	406.67 µl
	1 ml

Electron Microscopy Sciences formaldehyde is used for this protocol. It comes in 10 ml ampoules. After breaking open a ampoule, cover it with a lid from a 14 ml round bottom tube (BD 352059) and store it in the dark at room temperature. Discard all unused formaldehyde solution every few weeks to ensure freshness of formaldehyde used in embryo fixation.

MeOH

50 ml each of 25%, 50%, 70%, and 90% MeOH in 0.5X PBTw.

1% triethanolamine (store at room temperature)

triethanolamine	500 µl
0.5X PBTw	45.5 ml
	50 ml

Acetic anhydride solution (prepare immediately before use)

1% triethanolamine	500 µl
acetic anhydride	1.3 µl
	~500 µl

50X Denhardt's (store at -20° C)

Ficoil	5 g
polyvinylpyrrolidone	5 g
Bovine Serum Albumin	5 g
ddH_2O	to 500 ml
Final volume	500 ml

Hybe buffer (store at -20° C)

100% Formamide	25 ml
20X SSC (pH 6.0)	12.5 ml
100 mg/ml heparin	50 µl
10% Tween20	500 µl
10 mg/ml yeast RNA	500 µl
10% CHAPS	500 µl
50X Denhardt's	1 ml
sodium dodecyl sulfate	0.5 g
DEPC H_2O	9.95 ml
Final volume	50 ml

Plain Hybe buffer (store at -20° C)

100% Formamide	25 ml
20X SSC (pH 6.0)	12.5 ml
10% Tween20	500 µl
DEPC H_2O	12 ml
Final volume	50 ml

20X SSC buffer (store at room temperature)

NaCl	175.3 g
Sodium Citrate	88.2 g
ddH_2O	800 ml

adjust pH to 7.0

Fill to 1 L with H_2O. Use ddH_2O to dilute to working concentrations. Add CHAPS to 0.1%.

Maleic Acid Buffer (MAB) pH 7.5 (store at room temperature)

Maleic Acid	11.61 g
NaCl	8.77 g
NaOH pellets	7.2 g
Sterile H_2O	500 ml

adjust pH to 7.5

fill to 1 L with H_2O

10 % Blocking reagent solution (BRS) (store at 4° C)

Boil 50 ml of MAB in a sterile 250 ml glass bottle.

Slowly add 5 g of Blocking Reagent (Roche 11096176001) to the MAB, while intermittently swirling the solution.

Autoclave BRS.

Blocking buffer (store at 4° C)

Bovine Serum Albumin	1 g
BRS	25 ml
0.5X PBTw	25 ml
Final volume	~50 ml

AP Developing solution buffer (make fresh)

1 M Tris HCl (pH 9.5)	1 ml
5 M NaCl	200 µl
1 M $MgCl_2$	500 µl
10% Tween20	100 µl
ddH_2O	8.2 ml
Final volume	10 ml

BCIP/NBT PLUS solution (Southern Biotech 0302-01)

Supplies

35x10 mm petri dishes (BD 351008)

1.5 ml low retention tubes (Fisherbrand 02-681-320)

25-gauge needle (BD 305125)

Mobicols (Boca Scientific)

Mobicol mini-columns with Luer-lock cap, closing cap, and plug (M1002)

Large Filters for Mobicols, 10um pore size (M2210)

Bottom Filters for Mobicols, 10um pore size (M2110)

2 ml collection tube

1 ml syringe (BD 305125)

9” glass Pasteur pipette (Fisherbrand 13-678-20C)

Equipment

-20° C freezer

4° C refrigerator

Hybridization oven

Water bath

Heat block

Incubation chamber

Place a flat wet paper towel in a 150 x 15 mm plastic petri dish (BD 351058)

Mouth-pipets

50 µl calibrated pipets (WVR 53432-783) are used for this protocol. Pipets are pulled by hand over a bunsen burner. Next, the tip of a pulled pipet is broken off with clean forceps,

leaving an opening just large enough to allow an adult tardigrade to pass through. Then the pipet is inserted into an aspirator that comes with the pipets.

Unless otherwise noted, perform all embryo and adult transfer steps with a mouth-pipet.

Method

In-situ probe synthesis (2-3 days)

1. A 722 base pair fragment of *H. dujardini Distal-less* (*Dll*) was amplified with PCR from *H. dujardini* embryonic cDNA and cloned into the pCR 4-TOPO vector, following the manufacturers protocol. M13 forward and reverse vector primers were used to amplify *Dll* from the vector. This fragment included a vector T3 promoter site at one end and vector T7 promoter site at the other end. T7 or T3 RNA polymerase and DIG RNA labeling mix were used to produce either a sense or antisense DIG labeled probe. All standard approaches used to produce DIG labeled in-situ probes are suitable for this protocol. The strategy adopted is at the investigator's discretion.

Embryo collection (1 hr/200 embryos)

2. The *H. dujardini* in lab cultures are all parthenogenetic females. Collect molting adults that are in the process of depositing embryos into their exuviae. Adults lay between 3 and 12 embryos. Place these adults in a 35 x 10 mm petri dish filled with Poland Springs water (or another brand of spring water tested for suitability of rearing tardigades). Collect embryos for ~1

hour. At the end of this hour, most adults have exited their exuviae, and embryos are approximately at first cleavage.

3. The following steps take place in the embryo collection dish. Roughly two hours before embryos reach the developmental stage of interest, slice through the maternal exuvia near its middle, with a 25-gauge needle attached to a sterile 1 ml syringe. Most embryos will simply spill out. With the needle, gently push down on the exuviae to force any remaining embryos out (Supplementary video 1). Continue excising embryos from exuviae for 1 hour.

4. Transfer embryos to an autoclaved 1.5 ml low retention tube filled with 1 ml of 0.5X PBTw. Transfer as little water as possible.

Primary permeabilization (~1.5 hrs)

5. Centrifuge 1.5 ml tube containing embryos at 18,500 rcf for 3 minutes. At this point you should be able to see a pellet of embryos at the bottom of the tube. Remove supernatant using a 25-gauge needle attached to a syringe, leaving the embryos suspended in approximately 20 µl of 0.5X PBTw. Keep the needle tip close to the surface of the buffer in the tube in order to avoid sucking up embryos. By using a needle and syringe, very few embryos are lost during wash steps.

6. Spin Chymotrypsin/Chitinase solution on a bench top centrifuge briefly. Add 20 µl of this solution to the embryo tube and let stand for 1 hr at RT.

7. Wash 3 times for 5 minutes in 0.5X PBTw, following the procedure from step 5 to remove supernatant. Leave ~50 µl of 0.5X PBTw in the tube between washes.

Paraformaldehyde fixation (~1 hr)

8. Add 1 ml of fixative solution to the tube containing the embryos. Tape the tube on its side on a shaker and shake vigorously for 30 minutes. A New Brunswick Scientific Classic Series C1 Platform Shaker, set at speed 80, was used for development of this protocol.

It is critical that the following steps take place in an RNAse free environment. Wipe down all surfaces of work area with RNAse AWAY before continuing with the protocol.

9. Wash 5X-5 min. in 0.5X PBTw as in step 5.

Preparing and using Mobicol mini-columns

Performing methanol dehydration/rehydration and hybridization steps in a 1.5 ml tube leads to significant loss of embryos. This problem was circumvented by performing these steps in Mobicol mini-columns (Irvine, 2007). To use the mini-columns, insert the small filter and large filter into a mini-column with the tools provided by the manufacturer. Place the mini-column in a 2 ml collection tube in a tube rack. At this point, you can add up to 600 µl of liquid to the mini-column. Screw a Luer-lock cap onto the mini-column and attach a 1 ml syringe into the cap (Fig. 1A–B). To pass liquid through the mini-column, gently push down on the syringe

plunger until liquid is slowly dripping into the collection tube. When embryos are in the column, they must remain suspended in liquid at all times. To prevent desiccation, pull the syringe out of the mini-column before all the liquid has passed through (black dotted line in Fig. 1A). Pull out the mini-column and dump supernatant from the 2 ml collection tube. Replace the mini-column into the collection tube and remove Luer-lock cap/syringe to add more liquid.

Cleaning Mobicol mini-columns (~5 min)

10. Immediately before using, pass 600 µl of RNAse away through the mini-columns, followed by 4 washes of 600 µl of DEPC H_2O.

Methanol dehydration (~1 hr)

11. After the final embryo wash (step 9), centrifuge the tube again. With a 9" glass Pasteur pipette, carefully suck the embryos out of the bottom of the tube and transfer the embryos to a Mobicol mini-column. Be careful to not pull embryos beyond the shoulder of the glass pipette or the embryos may get stuck. To ensure as many embryos as possible are transferred, repeat step 10 until approximately 500 µl of 0.5X PBTw has been transferred.

12. Pass the 0.5X PBTw through the mini-column, leaving enough buffer to keep embryos submerged.

13. Wash embryos in 500 µl of 25% MeOH in 0.5X PBTw for five minutes. Pull back on the syringe gently to form a vacuum in the mini-column between washes, so there is not excessive loss of 0.5X PBTw.

14. Repeat step 13 with room temperature 50%, 70%, and 90% MeOH in 0.5X PBTw.

15. Wash the embryos 3 times in 100% MeOH. After adding the final wash of 100% MeOH, insert a bottom plug into the column and replace the Luer-lock cap with a closing cap (Figure 2C). Leave the tube at -20° C for at least 20 min.

At this stage, the embryos can be stored indefinitely at -20° C.

Methanol rehydration (~1 hr)

16. Remove the bottom plug and replace the closing cap with the Luer-lock cap and syringe. Wash the embryos for 5 minutes each in 500 µl of 90%, 70%, 50%, and 25% MeOH in 0.5X PBTw, followed by three washes of 500 µl 0.5X PBTw.

Secondary permeabilization (~1 hr/ 100 embryos)

The *H. dujardini* eggshell is impermeable to in situ probes and antibodies and was found to be resistant to chemical means of permeabilization. To circumvent this issue, the following simple procedure for removing the eggshell was developed.

17. After the final wash, pull the embryos out of the mini-column using a 9" glass Pasteur pipette, being careful to not suck embryos up past the shoulder of the pipette. Transfer the embryos into a 35 mm petri dish filled halfway with 0.5X PBTw.

18. To ensure most of the embryos are transferred, repeat step 17 until all 0.5X PBTw has been removed from the mini-column. Debris from the column is also transferred during this step. To ensure that the embryos are dissected in a sterile environment, transfer them to a new 35 mm petri dish filled halfway with 0.5X PBTw, being careful not to transfer debris.

19. With the sharp edge of a 25-gauge needle attached to a syringe, gently roll the embryo in the dish. When the eggshell has been penetrated, a space between the embryo and eggshell will become apparent as it fills with 0.5X PBTw (Supplementary video 2), or the eggshell may collapse onto the embryo. It is sometimes necessary to gently apply pressure on the eggshell to force the embryo to fully emerge from it.

20. Recollect the embryos in a new mini-column filled with 0.5 ml of 0.5X PBTw.

Acetylation (~15 min)

The acetylation step is used to reduce background.

21. Wash embryos with 500 µl of 0.5X PBTw.

22. Wash embryos twice with 500 µl of 1% triethanolamine in PBTw.

23. Prepare the acetic anhydride solution in a sterile 1.5 ml tube and vortex briefly. Wash the embryos twice for 5 minutes in 500 µl of this solution.

24. Wash the embryos 3 times with 500 µl of 0.5X PBTw.

The following steps that take place in mini-columns include long wash steps. For 20 minute–2 hour washes, pull back gently on the syringe to form a vacuum in the mini-column. For overnight incubations, gently pull back on the syringe, then insert the bottom plug (Fig. 1C). These precautions will prevent excessive loss of liquid during incubation periods.

Prehybridization (~3 hrs)

25. Pass ~half the 0.5X PBTw through the mini-column and replace it with room temperature Hybe buffer (resulting in 1:1, 0.5X PBTw:Hybe). Shake very gently for 20 min at RT.

A New Brunswick Scientific Classic Series C1 Platform Shaker set at speed 20 was used for development of this protocol.

26. Wash with room temperature Hybe while shaking gently for 20 min at RT.

27. Wash with Hybe heated to 60° C in a water bath. Keep the embryos in a hybridization oven at 60° C for 2 hr.

A Precision 180 Series Water Bath was used for warming buffers and a Lab-Line 120 Compact Incubator was used for heated incubation steps during development of this protocol.

Hybridization (~16 hrs)

28. Incubate DIG-labeled riboprobe with 500 µl of Hybe buffer (final concentration ~ 0.5 µg/ml DIG-labeled riboprobe) for 5 min at 80° C.

A Fisher Scientific Dry Bath Incubator was used for this step. Different riboprobes may have different optimal concentrations. Reduce the riboprobe concentration if a lot of background is produced during the detection (step 50).

29. While the riboprobe is incubating, prepare herring sperm (40 mg/ml). Boil water in a small beaker in the microwave. When the water starts to boil, immediately submerge 20 µl of herring sperm in a 1.5 ml tube into the hot water. After 20 seconds, shear the herring sperm by pulling it in and out several times through a 25 gauge needle attached to a 1 ml syringe. Refrain from pulling the herring sperm into the syringe so that it is not lost.

30. Repeat step 29 three times.

31. Add 1.0 µl of boiled and sheared herring sperm to the DIG-labeled riboprobe solution and mix well with the pipette tip.

The sheared DNA from the herring sperm acts as a blocking reagent.

32. Pass most of the buffer that the embryos are suspended in through the mini-column and add the riboprobe solution.

33. Hybridize overnight at 60° C in a hybridization oven.

Different riboprobes may have different optimum hybridization temperatures. Between 55° C and 60° C is typical for most in-situ protocols.

Post-hybridization washes (~4.5 hours)

At this time, it is no longer necessary to work in an RNAse free environment. In the following steps, all buffers should be preheated to 60° C in a water bath and the embryos should be incubated in a 60° C a hybridization oven, unless otherwise specified. The temperature used here is the same as the hybridization temperature used. Adjust accordingly.

34. Wash the embryos 5 times quickly with 500 µl of Plain Hybe buffer.

35. Wash the embryos 5 times for 20 minutes with 500 µl of Plain Hybe buffer.

36. Wash the embryos 5 times quickly with 500 µl of 2X SSC, 0.1% CHAPS.

37. Wash the embryos for 30 minutes with 500 µl of 2X SSC, 0.1% CHAPS.

38. Wash the embryos twice for 30 minutes with 500 µl of 1X SSC, 0.1% CHAPS.

39. Remove the embryos from the incubation oven. Wash the embryos twice with room temperature 0.5X PBTw.

Immunohistochemistry (overnight)

40. Incubate the embryos in 500 µl of blocking solution for 2 hours at room temperature.

41. Incubate the embryos overnight in 500 µl of 1:1500 anti-DIG antibody:blocking solution at 4° C.

Post-antibody washes (~1 hour)

42. Wash the embryos 5 times quickly with 500 µl 0.5X PBTw, followed by five 10-minute washes of 500 µl of 0.5X PBTw.

Detection

43. Wash the embryos 3 times quickly with 500 µl of AP developing solution, followed by 1 ten-minute wash in AP developing solution.

44. Pull the embryos out of the mini-column using a glass Pasteur pipette, being careful to not suck embryos up past the shoulder of the pipette.

45. Transfer the embryos to a well of a clean Pyrex 12 well dish.

The following steps are performed on a dissecting microscope.

46. Transfer the embryos in the smallest volume possible to a new well filled with 500 µl of AP developing solution. Be careful not to transfer mini-column debris. Before transferring to the new well, it may be necessary to clean debris off of embryos by pipetting them in and out several times.

47. Transfer the embryos to a well with 500 µl of BCIP/NBT solution, being careful to transfer the smallest volume of AP developing solution as possible.

48. Keep the 12 well dish in an incubation chamber at room temperature in the dark. To prevent overstaining, check the embryos at least once an hour on a dissecting microscope against a white background.

49. To stop the reaction, transfer the embryos in the smallest volume possible to a well filled with 0.5X PBTw.

50. Stained embryos can be stored in mounting medium on microscope slides. However, glycerol in mounting medium alters morphology of *H. dujardini* embryos, so images should be taken of embryos in PBTw before mounting for long-term storage.

References

Irvine, S.Q., 2007. Whole-mount in situ hybridization of small invertebrate embryos using laboratory mini-columns. *BioTechniques* 43, 764–768.

Seydoux, G., Fire, A., 1995. Whole-mount in situ hybridization for the detection of RNA in *Caenorhabditis elegans* embryos. *Methods Cell. Biol.* 48, 323–337.

Tenlen, J.R., McCaskill, S., Goldstein, B., 2012. RNA interference can be used to disrupt gene function in tardigrades. *Dev. Genes. Evol.* 1–11.

Tomoyasu, Y., Arakane, Y., Kramer, K.J., Denell, R.E., 2009. Repeated co-options of exoskeleton formation during wing-to-elytron evolution in beetles. *Curr. Biol.* 19, 2057–2065.

Figure 1. (A) The mobicol mini-column configuration used in this protocol. The black dashed line denotes the approximate level to which we reduce the embryo suspension during wash steps. (B) The mini-columns are kept in a tube rack for this protocol. (C) The mini-column configuration while the embryos are stored in MeOH at -20° C.

Figure 1.

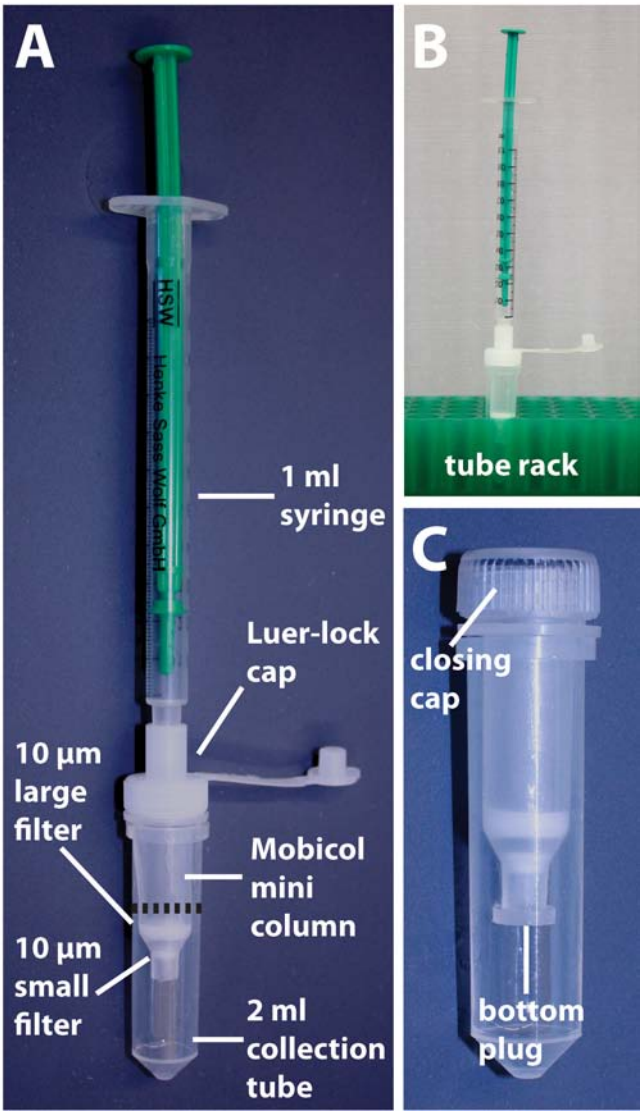
A
HSW
Henke Sass Wolf GmbH
1 ml
syringe
Luer-lock
cap
10 µm
large
filter
Mobicol
mini
column
10 µm
small
filter
2 ml
collection
tube
B
tube rack
C
closing
cap
bottom
plug

Supplementary materials

Supplementary video 1.

(http://edenrcn.com/protocols/Individual%20Protocols/Smith_tardigrade_movie1.mov). This recording shows the dissection of a maternal exuvia containing four embryos. At 3 seconds, the exuvia is cut open, using a slicing motion and the sharp edge of a 25-gauge needle attached to a syringe. The middle region of the exuviae, right between the 2nd and 3rd embryo was targeted. At 4 seconds, the first embryo spills out of the exuviae. By gently pushing against the other embryos, they are also forced out of the opening in the exuvia.

Supplementary video 2.

(http://edenrcn.com/protocols/Individual%20Protocols/Smith_tardigrade_movie2.mov). This recording shows an embryo being dissected out of its eggshell. Using the sharp end of a 25-gauge needle, the eggshell was targeted by carefully attempting to roll the embryo along the bottom of the dish. At 14 seconds, the eggshell is penetrated. At 15 seconds the eggshell becomes apparent as buffer rushes in and it expands away from the embryo. At this point the embryo begins to fall out of the eggshell. At 20 seconds the eggshell is completely pulled of the embryo.